

DISSERTATION

MICROBIAL SUCCESSION IN HUMAN RIB SKELETAL REMAINS AND FLY-HUMAN
MICROBIAL TRANSFER DURING DECOMPOSITION

Submitted by

Heather Leigh Deel

Graduate Degree Program in Cell and Molecular Biology

In partial fulfillment of the requirements

For the Degree of Doctor of Philosophy

Colorado State University

Fort Collins, Colorado

Spring 2022

Doctoral Committee:

Advisor: Jessica L. Metcalf

Carol Wilusz
Pankaj Trivedi
Michael Pante

Copyright by Heather Leigh Deel 2022

All Rights Reserved

ABSTRACT

MICROBIAL SUCCESSION IN HUMAN RIB SKELETAL REMAINS AND FLY-HUMAN MICROBIAL TRANSFER DURING DECOMPOSITION

Human decomposition is a dynamic process partially driven by the actions of microbes. It can be defined by the fresh, early decomposition, advanced decomposition, and skeletonization stages. The microbial communities that facilitate decomposition change in a predictable, clock-like manner, which can be used as a forensic tool for estimating postmortem interval. Chapter 1 introduces this concept by describing the stages of decomposition in detail and how high-throughput sequencing methods can be used with microbes to develop models for predicting postmortem interval. Chapter 1 also describes which sample types are most useful for predicting postmortem interval based on the stage of decomposition, the knowledge gaps in the field, and the steps necessary for adoption of this tool into the justice system.

During fresh and early decomposition, microbial succession of the skin and soil sample types are most predictive of postmortem interval. However, after approximately the first three weeks of decomposition, the changes in the microbial communities that are used for predictions begin to slow down and the skin and soil sample types become less useful for estimating postmortem interval. Chapter 2 of this dissertation shows that microbial succession of the bone microbial decomposer communities can be used for estimating postmortem interval during the advanced and skeletonization stages of decomposition. First, the bone microbial decomposer community was characterized using 16S ribosomal RNA sequencing from six human donor subjects placed in the spring and summer seasons at the Southeast Texas Applied Forensic Science Facility. A core bone decomposer microbiome dominated by taxa within phylum Proteobacteria was discovered, as well as significant overall differences in the bone microbial community between the spring and summer seasons. These microbial community data were used to develop random forest models that predicted postmortem interval within +/- 34 days over a 1–9-month time frame of decomposition. To gain a better understanding of where the microbes in the

decomposed bone were coming from, as healthy, living bone is typically sterile, SourceTracker2 was used with paired skin and soil samples taken from the same decedents. Results showed that the bone microbial decomposer community is likely sourced from the surrounding environment, particularly the skin and soil communities that occur during the advanced stage of decomposition.

Chapter 3 of this dissertation focuses on the influence of the blow fly (Calliphoridae) microbiome on human cadaver microbial community assembly. In early decomposition, volatiles attract blow flies to the cadaver, which serves as a source of nutrients and a safe place to lay eggs. It is likely that during this interaction between hosts, there is a mechanical transfer of microbes that subsequently alters each of their microbial communities. While studies have shown that blow flies have their own microbiome, they were not conducted in a decomposition environment. First, Chapter 3 shows the characterization of the blow fly microbiome by organ and season in a terrestrial, human decomposition environment. This was performed by placing ten cadavers across the winter, spring, and summer seasons at the Southeast Texas Applied Forensic Science Facility, collecting the first wave of colonizing flies for each cadaver, and sequencing the 16S ribosomal RNA gene of the labellum (mouth parts), tarsi (leg parts), and oocytes. Results showed that the previously defined universal fly microbiome persists even in a decomposition environment, with notable differences still present between organs and seasons. Additionally, results from using the tool SourceTracker2 showed that the labellum and tarsi act as substantial bacterial sources of the human decomposer bacterial community, and this source contribution varies by season.

In summary, this dissertation provides the first quantitative estimate of postmortem interval of terrestrially decomposed human skeletal remains using microbial abundance information. This is a significant contribution to the criminal justice system; anthropologists typically use visual evidence to provide postmortem interval estimates of skeletal remains with errors ranging from months to years, whereas our approach provides estimates with errors of approximately one month. Furthermore, this dissertation shows evidence that there is a mechanical transfer of microbes between blow flies and human cadavers during the early stage of decomposition, which provides ecological insight into human cadaver microbial community assembly.

ACKNOWLEDGMENTS

Work in this dissertation was supported by the National Institute of Justice grant numbers 2012-DN-BX-K023 and 2018-R2-CX-0018. Throughout my graduate career, I was also financially supported by many of the fantastic organizations at Colorado State University, including the GAUSSI Program, the Cell and Molecular Biology Program, the Vice President of Research Fellowship Program, and the Graduate Student Council. Together, these organizations have provided me with funds for conferences, funds for student fees, and many professional development opportunities that were instrumental for my success as a graduate student.

I have a multitude of people to thank for supporting me during these five years, and I first have to start with my incredible advisor, Jessica Metcalf. When I first came to graduate school, I honestly had no idea what I was doing. I came from a moderately sized college in Huntsville, TX, a college I chose to go to because it was the most cost effective, and all I knew was that I wanted to work hard and make something of myself. Jessica welcomed me as one of the first graduate students into her lab with open arms. Throughout my time in her lab, she has provided me with countless opportunities to develop my professional skills through presenting at conferences, attending some amazing summer courses on both the east and west coasts, teaching at workshops, and contributing to publications. She went out of her way to make sure I had the tools to succeed. There were many times that I struggled to keep up, and Jessica mentored me with an amount of patience and grace that I will forever be grateful for. I did not come from a world of higher education, and I am the scientist that I am because of her.

Next, I want to thank others in the Metcalf lab. I was so happy to have Aerial Belk as my lab mate. Since we started graduate school at the same time, we learned everything together – from day one about how to open a terminal all the way through teaching workshops towards the end of our graduate careers. Aerial is probably the most positive person I know, and her attitude was the highlight of every lab meeting. Her eagerness for figuring out some new code, finding new ways to display data, and even color palettes spilled over into my own work, and I will forever look back on our adventures both in and out of

the lab fondly. Alex Emmons and Zachary Burcham, who were postdocs in our lab, were both so helpful for me to just ask questions to and for helping me figure out bugs in my code. Victoria Niececki has also been so fun to have around for bouncing ideas off each other and talking through experiments. The lab managers who contributed to my projects, Holly Archer and Kris Otto, were both so incredibly helpful and supportive of me figuring out and doing bone extractions, especially because probably 97% of my work was computer-based and it took a little while to learn the ropes of the wet lab.

I also want to thank the members of my committee. Carol Wilusz, who is also the director of the Cell and Molecular Biology Program, surely had my best interests at heart. She has always taken the time to meet with me and has provided valuable advice that has made me a better scientist. I always enjoyed a conversation with Pankaj Trivedi (and most definitely learned something new every time), and I have valued his intellectual input. I first met Michael Pante when I took his From Death to Discovery class in the Anthropology Department. While this class was out of my wheelhouse, he provided some much-needed perspective on bioerosion of bone.

I would not have pursued a PhD if not for the many teachers and professors I've had who fostered my sense of curiosity for the sciences. I had two amazing high school teachers – Jason Gaspar and Naomi Nassar – who taught me the foundations of studying hard. From Sam Houston State University, Aaron Lynne, Sibyl Bucheli, Chris Randle, and Anne Gaillard gave me the foundations of biology that undoubtedly got me through my first two years of graduate classes. Sibyl and Aaron both deserve a special thank you for connecting me with Jessica, teaching me the ropes of doing research at an anthropological facility, and for their invaluable collaboration while I was in graduate school. I also want to thank my college roommate, Michelle Harrel. She was a constant guidepost and best friend during my time at Sam Houston State University, and she was most assuredly with me in spirit as motivation and inspiration during graduate school.

So much of who I am today is also because of my friends and family. My dad instilled a sense of hard work in me from a very young age, and that is something I have carried with me. My mom and Mike have been so incredibly supportive of my decision to move to another state for my PhD. I wouldn't have

had the courage to do it without them – for my entire life, they have fostered a love for learning and a love for travel. I will never take the family road trips, camping trips, and vacations that they sacrificed for us to go on for granted because it made me a better and braver person. I also want to thank my grandpa (“Gramps”) – when he would visit Fort Collins just because he could, it was always the highlight of my weekend. I have loved having Michelle and Paul Phipps, my future in-laws, as my “Colorado parents.” Other family I want to thank are my Aunt Chell, my sister Amy, and my grandmothers Becky and Bonnie. They are all a solid ground and have always been there just to talk to. I’ve also had many friends in Fort Collins who have helped me escape work when I needed it through trivia nights, movie nights, Jackbox nights, Pokémon Go park trips, hikes, and some darn good Sea of Thieves sessions. Thank you, Coleen, James, David, Matt, Amber, Manny, Alex, and Anna. You have all become dear to my heart over the last couple of years, and COVID was a lot less sucky because of all of you.

Finally, this last paragraph is for my fiancé, Nate. I don’t quite have the words to describe what our relationship has meant to me (maybe I’ll get it right when we exchange vows in August), but I do know that his constant and unflinching love and support have kept me going through finishing a PhD during a pandemic. When COVID pulled the rug out from under all of us, and much of my support system at CSU was just gone, Nate was there to help when I needed to vent and cry, when I needed silent company, when I needed to lock myself in a room to figure something out, when I had news (good or bad), when I just needed some time alone, and when I needed tacos. Even now, as I write this, he is making dinner while I’m working late. No matter what kind of day I was having, his voice was always there just to tell me that it would be okay. Thank you, Nate – I love you more than you know.

TABLE OF CONTENTS

ABSTRACT	ii
ACKNOWLEDGEMENTS	iv
CHAPTER 1: AN INTRODUCTION TO USING MICROBIOME TOOLS FOR ESTIMATING POSTMORTEM INTERVAL	1
Summary	1
Introduction	1
Decomposition and Estimation of the Postmortem Interval	3
Stages of Decomposition	3
Estimating the Postmortem Interval	6
The Microbial Clock	10
Using Decomposition Studies to Build Regression Models for Predicting PMI	11
Early Studies of Microbial Ecosystems	13
The use of Mammalian Model Systems to Develop a Microbial Clock	15
Human Decomposition Studies	16
The Microbial Clock of Different Sampling Environments	17
Human Body: Externally Accessible Locations	17
Human Body: Internally Accessible Locations	18
Bone	20
Soil	20
The Effect of Environmental Variables on the Microbial Clock	22
Knowledge Gaps and Areas of Investigation	24
Adoption of Technology	24
Conclusions	27
REFERENCES	29
CHAPTER 2: A PILOT STUDY OF MICROBIAL SUCCESSION IN HUMAN RIB SKELETAL REMAINS DURING TERRESTRIAL DECOMPOSITION	37
Summary	37
Introduction	38
Results and Discussion	39
Progression of Decomposition and Rib Sampling	39
Quality of Amplicon Sequence Data	40
What Microbes Invade the Bone, and Where are they Coming From?	40
Is there a Difference in the Microbial Community Assembly in Ribs from Cadavers Placed During Different Seasons?	45
Can we use Microbial Invasion into Bone to Estimate PMI?	47
Conclusions and Limitations	51
Materials and Methods	53
Decedent Placement and Sampling	53
Rib Bone Processing	54
Extraction and Purification	55
Amplification and Sequencing	56
Data Analysis	56
16S rRNA Preprocessing	56
18S rRNA Preprocessing	56
Diversity Estimates	57
Identifying Core Features and Features Different Between Seasons	58
Source Tracking	58

Model Testing	60
REFERENCES	61
CHAPTER 3: THE MICROBIOME OF BLOW FLY ORGANS AND FLY-HUMAN MICROBIAL TRANSFER DURING DECOMPOSITION	70
Summary	70
Introduction.....	71
Results and Discussion	73
Fly Occurrence.....	73
Quality of Amplicon Sequence Data	74
The Core Fly Microbiome	75
How Does the Fly Microbiome Compare Between Organs (Tarsi, Oocyte, Labellum)?	77
How Does the Fly Microbiome Compare Between Seasons?	80
Do Fly-Associated Bacteria Appear in the Human Decomposition Microbiome, and How Does this Differ Between Placement Seasons?	82
Conclusions.....	85
Materials and Methods.....	85
Study Site	85
Cadaver Placement and Monthly Temperature Calculations	85
Fly Collections	86
Human Sampling	86
Identification of Flies.....	87
Dissections	87
Sample Processing and Sequencing.....	87
Data Cleaning and Analysis.....	88
Data Availability	89
REFERENCES	90
CHAPTER 4: CONCLUSIONS AND FUTURE DIRECTIONS	100
APPENDIX A: CHAPTER 2 SUPPLEMENTARY MATERIALS.....	102
APPENDIX B: CHAPTER 3 SUPPLEMENTARY MATERIALS.....	112

CHAPTER 1: AN INTRODUCTION TO USING MICROBIOME TOOLS FOR ESTIMATING POSTMORTEM INTERVAL¹

Summary

Estimating the postmortem interval (PMI) of human remains is important in criminal investigations. Microbes play an important role in the process of decomposition and can provide clues about the time elapsed since death. Host-associated and environmental microbial communities undergo succession in a predictable, clock-like manner during decomposition. High throughput DNA sequencing can be used to inexpensively and rapidly track these microbial community shifts, and machine learning techniques can use these data to develop predictive models. In this chapter, we discuss the development of a microbial clock for estimating PMI, as well as remaining knowledge gaps and hurdles to technology adoption.

Introduction

The postmortem interval (PMI), or the time elapsed since death, is critical to establish in forensic investigations. During death investigations, testimonies are often incomplete and inaccurate, and the use of physical evidence (such as microbes or insect activity) to estimate PMI is important. Narrowing down PMI can aid testimonial evidence by validating or refuting alibis, identifying suspects and witnesses, and reconstructing the death scene. Additionally, it can help with the issuing of death certificates and the distribution of assets defined in wills. However, PMI can be difficult to determine. Estimating PMI to the hour of death is often impossible. That level of precision is virtually nonexistent. Additionally, current methods for estimating PMI, such as gross postmortem changes, last communications, and visual sightings become limited in their accuracy as PMI increases. Forensic entomology, the study of insect

¹ This work has been previously published: Deel, H., Bucheli, S., Belk, A., Ogden, S., Lynne, A., Carter, D. O., Knight, R., & Metcalf, J. L. (2020). Chapter 12 - Using microbiome tools for estimating the postmortem interval. In B. Budowle, S. Schutzer, & S. Morse (Eds.), *Microbial Forensics (Third Edition)* (pp. 171–191). Academic Press.

activity in a death investigation, can be useful for PMI estimations of remains that have been decomposing for days to weeks, but these methods are not always consistent due to a lack of insect activity during the winter and the relative absence of insects indoors. Therefore, novel tools for estimating the PMI of remains over the timeline of decomposition are needed.

Microbes play an important role in the process of decomposition, and host-associated and environmental microbial communities have been shown to change in a predictable, clock-like manner during decomposition. Therefore, the microbial communities associated with human remains may have the potential to be applied as a forensic tool by estimating PMI on longer or broader timescales than can be determined by traditional methods. The use of microbiome data (high throughput characterization of microbial communities) to profile microbial communities associated with decomposing remains and its development into a “microbial clock” to estimate PMI is a promising new method for which proof-of-concept studies have been published by independent research groups over the last several years (e.g. (1–3)).

In this chapter, we will describe the potential use of microbes as predictors of PMI. We begin the chapter with a description of human decomposition, including the major stages of decomposition and how they are identified. We then describe benefits and limitations of current methodologies for estimating PMI. Next, we define how to create a model to predict PMI using microbial data, including different sequencing and computational approaches. To follow, we describe early studies that lead to the development of the microbial clock and its use in mammalian model systems, including human remains. An explanation for different sample types that can be collected during human decomposition studies and how that may affect the microbial clock will then be provided. Next, we describe environmental variables that could affect the microbial clock, followed by current knowledge gaps in creating a microbial clock for estimating PMI. Lastly, we conclude with how to integrate this tool into the justice system.

Decomposition and Estimation of the Postmortem Interval

Human decomposition is a dynamic process that is dependent upon many factors from the condition of the remains in life, the circumstances under which death occurred, and the environment in which the remains are decomposing. During decomposition, a cadaver is returned to its elemental basics through chemical degradation and the action of organisms that can consume tissues. These organisms are active from the inside out (primarily microbes) and the outside in (microbes, vertebrate and invertebrate scavengers). Climate, weather, and geography also influence how decomposition progresses. Therefore, decomposition is a product of the larger habitat in which it occurs, and alteration of ecosystem components will have an impact on the tempo and mode of decomposition. It follows then that studies of biology and chemistry are the main ways in which scientists understand generalities and variances that may occur during decomposition (4–6). Accurate measurements of biotic and abiotic ecosystem components combined with qualitative assessments of the remains allow scientists to estimate PMI. There are several methods available to estimate the PMI, each with strengths and limitations. The robustness of a method depends on the extent to which decomposition is influenced by the habitat as well as an investigator's ability to assess these variables to accurately incorporate them into a model. Because investigators are working backwards through time, the conditions of death may never be known, but the more clock-like the method to estimate the PMI, the more reliable are the assessment and conclusion.

Stages of Decomposition

Decomposition can be classified into major stages, which progress one after the other. Each stage has taphonomic landmarks, but the overall process is that a wet environment, after purging of the fluids of decomposition, becomes a dryer one (4, 5, 7). The number of decomposition stages that exist is debated in forensic science. Megyesi et al. (7) defined 4 stages of decomposition, a modification of the Galloway (8) system: fresh, early decomposition, advanced decomposition, and skeletonization, although these stages can co-occur.

The first stage, fresh, shows few postmortem changes with little to no discoloration (7). However, at the cellular level, deprivation of oxygen results in a cascade of biochemical events. The body begins to equilibrate to ambient temperatures (*algor mortis*). Actin and myosin proteins (responsible for normal muscle contractions) lock due to limited adenosine triphosphate (ATP; necessary to unlock the proteins) in the cells, causing the entire body, from the face and shoulders to the larger muscle groups such as the trunk and limbs, to stiffen (*rigor mortis*). Body areas in contact with surfaces will discolor from pooling of blood due to gravity (*livor mortis*). Eventually *autolysis* occurs, ending *rigor*; digestive enzymes, stored in cellular organelles called lysosomes, begin self-decomposition causing cellular membranes to lose integrity and cell-to-cell junctions to be destroyed (5, 9–14). Bacteria that are able to survive independent of the host or are no longer kept in check by the host's immune system reach increased levels of activity (15, 16). Flies (Diptera) may lay eggs at this stage. Those in the family Calliphoridae, blow flies, are attracted to fresh remains, and females will lay their eggs in protected areas such as the eyes, nose, and ears. Eggs will also be laid at body-ground and body-body interfaces and sometimes in thicker hair. Egg-laying by a female is an attractant to other females to do the same, and egg masses may consist of hundreds or thousands of eggs. Occasionally beetles (Coleoptera), such as carrion beetles (Silphidae) and rove beetles (Staphylinidae), and ants and wasps (Hymenoptera) are attracted to the fly eggs (6, 17–21); pers. obs. Bucheli Laboratory).

Early decomposition is rapidly changing at the biochemical, microbial, scavenging, and taphonomic levels. Skin begins to slip off, sometimes in large sheets, and the hair falls, marking the transition from fresh to the first state of early decomposition (5, 7). The remains are engaged in active putrefaction with fermentation and proteolysis (13). Fatty acid decomposition is either aerobic or anaerobic, sometimes both occurring on the same subject (5, 13). The remains shift from a pink-white color to gray-green color and finally to black (7, 8). During this color shift, a marbling effect often occurs that Pinheiro (5) refers to as “posthumous circulation.” As the gut decomposes, bacteria are able to enter into and move through the circulatory system, metabolizing the blood and creating a blackish residue. Visible through the waxy skin, the effect is like marbled stone. The internal condition of the remains is

now anoxic and acidic, and the anaerobic bacteria proliferate and produce gases as a metabolic byproduct. The gases inflate the remains (bloat) and eventually force accumulated fluids from orifices of the head and trunk (purge) (5, 13, 22). Megyesi et al. (7) note that for the trunk, bloating with purge represents the third state of early decomposition, and for the head and neck, purge represents the fourth state of early decomposition. Insect activity intensifies during this stage, reaching its peak. Many adult flies are attracted to the remains to lay eggs and to feed from fluids. The eggs of the initial colonizing Diptera, now hatched, represent the oldest larvae; however, Diptera are attracted to the remains and lay eggs in waves and the potentially large “maggot mass” (conglomerate of actively feeding larval Diptera) consists of many species, even families, at variable ages. The maggot mass travels around the body, feeding as it goes and physically tearing at the flesh with modified mouthparts. This activity will greatly facilitate decomposition of wet tissues, as the maggots spread digestive enzymes and bacteria as they move. It is also common to encounter necrophagous beetles, especially larvae and adults of the family Silphidae, and predatory insects as observed in the fresh stage (6, 17–21); pers. obs. Bucheli Laboratory.)

Megyesi et al. (7) mark the onset of advanced decomposition, the third stage, with caving of the flesh of the eyes, throat, and abdominal cavity, though others have marked post-purge as the onset of advanced decomposition. Although the cadaver has now entered the drier stages of decomposition, putrefaction continues. For the limbs, Megyesi et al. (7) note that moist decomposition with bone exposure (less than 50% of the total area) is followed by mummification with bone exposure (less than 50% of the total area). Galloway (8) adds the formation of adipocere as the end state of advanced decomposition in some cases. Diptera activity slows as tissues dehydrate, but Coleoptera that prefer drier remains can present variable levels of activity during decomposition, particularly taxa from families Silphidae, Cleridae, Scarabaeidae, Trogidae, and Dermestidae (6, 17–21); pers. obs. Bucheli Laboratory.)

During the final stage, skeletonization, all soft tissues are eliminated from the remains so that only dry bone is left. Insect activity decreases from sparse to nonexistent (7) and scavenging activity is decreased (6, 17–21); pers. obs. Bucheli Laboratory.), excluding scavengers that are attracted to bones (some rodents, some birds (23), coyotes (pers. obs. Bucheli Laboratory,) snails (24), and occasionally

millipedes (pers. obs. Bucheli Laboratory.) This last stage may take an extended period of time, months to years.

Estimating the Postmortem Interval

Chronological time can be linked to stages of decomposition in a number of different ways, allowing for a variety of methods for estimating PMI, each of which has strengths and limitations. One main challenge is that the route taken to get to the final stage of skeletal remains can vary based on the conditions of the decedent in life, at death, and parameters of the ecosystem in which the remains decompose. Though predictable to a degree, alteration of temperature, humidity, rainfall, or soil conditions may change the tempo and mode of decomposition, allowing remains to indicate multiple stages of decomposition at once, bypass a stage, or prolong a stage, all of which could lead to inaccurate interpretation of the PMI. Decomposition is also greatly influenced by organisms adapted to consume putrefying tissues. Vertebrate scavengers are common outdoors and can greatly increase the rate of decomposition by removing flesh, but their attraction to and ability to consume remains is difficult to predict. Insects are highly successful necrophagous feeders. These organisms will colonize the remains at particular stages of decomposition. This resource partitioning results in ecological succession—a predictable change in the community structure that is driven by the cadaver ecosystem shifting from wet to dry. Using information extracted from the necrophagous insect fauna can also have challenges. The benefits and drawbacks of various methods are discussed below.

Early landmark taphonomic events of decomposition occur during an established timeline. Although variable, *rigor mortis*, *livor mortis*, and *algor mortis* are well studied processes that may be useful to estimate the PMI during the first few days after death. Some general observations are that, under ambient temperatures of ~20°C (12), *rigor mortis* sets in at 2 - 6 hours after death, with rigidity established in all muscle groups by 6 hours postmortem, persisting for 24 - 84 hours postmortem until autolysis destroys cells (11–13). *Rigor mortis* onset and duration times can be altered by temperatures. Increased body temperatures just before death (through increased activity or fever) can shorten the onset

time (9, 11, 13). Colder ambient temperatures can shorten onset time and increase the duration of *rigor*, while warmer temperatures may delay the onset time and/or prevent full development of *rigor* (13). *Livor mortis* begins between 30 minutes and 3 hours after death and will continue to develop for the first 12 hours postmortem, becoming fixed (with a reddened skin color that no longer turns white when pressure is applied) after 18 - 24 hours postmortem. Colors of lividity then change as a result of biochemical events with the initial red of oxygenated blood giving way to purple as oxygen unbinds from hemoglobin. Temperature can affect this color change, as colder temperatures may delay the release of oxygen from hemoglobin. *Livor mortis* persists until putrefactive changes dominate (9, 11). Estimates of the postmortem interval by analyzing *algor mortis* are based on the time it takes a cadaver to reach the ambient temperature. The average temperature of life for a human is 37.4°C. Postmortem, the remains cool at a rate dependent on time but can also be affected by activity just before death, body mass, clothing, and the ecosystem surrounding the remains at death. There is extensive literature on estimates of the time since death based on body cooling and all variables that must be considered. Hayman and Oxenham (9) provide a useful review.

As decomposition advances past the first few days, methods to estimate the time since death become fraught with variables, making accurate estimates more difficult as the timeline progresses. To predict the time of death using the Megyesi et al. (7) system, state of decomposition for three major body regions (head/neck, limbs, and trunk) is assessed and a total body score (or TBS) is generated and used in a regression to calculate the accumulated degree day (ADD) (see **Box 1.1** for more information).

For organisms that are cold-blooded or for chemical reactions, the ambient temperature dictates the speed of physiological or chemical reactions (i.e. higher temperatures speed up reactions while lower temperatures slow them down or stop them completely). Therefore, the same physiological or chemical reaction taking place at two locations with varying temperatures may occur at different speeds. To account for this, decomposition scoring systems and models include a minimum threshold temperature, or base temperature, below which the reactions cease or are greatly slowed. Accumulated degree hours (ADH) measures total heat units spent above the base temperature and accumulated degree days (ADD) converts this measurement to calendar time. Including these parameters ensures more valid comparisons between subjects decomposing at different ambient temperatures.

Box 1.1. ADH and ADD to estimate physiological time.

With this approach, a previously qualitative method is made quantitative. The Megyesi et al. (7) system seeks to diminish user error and standardize the degree of decomposition across seasons and geographic locations; it is unique in that it allows the user to assess and score the state of decomposition of the remains as three separate areas. This system, according to Megyesi et al. (7), hypothetically works at all time points postmortem until the recovery of skeletal remains. A valid concern of the Megyesi et al. (7) TBS system is user error. However, Dabbs et al. (25) demonstrated there was no difference in TBS scores produced by different observers, and that photographs of remains are as reliable for assessment as the cadaver itself, if it is no longer available (26, 27). Another concern of the Megyesi et al. (7) TBS system is the reliability of the regression models used to calculate the ADD, which Moffatt et al. (28) corrected by using a more appropriate regression model.

Yet another challenge is the reliability of the equation in other climates, which may not be representative of how remains decompose in areas of high temperatures or high humidity where decomposition may be accelerated or stopped (29) via mummification and saponification (see below). Progressive color change is also plastic with remains experiencing nonlinear or composite color changes, with earlier mummification possible and then reversal of mummification at times of intense rain (29). Though Megyesi et al. (7) do not record bloat in the head, neck, and limbs, Bucheli et al. (30) recorded noticeable bloat in these areas using LiDAR. Bucheli et al. (30) also observed diurnal periods of bloating (inflation during the day and deflation at night) and that remains of similar PMIs even in close proximity may experience different trajectories of decomposition given slight variation of ecosystem components (31).

A final valid concern for estimating PMI using TBS is the timing of saponification and mummification. Saponification (adipocere formation) and mummification are both processes that occur in opposition to decomposition; that is, they are preservation processes. While Galloway (8) and Megyesi et al. (7, 8) include mummification as later stages of advanced decomposition, and Galloway (8) includes saponification as the final stage of advanced decomposition, Pinheiro (5) records these processes as able to occur at any stage of decomposition. Saponification is the result of hydrolysis and hydrolyzation of

adipose tissue to form a waxy but brittle substance (5), facilitated by warm temperatures and water. It can begin immediately after death, with visible signs showing later. Mummification, caused by desiccation of tissues, is frequently seen in arid climates. The onset of desiccation can be immediate but not noticeable until weeks later. Pinheiro (5) notes that on a single cadaver, saponification and mummification can occur at the same time. Only a small amount of water is necessary for saponification, as little as what is naturally found in human tissues, and use of cellular water for saponification may result in dehydration of nearby tissues (5).

Insect colonization, or the arrival time and duration of the insect on the cadaver, frequently correlates to the PMI and therefore can be used to estimate the time since death (17). Two methods are useful in this regard: the age of the maggot (shorter-term evaluation) and the succession pattern of an insect community (longer-term evaluation). If female flies arrive nearly immediately after death to lay their eggs, the age of the oldest maggot (sometimes the largest) should be indicative of PMI. Using information of the ambient temperature of the maggots during development compared to a standardized growth curve, the ADH (with the base temperature of insect metabolism figured) can be calculated. This ADH will correlate to the ADH of the cadaver and therefore the PMI. Maggot ADH models work best when the first colonizing maggots are used for estimates. Generally speaking, at 25°C and 60-70% humidity, it takes the eggs of the blow fly *Lucilia coeruleiviridis* approximately 24 hours until hatching and another 7-13 days of feeding until pupation (32). This time frame can be greatly altered by temperature (as temperatures increase, the rate of maggot development is accelerated). Noteworthy, however, is that each species of fly has its own unique developmental ADH and base temperature. A researcher must be familiar with these species-specific values to use the ADH approach. If those oldest maggots have completed their lifecycle and departed as adults, investigators may misinterpret the second oldest maggots as the first (21), greatly underestimating PMI.

The second entomological method to estimate PMI uses long-term colonization patterns of insects that are tracking cadaver resources through time as dehydration of the body advances. Certain insects are attracted to the remains at particular stages of decomposition (see above for general patterns). These

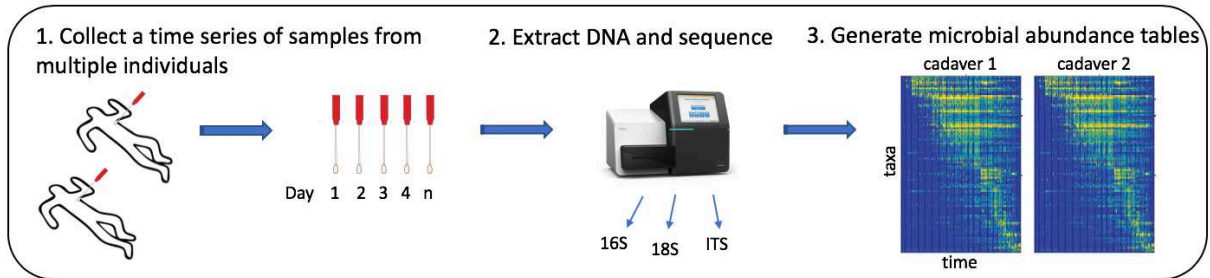
insects will attend the remains as long as it is palatable, giving way to other insects as decomposition progresses so that certain combinations of insect colonizers found at the cadaver at certain states of decomposition can be indicative of a long term PMI, on the order of weeks or months. Insect successional patterns work best when they can be compared to a well-curated insect library generated through long-term studies of biodiversity of necrophagous insects (21, 33). Insect models to estimate the PMI can also be problematic. Maggot ADH methods require laboratory equipment to rear insects. Successional patterns to estimate PMI require long-term studies of remains. Both of these methods are highly influenced by geography and season and therefore are a regionally specific science. One must also have extensive knowledge of insects of the area to be able estimate PMI based on insect data. Studies conducted in one area are not immediately applicable to other areas. Other pitfalls to using insects to estimate the PMI include instances when the maggot ADH and the time since death are not the same as in situations of extreme heat or extreme cold (may speed up or slow down insect development, respectively), delayed or expedited colonization by the insect (restriction of the insect by loose or semi-open physical barrier or antemortem access to wound sites), or complete restriction from the remains (burials, aquatic environment, tightly closed chambers) (21). Other unique circumstances of insect biology can alter the timing of egg laying by flies and slow insect successional patterns, greatly skewing PMI estimates (34).

The Microbial Clock

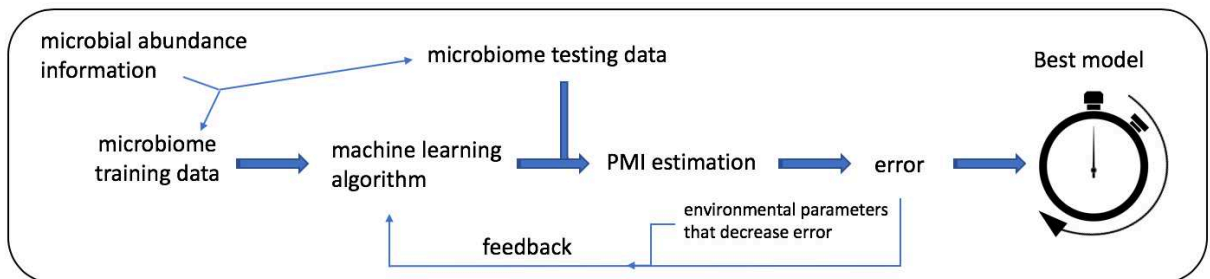
Similar to insects, the succession of different microbial communities can indicate PMI. This temporal succession of microbes during decomposition was first noted in early studies in the 1980s (35, 36). After the advent of next generation high throughput sequencing, microbial succession patterns have been more accurately and comprehensively characterized by rapid and inexpensive profiling of thousands of microbial taxa per sample. For example, microbial community changes during decomposition have been shown to be relatively predictable and clock-like across individuals decomposing within the same environment (1, 2, 37). Due to the predictable nature of microbial succession associated with

decomposing bodies, researchers have been exploring the potential of building regression models from microbiome data that can predict the PMI of a cadaver-associated sample with unknown PMI (**Figure 1.1**).

A. Conduct temporal decomposition study



B. Build and refine model



C. Use model to estimate unknown PMI

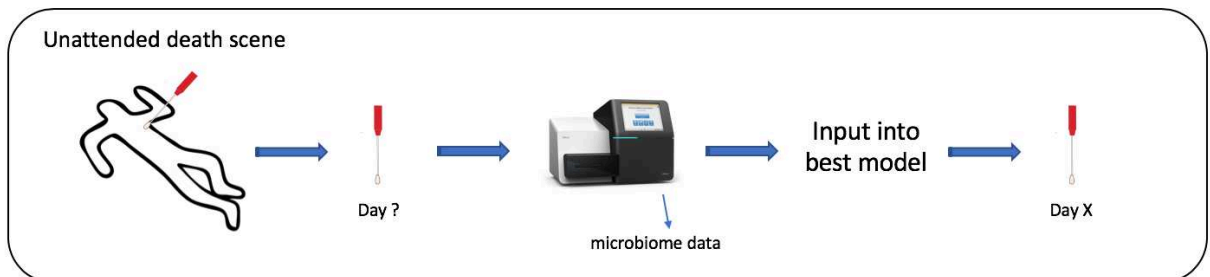


Figure 1.1. Building and using a microbial clock model. Controlled experiments are conducted to observe and harness the patterns of microbial succession on human remains over a timeframe of PMI. The microbial community data resulting from these experiments can be used to build a machine learning model, which can then be used to predict the PMI of testing data and, eventually, microbiome samples of unknown PMI.

Using Decomposition Studies to Build Regression Models for Predicting PMI

Building a microbial model for estimating PMI requires data generated from a decomposition study of multiple decomposing individuals (**Figure 1.1A**). These decomposition studies can be accomplished with either nonhuman mammalian models in laboratories or outdoor facilities, or with

human donors at anthropological research facilities, which provide the infrastructure for research on decomposing human remains. Generally, in decomposition studies, sterile cotton swabs are used to collect a sample of microbes from a chosen site (e.g. skin of the cheek). To build a robust model with low error rates, a time series of samples is required to capture the microbial succession that occurs at the sample location during decomposition. Therefore, remains are often sampled daily or in 2-3 day intervals to build models with error rates in these time frames (since the error rate cannot be smaller than the sampling frequency). Swabs are then frozen to prevent continued microbial growth until further analysis can be conducted. To process the samples, DNA is extracted, and polymerase chain reaction (PCR) is used to amplify a taxonomically informative DNA region. For example, the 16S ribosomal RNA (rRNA) amplicon is commonly used to survey bacterial and archaeal populations present in a microbial community. The 18S rRNA amplicon is typically used for eukaryotic characterizations, and the internal transcribed spacer (ITS) gene region is used for fungi. Each of these amplicons are universal, taxonomically informative, and relatively cheap to sequence.

Once sequence data are generated, they can be summarized into a count table representing the relative abundance of each microbial taxon for each sample (**Figure 1.1A**). With thousands of microbial taxa and potentially hundreds to thousands of samples, these datasets are big and complex. Machine learning is a powerful tool for discovering patterns in complex microbiome data (see **Box 1.2**) and can be used to build predictive models for estimating unknown PMIs by using a time series of samples from remains with known PMIs. The microbial abundance information is partitioned into training and testing datasets, and the abundance patterns in the training dataset are used to “program” the machine learning algorithm (**Figure 1.1B**). The testing dataset is then used to determine the accuracy of the model, which calculates error based on predicted versus known PMI. In addition to modeling based on microbiome data, environmental parameters (e.g. temperature) can be added to improve model accuracy. The modeling process is repeated until the lowest error for PMI estimations is achieved, which represents the best model (**Figure 1.1B**).

Once the best regression model is generated, microbiome swabs collected from remains with unknown PMIs can be processed in the same manner as those from the decomposition studies (**Figure 1.1C**). The microbial abundance information obtained from sequencing can then be input into the best model, which uses the microbial clock to estimate PMI with error rates (e.g. 10 days +/- 3 days).

Machine learning predictive tools for microbiome data

Microbiome datasets are large and complex. Therefore, they are well-suited for modeling and classifying using machine learning approaches. Machine learning is the construction of systems that learn from data. Data are input into an algorithm, which uses these data to build a model. Then, the machine learning algorithm uses another set of data to test the model and refines it based on the error. In simple statistics this second step does not occur, which is what makes machine learning unique. Furthermore, when using machine learning the researcher is able to relax assumptions (i.e., that the data are normally distributed) and work with more general models than in basic statistics.

There are numerous algorithms for building machine learning models, most of which follow similar constructions. The microbiome data are used to train a model for either classification or regression based on a metadata variable. Classification models are built to predict a categorical outcome. For example, microbiome data could be trained to classify patients into different disease states or risk groups. Regression models predict continuous variables. For example, microbiome data could be trained to predict sample pH, geolocation, or patient age. Both of these models have been applied to predict PMI, by creating a binary to predict whether the sample is from an early PMI or middle PMI as a categorical variable, or by using days since death as a continuous variable.

Algorithms that have been used with some success in PMI prediction include Random Forest, K-nearest neighbors, and Linear Regression. These algorithms all work to generate predictive models, generally through subsetting the data into training and testing sets. The model is built on the training set, then applied to information from the testing set. The model will then have both the “true” response and the “predicted” response, and the difference between these two is used to calculate the model error rate. The main distinction between these three algorithms, then, is how they train the model.

Box 1.2. Machine learning tools for building regression models with microbiome data sets.

Early Studies of Microbial Ecosystems

Before the advent of high throughput sequencing, studies of microbial succession relied on culture and microscopy methods. But, this did not prevent scientists from proposing the use of microbial change to model PMI. This concept was investigated by Melvin et al. as early as (35). In this study, researchers removed a portion of the small intestine from mice and suspended it in a beaker of saline. Using this model, they were able to monitor the movement of microbes, known as transmigration, from

the luminal contents to the surface of the intestine. Melvin et al. showed that the time required for this transmigration was dependent on the temperature but, using electron microscopy, the researchers identified specific organisms that translocate and the order in which they appear on the intestinal surface. These were, in order, *Staphylococcus* spp., coliforms and fungi, then coliforms and anaerobes. This was critical information to establish the concept of a microbial clock because it demonstrated that microorganisms appeared repeatedly at different time points, though this was only in an *in vitro* model.

After the initial hypothesis of microbial succession patterns, several other studies were conducted to monitor the microbial changes during mammalian decomposition. Micozzi (36) published a study that compared the decomposition patterns of rat remains that were either freshly killed or frozen and thawed. In this investigation, Micozzi further demonstrated a succession of microbial taxa that was consistent across all remains sampled. As in Melvin et al., *Staphylococcus* appeared in the earliest stages of decomposition, day 0 in the frozen-thawed remains and day 2 in the fresh. However, he found other microorganisms as well, including *Enterococcus*, *Streptococcus*, *Bacillus*, and other non-identified gram-negative rods. These microorganisms persisted for most days of decomposition, but by the final sampling point (day 6), only *Enterococcus*, *Streptococcus*, *Bacillus*, and *Staphylococcus* were still found in the samples, with the addition of *Proteus* and *Clostridium*. Though not as clear as in the previously described experiment, there was still evidence of a bacterial succession pattern. Micozzi did not culture for fungi, so it is unclear if fungal succession was also a part of the decomposition pattern in his experiment. In addition to the contributions to the body of evidence surrounding the microbial clock hypothesis, this study also helped to direct experimental methodology as investigation continued in this field. In the comparison of fresh versus frozen-thawed rat remains, Micozzi found that the postmortem changes were different. Specifically, Micozzi concluded that the frozen-thawed remains were more susceptible to external insects and microorganisms and aerobic decay. Due in part to this evidence, current research prioritizes the use of fresh (never frozen) cadavers.

The use of Mammalian Model Systems to Develop a Microbial Clock

Model organisms are often used in all facets of biological and biomedical research. There are several advantages that smaller model systems have over using human hosts, including larger sample sizes, ease of manipulation, lower cost, greater accessibility, and more rapid growth and reproduction (38). This holds true for decomposition research, and as a result many of the experiments using next-generation sequencing methods were conducted using nonhuman models, including rats, mice, fish, and swine. Another advantage to using these models in decomposition studies is that the experiments can be conducted in an animal facility, which many universities have, while human remains studies require a specialized facility. These mammalian model studies have been critical for demonstrating a proof of concept for the predictability of microbial succession during decomposition. For example, Metcalf et al. (2) published a proof-of-concept study in which mice decomposed over 48 days, and microbiomes of the skin, abdomen, and soils were characterized using amplicon sequencing for the 16S rRNA and 18S rRNA genes. They found that the microbial community composition changed significantly and consistently as decomposition progressed. Similar to the early studies, researchers identified bacterial taxa that changed in abundance during decomposition, but in this case these organisms were determined based on relative abundance of DNA sequences as opposed to presence in culture. To determine whether this observed succession could result in an accurate model of PMI, they generated regression models and discovered that PMI could be predicted within approximately 3 days over 48 days of decomposition, thus providing evidence for developing a novel tool for estimating PMI.

Swine have also been used to build models for human decomposition, as they are similar to humans in their internal anatomy, fat distribution, lack of fur, and diet, which indicate a similar initial gut fauna (39). In another important proof-of-concept study, Pechal et al. (1) evaluated the bacterial succession during the decomposition of three swine carcasses and used these data to predict PMI. This study was conducted outdoors instead of in a laboratory, so the carcasses were exposed to weather conditions, though they were covered in cages to prevent scavenging. These carcasses were sampled at 1, 3, and 5 days after placement, and the extracted DNA was sequenced using the 16S rRNA gene amplicon.

Similar to Metcalf et al. (2), researchers found that there were significant changes in bacterial community structure and diversity. In this experiment, models were also generated using Random Forest regression. This resulted in accurate predictions of PMI, further suggesting this method could be used as a forensic tool.

Human Decomposition Studies

The use of model organisms permitted controlled, repeatable experiments, which provided proof-of-concept studies for microbial clock applications for predicting PMI. Before microbiome data can be used as a forensic tool, however, it is important to show that the microbial clock can also be used to estimate PMI of human remains. To evaluate this, decomposition studies tracking microbial succession using donated human remains have been conducted at specialized anthropological research facilities (3, 37, 40–49).

A challenge with many of these studies is the low sample size that results from the high cost and low availability of human cadavers. To remedy this, Pechal et al. (44) conducted a large-scale PMI experiment using 6 external skin swabs from 188 cases that were collected in death investigation cases. Due to the nature of the sample collection process, this study focused on the early decomposition period. Researchers analyzed the microbiome data using 16S rRNA amplicon sequencing, then inferred the gene pathways to investigate the potential ecological functions of these communities. Based on these results, investigators suggested that the microbiome is more stable in the first 48 hours, and after two days, the variability increases despite fewer taxa. They concluded that while there was bacterial succession throughout PMI, microbes may not be informative of PMI until after 48 hours postmortem. In another study underway by the authors of this chapter, 36 human cadavers were placed at three anthropological research facilities and microbial communities were sampled for the first 21 days of decomposition. Together, these two studies lay a foundation for building a microbial clock based on human samples.

The Microbial Clock of Different Sampling Environments

While generalized trends in the microbial processes that drive corpse decay are somewhat pervasive throughout each stage of decomposition, the precise pattern of community succession observed at various points in decay could be significantly impacted by the location from which samples are collected. It is also possible that some sample types may provide a more accurate clock for predicting PMI than others. Research examining microbial community change has been conducted on samples associated with mammalian cadaver skin (2, 43, 45, 50), gastrointestinal/rectal locations (41, 42, 44, 45, 50), oral sites (44, 45, 50), nasal, eyes, and ear cavities (44, 48), internal organs (46), bones (40), and cadaver associated soils (43), each providing useful information regarding the impact of sample environment location on microbial succession. Each sample type harbors its own set of limitations and benefits that should be carefully considered when deciding what locations to use. For example, samples taken from organs may be accurate early in decay (46), whereas bone samples provide increased accuracy for longer decay time frames (40). Certain sampling locations may be more or less accessible, depending on the stage of decay and the nature of the death scene. Furthermore, some sampling locations may be less invasive during a death investigation. For example, skin samples may be more accessible and less invasive at a death investigation than a gastrointestinal sample. All of these factors are important considerations to make when using microbial clocks as a forensic tool. Below, we discuss these considerations in more detail regarding each sample type.

Human Body: Externally Accessible Locations

External sample locations have been frequently chosen in decomposition studies, including skin, rectal, oral, nasal, eye, ear, and umbilicus sites. These locations are often beneficial because they are easily accessible, and only a simple, non-invasive swab is required to sample the microbiome. However, since there are numerous external sites from which to sample, it is important to consider whether microbes from different locations change similarly throughout decomposition.

The skin is a common sample site in decomposition studies, and it has been chosen for model organisms including mice (2, 43), swine (50), and humans (43, 45, 51). Since the skin is a very large organ, there are multiple locations to consider when choosing from where to sample. In one experiment by Hyde et al. (45), two human subjects were sampled from the mouth, external left/right cheeks, external left/right biceps, torso, and rectal regions. Although the succession of microbes was not identical, both subjects exhibited similar changes in phyla abundance through time for all sites sampled. Other recent studies have investigated whether certain skin sites increase the accuracy of PMI estimations to allow for a better microbial clock. For example, in Johnson et al. (48), machine learning revealed lower error models from skin samples collected from the inner ear canals compared to the inner nasal surfaces. Belk et al. (51) compared models using samples collected from the skin of the torso and the head, revealing that both sites could accurately estimate PMI. While these promising results suggest that the skin can build an accurate microbial clock, it would be useful to compare a wider array of skin locations within one study to determine which site provides a more clock-like succession of microbes.

In addition to the skin, other external sample sites have been studied for potential use as PMI estimators. Pechal et al. (44) used samples from a variety of locations, including the eyes, ears, nares, mouth, and rectum to determine if models generated for each sample type could be used to classify the PMIs within the temporal categories of less or greater than 48 hours. Each model except the one created using rectal samples was successfully able to accomplish this task, suggesting that a wide variety of externally accessible sample types can be used to achieve similar ends when estimating PMI.

Human Body: Internally Accessible Locations

In decomposition studies, researchers can also choose to sample the internal “thanatomicrobiome,” or the microbiome of the blood and internal organs (46, 52). These sites are not directly influenced by the same environmental factors (such as pH, temperature, insects, and scavengers) as external sites are. Furthermore, the internal thanatomicrobiome may not be affected by gut-associated microbes that flourish after death. While it was previously thought that internal organs were sterile, it was

demonstrated in the Human Microbiome Project that some internal organs may contain distinct microbial communities (52). Therefore, it is possible that microbial succession varies among organs during decomposition. Javan et al. (46) sampled the brain, heart, liver, spleen, buccal cavities, and/or blood from 27 human corpses from criminal cases with known PMIs. Results demonstrated that there were statistically significant, organ-dependent differences in microbial succession.

The gut microbiome has also been investigated as a potential source of clock-like microbial community change. For example, Hauther et al. (41) repeatedly sampled the gut microflora from 12 human subjects by making an incision in the abdomen and inserting a sterile swab into the cecum. Sequencing of the 16S rRNA gene revealed that *Bacteroides* and *Lactobacillus* populations declined with increasing decomposition, indicating that these taxa could be used as indicators of PMI. To further study microbial decomposers in the gut, Debruyne and Hauther (42) allowed four more human subjects to decompose. They then sampled the gut and sequenced the 16S rRNA gene as in their previous study. Results showed that the bacterial community in the gut gradually changed towards a common decay community, with a decline in Bacteroidales (*Bacteroides*) and an increase in Clostridiales and Gammaproteobacteria. Studies investigating microbial succession of the gut with increasing PMI have some results in common (2, 41, 42), such as a decline in *Bacteroides*, but they have also revealed differences in microbial succession, such as the presence of *Lactobacillus*, Clostridiales, and Gammaproteobacteria in some gut communities but not detected in others. Thus, it would be useful to conduct more experiments of this nature to determine if these differences impact the microbial clock.

While these sites can be informative for internal microbial succession and possibly PMI, it can be very destructive for the remains, and therefore difficult to study. During a decomposition study, it is important that sampling of remains does not have a major impact on the outcome of the experiment. For this reason, choosing a sampling site that allows for non-invasive sampling can be critical.

Bone

As decomposition progresses into the skeletonization stage, our ability to estimate PMI becomes more difficult (40). This is partially due to the loss of soft tissue, which prevents the regeneration of maggot masses and subsequently causes a shift in the decomposer community. Recent work has mostly focused on characterizing the diversity of decomposer communities leading up to skeletonization, but there are few studies characterizing the communities associated with skeletal remains.

Microbial invasion into bones is likely a slow process in that it potentially occurs for up to one year of decomposition, while the flesh can decompose within a few weeks. Therefore, the succession of microbes into bones after death could be tracked by collecting a time series of bone samples, providing a microbial clock of death for a longer time frame. Damann et al. (40), collected one rib bone from 12 bodies that were allowed to decompose over a wide time range (approximately 500-19,000 ADD). This allowed for the characterization of microbial succession over a longer time frame of decomposition than would have been possible using another sample type, such as skin, which is processed by microbial decomposers at earlier ADDs. Results indicated an interstage taxonomic succession of Firmicutes, Bacteroidetes, then Actinobacteria and Acidobacteria from partially skeletonized remains to completely dry remains. Additionally, researchers were able to identify an apparent source; the microbial communities associated with partially skeletonized remains resembled the human gut, while those of dry remains resembled the soil. This study suggests that there is potential for using rib bones as an extension to the microbial clock.

Soil

Studies have revealed that there are approximately eight million bacterial species per gram of soil (53). Carcasses serve as a nutrient-dense source for soil microbial decomposer communities. The decomposition of a mammalian corpse selects for specialized soil microbial communities that appear in consistent patterns. Multiple studies have shown that Proteobacteria is the dominant phylum during decomposition (2, 3, 49), while Acidobacteria generally decrease (2); (3) and Firmicutes increase (49); (3)

as decomposition slows. Additionally, human-associated *Bacteroides* are highly concentrated in soils during decomposition (3). Finally, Metcalf et al. (2, 43) demonstrated that soils associated with decomposing carcasses (gravesoils) provided accurate estimates of PMI, with errors similar to skin sites (51).

It is important to consider depth when sampling gravesoils in decomposition studies. Finley et al. (49) showed that in the decomposition soils of 18 human subjects (14 on the surface, 4 buried), there was a decrease in taxon richness (the number of species), evenness (the abundance of each species), and diversity of surface soils. In the soils associated with buried remains, there was an increase in taxon richness with decreasing evenness and consistent diversity. While Proteobacteria were dominant in all gravesoils, there was a decrease in Acidobacteria and an increase in Firmicutes only in the surface soil communities, which contrasts with the consistent community composition of the buried soil communities. Therefore, the sampled depth of gravesoils can affect the observed microbial composition and should be taken into consideration during sampling and PMI estimations.

It is critical to consider sample location when studying microbial succession of decomposing remains. External sites, such as the skin, rectum, mouth, nose, eyes, and ears, are easily accessible and have shown to provide accurate microbial clocks, but these locations can be influenced by the environment in which the remains are located. Internal sites, including the blood and internal organs, are likely less impacted by the environment, but sampling requires invasive dissection and introduces unreliability into the microbial clock. For researchers who aim to estimate PMI on a longer time scale, bone may be a good choice, as collecting a time series of rib bones may be able to extend the microbial clock. Soil as a sample site also shows great potential, as gravesoil microbial succession plays an important role as a possible source of microbial decomposers and a sink for ammonia rich post-rupture fluids associated with decomposition (43). Researchers interested in conducting a study of this nature should carefully consider one or a combination of these sample types based on invasiveness and the decompositional time frame of interest.

The Effect of Environmental Variables on the Microbial Clock

Although the proof of concept for the microbial clock has been demonstrated, the suite of variables that may affect the clock-like pattern of microbial decomposers is not well established. Some studies have investigated how some factors such as soil type, season, and insect activity affect the predictable succession of microbes during decomposition. Soil microbial community composition is partially driven by pH (54). Therefore, it is possible that different soil types will seed remains with different decomposer microbial communities. To test this hypothesis, Metcalf et al. decomposed mice on three soil types, including desert, shortgrass, and forest, which had different resident microbial communities (43). They showed that soil microbiomes from the different sources became more similar to each other as decomposition progressed. Importantly, when soil type was included as additional information (a feature) in regression models, it did not improve model accuracy. These results suggest that the microbial clock of decomposition ticks similarly across soil types, despite different endogenous soil communities - a promising result for developing a new forensic tool that is robust to environmental variation.

Another environmental parameter of interest is season, which captures major changes in temperature, humidity, and UV intensity. Carter et. al. (55) tested whether the microbial communities are similar across different seasons. Within a sample type (summer control, winter control, summer gravesoil, winter gravesoil) the microbiomes were similar, which confirmed the idea of a reproducible microbial succession pattern. Interestingly, season did influence the microbial communities, as bacterial and eukaryotic diversity was higher in the summer. Furthermore, in Metcalf et al. (43), regression models were trained on two human donor bodies placed in spring season, and the resulting model was used to predict PMI for two bodies in the winter season. By using ADD (see **Box 1.1**) in the regression, they found predictions across seasons to be much better than random.

Another variable that may impact the microbiome is carcass mass. Many studies in this area suggest that smaller carcasses decompose faster, though the mechanism is not well understood (56–59). Additionally, it has been demonstrated that larger carcasses release higher levels of total nitrogen, which

is an important nutrient for microbial growth, so release at differing levels could affect the microbial communities (56). This is an important research question, both because it is a critical variable in the construction of microbial clock models, and because it could influence whether small nonhuman models like rodents and pigs actually serve as valid model organisms. The effect of carcass size on the microbial community was investigated by Weiss and collaborators using swine as the model organism (60). Researchers found that the bacterial and eukaryotic signature changed similarly over decomposition, and carcass mass did not have a significant impact on the microbial clock. These findings support the use of model organisms to mimic human decomposition in the development of microbial models, though this study should be repeated with a larger sample size to support this more conclusively.

Finally, Guo et al. (61) conducted a study to determine if specifically insect exclusion would change the pattern of microbial succession. Researchers noted that, for both insect and insect-exclusion groups, they were able to identify specific taxa that changed significantly and in a repeatable manner during decomposition, providing further evidence of a microbial clock. They found that insect-exclusion rates decomposed more slowly, however they were unable to find a significant difference in taxa between the two groups; the only differences were in very low-abundance organisms. There is still a need for more research before it is fully known whether insect activity impacts the microbial clock.

These studies successfully demonstrate that environmental variables can influence microbial communities in some cases (e.g. soils, season), but do not necessarily affect the decomposer microbial community (e.g. soils). The evidence presented above clearly demonstrates that the microbial communities associated with decomposing mammalian tissue change and succeed each other in a significant and reproducible pattern. Furthermore, this pattern is sufficient to predict PMI in both early and advanced decomposition periods. By conducting these experiments, researchers were able to isolate variables to create an understanding of which factors impact the microbial clock.

Knowledge Gaps and Areas of Investigation

Although research has shown that a microbial clock is useful for predicting PMI, there are still important knowledge gaps that remain. These include a complete understanding of whether nonhuman models are useful for the development of microbial clocks, the time frame(s) for which microbes are most informative for building a microbial clock, which environmental variables are most useful for model improvement, the effect of the initial condition of the remains on the microbial clock, the sample type that is most informative for estimating PMI, and robust methods and parameters for modeling. These knowledge gaps are outlined in a recent submission that is currently under review (62).

Adoption of Technology

Adopting new technologies into the justice system requires overcoming a number of hurdles, including both academic and legal. The process of introducing new technologies starts with a need in the forensic science community, a response by scientists with a proof of concept, followed by the development of a prototype, legal validation and acceptance, and finally technology adoption (**Figure 1.2**). The need for improved methods for estimating PMI is well established in the forensic science community, and considered an achilles heel in the field (63). Although researchers have been working to improve these methods for decades, the advent of next generation sequencing technologies has provided new opportunities for methods development. Resulting from these new technologies, independent research laboratories have provided a proof of concept for estimating PMI. By publishing these findings (1–3, 37, 40–46, 48–51, 54, 55, 60, 61, 64, 65) and sharing results through conference presentations (66, 67), workshops (68) and webinars (69), researchers have connected with potential end users to overcome an important legal requirement of peer-reviewed publication (**Figure 1.2**). The next steps include developing a robust microbial PMI model with quantifiable error rates and creating a prototype kit and analysis pipeline. Once a prototype is developed, the technique needs to be validated and accepted into the legal system by having an attorney introduce the technology for acceptance to the court system (**Figure 1.2**). At this point, a judge will decide whether the microbial clock meets the Frye and/or Daubert

standards. The Daubert ruling (70) expanded on the earlier Frye ruling by allowing a judge to ask if the science and technology have been published in peer-reviewed journals, taught at colleges or universities, and has an established error rate, all of which contribute to its validity and reliability (71). Finally, efforts are required to support the adoption of this new type of DNA sequencing technology into the forensic community, and become used in accredited laboratories. This may be accomplished by sharing the new technology broadly at conferences, providing workshop and training opportunities, and working with accrediting organizations such as NACE (the National Association of Corrosion Engineers, a non-profit organization that publishes standard practices for industry use) and IACME (the International Association of Coroners and Medical Examiners, an organization committed to determining accurate causes of death through science, medicine, and the law).

Transitioning New Tools and Processes from Research into Casework



Figure 1.2. Adoption of new technology into the justice system. The process begins with a need, which researchers then aim to address. After a proof of concept is established, a prototype should be developed and validated by the forensic science community before it can be accepted as a new tool for use in the

justice system. *This graphic was developed by RTI International in operating the Forensic Technology Center of Excellence <http://www.forensiccoe.org/>, under Cooperative Agreement Award 2016-MU-BX-K110 from the U.S. Department of Justice, National Institute of Justice.*

Conclusions

Establishing PMI is often critical to the success of death investigations, as it can be used to validate alibis, identify suspects and witnesses, and reconstruct the death scene. Current tools for estimating PMI, such as gross postmortem changes and entomological evidence, have limited accuracy with increasing decomposition and are sometimes unavailable or unreliable. However, microbes are consistently present throughout decomposition, and recent proof-of-concept studies have shown that microbial succession on remains is both predictable and clock-like. Researchers have begun to utilize this “microbial clock” to estimate PMI using newly developed technologies, including high throughput next-generation sequencing to profile microbial communities and machine learning techniques that use this information to create models that are generalizable across different environments. However, it is becoming increasingly clearer that there are numerous sample types (externally and internally accessible, bone, and soil) to choose from and environmental variables (temperature, humidity, UV intensity, and insect exclusion) to consider that could affect the observed microbial succession in decomposition studies. It is critical to establish which sample types and parameters should be included in models to give the highest accuracy for estimating PMI. Additionally, these will give a better understanding of whether a single, generalizable model can be used for estimating PMI across different regions, or whether PMI estimates are more accurate using multiple models specified for each type of environment. Filling in these knowledge gaps will allow for the integration of this microbial clock as a forensic tool into the justice system, which will aid in death investigations.

In this dissertation, this chapter provides important context for understanding the goals and approaches of Chapter 2 and Chapter 3. This chapter has explained in detail how microbial succession in decomposing remains may be used for developing PMI models. It also describes the reason that bone is the appropriate sample type for developing PMI models for remains found within late stages of

decomposition. These concepts are critical for understanding the motivation behind the experimental approaches in Chapter 2, “A Pilot Study of Microbial Succession in Human Rib Skeletal Remains During Terrestrial Decomposition”. Additionally, this chapter provides context surrounding the complex ecological dynamics of human cadaver microbial community assembly. We describe how the decomposer microbiome forms after 48 hours of decomposition, with interactions between cadavers and insects occurring during this time frame. This sheds light on the motivation for studying the influence of the fly microbiome on the human decomposer microbiome in Chapter 3, “The Microbiome of Blow Fly Organs and Fly-Human Microbial Transfer During Decomposition”.

REFERENCES

1. J. L. Pechal, T. L. Crippen, A. M. Tarone, A. J. Lewis, J. K. Tomberlin, M. E. Benbow, Microbial community functional change during vertebrate carrion decomposition. *PLoS One*. **8**, e79035 (2013).
2. J. L. Metcalf, L. Wegener Parfrey, A. Gonzalez, C. L. Lauber, D. Knights, G. Ackermann, G. C. Humphrey, M. J. Gebert, W. Van Treuren, D. Berg-Lyons, K. Keepers, Y. Guo, J. Bullard, N. Fierer, D. O. Carter, R. Knight, A microbial clock provides an accurate estimate of the postmortem interval in a mouse model system. *Elife*. **2**, e01104 (2013).
3. K. L. Cobough, S. M. Schaeffer, J. M. DeBruyn, Functional and Structural Succession of Soil Microbial Communities below Decomposing Human Cadavers. *PLoS One*. **10**, e0130201 (2015).
4. E. R. Hyde, D. P. Haarmann, A. M. Lynne, S. R. Bucheli, J. F. Petrosino, The living dead: bacterial community structure of a cadaver at the onset and end of the bloat stage of decomposition. *PLoS One*. **8**, e77733 (2013).
5. J. Pinheiro, in *Forensic Anthropology and Medicine: Complementary Sciences From Recovery to Cause of Death*, A. Schmitt, E. Cunha, J. Pinheiro, Eds. (Humana Press, Totowa, NJ, 2006), pp. 85–116.
6. C. P. Campobasso, G. Di Vella, F. Introna, Factors affecting decomposition and Diptera colonization. *Forensic Sci. Int.* **120**, 18–27 (2001).
7. M. S. Megyesi, S. P. Nawrocki, N. H. Haskell, Using accumulated degree-days to estimate the postmortem interval from decomposed human remains. *J. Forensic Sci.* **50**, 618–626 (2005).
8. A. Galloway, The process of decomposition: a model from the Arizona-Sonoran desert. *Forensic taphonomy: The postmortem fate of human remains*, 139–150 (1997).

9. J. Hayman, M. Oxenham, *Human Body Decomposition* (Academic Press, 2016).
10. J. Dix, M. Graham, *Time of death, decomposition and identification: an atlas* (CRC press, 1999).
11. J. P. Wyatt, T. Squires, G. Norfolk, J. Payne-James, *Oxford Handbook of Forensic Medicine* (Oxford University Press, ed. 1).
12. J. Payne-James, A. Busuttil, W. Smock, *Forensic Medicine: Clinical and Pathological Aspects* (Cambridge University Press, 2003).
13. H. Gill-King, Chemical and ultrastructural aspects of decomposition. *Forensic taphonomy: the postmortem fate of human remains*, 93–108 (1997).
14. D. O. Carter, D. Yellowlees, M. Tibbett, Moisture can be the dominant environmental parameter governing cadaver decomposition in soil. *Forensic Sci. Int.* **200**, 60–66 (2010).
15. A. A. Vass, Others, Beyond the grave-understanding human decomposition. *Microbiol. Today.* **28**, 190–193 (2001).
16. V. Mesli, C. Neut, V. Hedouin, in *Forensic Microbiology*, D. O. Carter, J. K. Tomberlin, M. E. Benbow, J. L. Metcalf, Eds. (John Wiley & Sons, Ltd., Chichester, UK, 2017), pp. 192–211.
17. J. Amendt, C. S. Richards, C. P. Campobasso, R. Zehner, M. J. R. Hall, Forensic entomology: applications and limitations. *Forensic Sci. Med. Pathol.* **7**, 379–392 (2011).
18. W. C. Rodriguez, W. M. Bass, Insect activity and its relationship to decay rates of human cadavers in East Tennessee. *J. Forensic Sci.* **28**, 423–432 (1983).
19. R. D. Hall, Medicocriminal entomology. *Entomology and death: a procedural guide. Joyce's Print Shop, Clemson, SC*, 1–8 (1990).

20. E. P. Catts, N. H. Haskell, Entomology & death (1990) (available at <http://agris.fao.org/agris-search/search.do?recordID=US201300704329>).
21. J. H. Byrd, *Forensic Entomology: The Utility of Arthropods in Legal Investigations, Second Edition* (CRC Press, 2009).
22. D. O. Carter, D. Yellowlees, M. Tibbett, Cadaver decomposition in terrestrial ecosystems. *Naturwissenschaften*. **94**, 12–24 (2007).
23. M. H. Cantu, LSU Master's Theses | Graduate School | Louisiana State University, (available at https://digitalcommons.lsu.edu/gradschool_theses).
24. M. F. Galvão, J. R. Pujol-Luz, C. V. de Assis Pujol-Luz, C. T. A. de Rosa, L. R. L. Simone, S. N. Bão, K. B. Barros-Cordeiro, L. Pessoa, G. Bissacot, Shells and Bones: A Forensic Medicine Study of the Association of Terrestrial Snail *Allopeas micra* with Buried Human Remains in Brazil. *J. Forensic Sci.* **60**, 1369–1372 (2015).
25. G. R. Dabbs, M. Connor, J. A. Bytheway, Interobserver Reliability of the Total Body Score System for Quantifying Human Decomposition. *J. Forensic Sci.* **61**, 445–451 (2016).
26. G. R. Dabbs, J. A. Bytheway, M. Connor, Comparing the Scoring of Human Decomposition from Digital Images to Scoring Using On-site Observations. *J. Forensic Sci.* **62**, 1292–1296 (2017).
27. A. Ribéreau-Gayon, C. Rando, R. M. Morgan, D. O. Carter, The suitability of visual taphonomic methods for digital photographs: An experimental approach with pig carcasses in a tropical climate. *Science and Justice* (2017), doi:10.1016/j.scijus.2017.12.001.
28. C. Moffatt, T. Simmons, J. Lynch-Aird, An Improved Equation for TBS and ADD: Establishing a Reliable Postmortem Interval Framework for Casework and Experimental Studies. *J. Forensic Sci.* **61 Suppl 1**, S201–7 (2016).

29. J. K. Suckling, M. K. Spradley, K. Godde, A Longitudinal Study on Human Outdoor Decomposition in Central Texas. *J. Forensic Sci.* **61**, 19–25 (2016).
30. S. R. Bucheli, Z. Pan, C. L. Glennie, A. M. Lynne, D. P. Haarman, J. M. Hill, Terrestrial laser scanning to model sunlight irradiance on cadavers under conditions of natural decomposition. *Int. J. Legal Med.* **128**, 725–732 (2014).
31. X. Zhang, C. L. Glennie, S. R. Bucheli, N. K. Lindgren, A. M. Lynne, Terrestrial laser scanning and a degenerated cylinder model to determine gross morphological change of cadavers under conditions of natural decomposition. *Forensic Sci. Int.* **241**, 35–45 (2014).
32. L. M. Weidner, J. K. Tomberlin, G. C. Hamilton, Development of *Lucilia coeruleiviridis* (Diptera: Calliphoridae) in New Jersey, USA. *Fla. Entomol.* **97**, 849–851 (2014).
33. N. K. Lindgren, M. S. Sisson, A. D. Archambeault, B. C. Rahlwes, J. R. Willett, S. R. Bucheli, Four Forensic Entomology Case Studies: Records and Behavioral Observations on Seldom Reported Cadaver Fauna With Notes on Relevant Previous Occurrences and Ecology. *J. Med. Entomol.* **52**, 143–150 (2015).
34. N. K. Lindgren, S. R. Bucheli, A. D. Archambeault, J. A. Bytheway, Exclusion of forensically important flies due to burying behavior by the red imported fire ant (*Solenopsis invicta*) in southeast Texas. *Forensic Sci. Int.* **204**, e1–3 (2011).
35. J. R. Melvin Jr, L. S. Cronholm, L. R. Simson Jr, A. M. Isaacs, Bacterial transmigration as an indicator of time of death. *J. Forensic Sci.* **29**, 412–417 (1984).
36. M. S. Micozzi, Experimental study of postmortem change under field conditions: effects of freezing, thawing, and mechanical injury. *J. Forensic Sci.* **31**, 953–961 (1986).

37. E. R. Hyde, D. P. Haarmann, A. M. Lynne, S. R. Bucheli, J. F. Petrosino, The living dead: bacterial community structure of a cadaver at the onset and end of the bloat stage of decomposition. *PLoS One*. **8**, e77733 (2013).
38. D. Simmons, The Use of Animal Models in Studying Genetic Disease: Transgenesis and Induced Mutation. *Nature Education*. **1**, 70 (2008).
39. K. G. Schoenly, N. H. Haskell, D. K. Mills, C. Bieme-Ndi, K. Larsen, Y. Lee, RECREATING DEATH'S ACRE IN THE SCHOOL YARD: Using Pig Carcasses as Model Corpses To Teach Concepts of Forensic Entomology & Ecological Succession. *Am. Biol. Teach.* **68**, 402–410 (2006).
40. F. E. Damann, D. E. Williams, A. C. Layton, Potential Use of Bacterial Community Succession in Decaying Human Bone for Estimating Postmortem Interval. *J. Forensic Sci.* **60**, 844–850 (2015).
41. K. A. Hauther, K. L. Cobaugh, L. M. Jantz, T. E. Sparer, J. M. DeBruyn, Estimating Time Since Death from Postmortem Human Gut Microbial Communities. *J. Forensic Sci.* **60**, 1234–1240 (2015).
42. J. M. DeBruyn, K. A. Hauther, Postmortem succession of gut microbial communities in deceased human subjects. *PeerJ*. **5**, e3437 (2017).
43. J. L. Metcalf, Z. Z. Xu, S. Weiss, S. Lax, W. Van Treuren, E. R. Hyde, S. J. Song, A. Amir, P. Larsen, N. Sangwan, D. Haarmann, G. C. Humphrey, G. Ackermann, L. R. Thompson, C. Lauber, A. Bibat, C. Nicholas, M. J. Gebert, J. F. Petrosino, S. C. Reed, J. A. Gilbert, A. M. Lynne, S. R. Bucheli, D. O. Carter, R. Knight, Microbial community assembly and metabolic function during mammalian corpse decomposition. *Science*. **351**, 158–162 (2016).

44. J. L. Pechal, C. J. Schmidt, H. R. Jordan, M. E. Benbow, A large-scale survey of the postmortem human microbiome, and its potential to provide insight into the living health condition. *Sci. Rep.* **8**, 5724 (2018).
45. E. R. Hyde, D. P. Haarmann, J. F. Petrosino, A. M. Lynne, S. R. Bucheli, Initial insights into bacterial succession during human decomposition. *Int. J. Legal Med.* **129**, 661–671 (2015).
46. G. T. Javan, S. J. Finley, I. Can, J. E. Wilkinson, J. D. Hanson, A. M. Tarone, Human Thanatomiobiome Succession and Time Since Death. *Sci. Rep.* **6**, 29598 (2016).
47. R. A. Parkinson, K.-R. Dias, J. Horswell, P. Greenwood, N. Banning, M. Tibbett, A. A. Vass, in *Criminal and Environmental Soil Forensics*, K. Ritz, L. Dawson, D. Miller, Eds. (Springer Netherlands, Dordrecht, 2009), pp. 379–394.
48. H. R. Johnson, D. D. Trinidad, S. Guzman, Z. Khan, J. V. Parziale, J. M. DeBruyn, N. H. Lents, A Machine Learning Approach for Using the Postmortem Skin Microbiome to Estimate the Postmortem Interval. *PLoS One.* **11**, e0167370 (2016).
49. S. J. Finley, J. L. Pechal, M. E. Benbow, B. K. Robertson, G. T. Javan, Microbial Signatures of Cadaver Gravesoil During Decomposition. *Microb. Ecol.* **71**, 524–529 (2016).
50. J. L. Pechal, T. L. Crippen, M. E. Benbow, A. M. Tarone, S. Dowd, J. K. Tomberlin, The potential use of bacterial community succession in forensics as described by high throughput metagenomic sequencing. *Int. J. Legal Med.* **128**, 193–205 (2014).
51. A. Belk, Z. Z. Xu, D. O. Carter, A. Lynne, S. Bucheli, R. Knight, J. L. Metcalf, Microbiome Data Accurately Predicts the Postmortem Interval Using Random Forest Regression Models. *Genes* . **9** (2018), doi:10.3390/genes9020104.

52. G. T. Javan, S. J. Finley, Z. Abidin, J. G. Mülle, The Thanatomicrobiome: A Missing Piece of the Microbial Puzzle of Death. *Front. Microbiol.* **7**, 225 (2016).
53. J. Gans, M. Wolinsky, J. Dunbar, Computational improvements reveal great bacterial diversity and high metal toxicity in soil. *Science.* **309**, 1387–1390 (2005).
54. C. L. Lauber, M. Hamady, R. Knight, N. Fierer, Pyrosequencing-Based Assessment of Soil pH as a Predictor of Soil Bacterial Community Structure at the Continental Scale. *Appl. Environ. Microbiol.* **75**, 5111–5120 (2009).
55. D. O. Carter, J. L. Metcalf, A. Bibat, R. Knight, Seasonal variation of postmortem microbial communities. *Forensic Sci. Med. Pathol.* **11**, 202–207 (2015).
56. A. Spicka, R. Johnson, J. Bushing, L. G. Higley, D. O. Carter, Carcass mass can influence rate of decomposition and release of ninhydrin-reactive nitrogen into gravesoil. *Forensic Sci. Int.* **209**, 80–85 (2011).
57. T. Simmons, R. E. Adlam, C. Moffatt, Debugging decomposition data--comparative taphonomic studies and the influence of insects and carcass size on decomposition rate. *J. Forensic Sci.* **55**, 8–13 (2010).
58. A. Sutherland, J. Myburgh, M. Steyn, P. J. Becker, The effect of body size on the rate of decomposition in a temperate region of South Africa. *Forensic Sci. Int.* **231**, 257–262 (2013).
59. S. Matuszewski, S. Konwerski, K. Frątczak, M. Szafałowicz, Effect of body mass and clothing on decomposition of pig carcasses. *Int. J. Legal Med.* **128**, 1039–1048 (2014).
60. S. Weiss, D. O. Carter, J. L. Metcalf, R. Knight, Carcass mass has little influence on the structure of gravesoil microbial communities. *Int. J. Legal Med.* **130**, 253–263 (2016).

61. J. Guo, X. Fu, H. Liao, Z. Hu, L. Long, W. Yan, Y. Ding, L. Zha, Y. Guo, J. Yan, Y. Chang, J. Cai, Potential use of bacterial community succession for estimating post-mortem interval as revealed by high-throughput sequencing. *Sci. Rep.* **6**, 24197 (2016).
62. J. Metcalf, Estimating the postmortem interval using microbes: knowledge gaps and hurdles. *Forensic Sci. Int. Genet.*
63. R. W. Byard, Timing: the Achilles heel of forensic pathology. *Forensic Sci. Med. Pathol.* **13**, 113–114 (2017).
64. C. L. Lauber, J. L. Metcalf, K. Keepers, G. Ackermann, D. O. Carter, R. Knight, Vertebrate decomposition is accelerated by soil microbes. *Appl. Environ. Microbiol.* **80**, 4920–4929 (2014).
65. M. E. Benbow, J. L. Pechal, J. M. Lang, R. Erb, J. R. Wallace, The potential of high-throughput metagenomic sequencing of aquatic bacterial communities to estimate the postmortem submersion interval. *J. Forensic Sci.* **60**, 1500–1510 (2015).
66. J. Metcalf, Perspective on Forensic Microbiology (2014).
67. J. Metcalf, Current Microbiology & Forensic Microbiology (2014).
68. J. Tomberlin, D. Carter, R. Knight, Forensic Microbiology: Where Do We Begin? Workshop at the 66th annual American Academy of Forensic Sciences (2014).
69. J. DeBruyn, The Necrobiome - Microbial Life After Death (2016), (available at <https://www.asm.org/index.php/public-outreach/microbes-after-hours>).
70. V. Daubert, Others, Merrell dow pharmaceuticals. *United States.* **509** (1993).
71. T. F. Kiely, *Forensic Evidence: Science and the Criminal Law, 2nd edition* (CRC Press, Boca Raton, FL, 2005).

CHAPTER 2: A PILOT STUDY OF MICROBIAL SUCCESSION IN HUMAN RIB SKELETAL REMAINS DURING TERRESTRIAL DECOMPOSITION²

Summary

The bones of decomposing vertebrates are colonized by a succession of diverse microbial communities. If this succession is similar across individuals, microbes may provide clues about the postmortem interval (PMI) during forensic investigations in which human skeletal remains are discovered. Here, we characterize the human bone microbial decomposer community to determine whether microbial succession is a marker for PMI. Six human donor subjects were placed outdoors to decompose on the soil surface at the Southeast Texas Applied Forensic Science facility. To also assess the effect of seasons, three decedents were placed each in the spring and summer. Once ribs were exposed through natural decomposition, a rib was collected from each body for eight time points at three weeks apart. We discovered a core bone decomposer microbiome dominated by taxa in the phylum Proteobacteria, and evidence that these bone-invading microbes are likely sourced from the surrounding decomposition environment, including skin of the cadaver and soils. Additionally, we found statistically significant overall differences in bone microbial community composition between seasons. Finally, we used the microbial community data to develop random forest models that predict PMI with an accuracy of approximately ± 34 days over a 1–9-month time frame of decomposition. Typically, anthropologists provide PMI estimates based on qualitative information, giving PMI errors ranging from several months to years. Previous work has focused on only the characterization of the bone microbiome decomposer community, and this is the first known data-driven, quantitative PMI estimate of terrestrially decomposed human skeletal remains using microbial abundance information.

² This work has been previously published: Deel, H., Emmons, A. L., Kiely, J., Damann, F. E., Carter, D. O., Lynne, A., Knight, R., Xu, Z. Z., Bucheli, S., & Metcalf, J. L. (2021). A Pilot Study of Microbial Succession in Human Rib Skeletal Remains during Terrestrial Decomposition. *mSphere*, e0045521.

Introduction

Terrestrial microbial decomposition of vertebrate remains includes a succession of communities of microbes from across the tree of life. Recent research has revealed that this succession can be repeatable and predictable enough that the composition of microbes can be used for estimating time since death, or postmortem interval (PMI) (1–6), which could be a useful tool for medicolegal investigations. Most microbial decomposition research has focused on timeframes immediately following death using sample types such as the skin or other organs of the decedent and/or the associated soil. However, at later time frames of decomposition, often the only sample types available from the decedent are bones and teeth. Research in this area has revealed a potential use of microbial succession in bone for predicting PMI (7, 8), but more information is needed about the accuracy of PMI estimates for determining whether this could be a useful tool in medicolegal investigations. Furthermore, a more in-depth study of the bone decomposer bacterial and microbial eukaryotic community would be useful for fields of forensic anthropology, archeology, paleontology, and ancient DNA because the role of the microbiome within these fields has been understudied.

Although decomposition is a continuous process, a decomposing body goes through visible changes that can be categorized into stages based on taphonomic landmarks (e.g., bloating), but are also related to changes in microbial processes. In the fresh stage, there are few visible changes to the decedent, with a cascade of biochemical events occurring at the cellular level (9). These events lead to discoloration, bloating, and the purging of fluids in the active decay stage, in which microbial processes are at their peak activity and decomposition is rapid. When the availability of nutrients for microbes decreases and the rate of decomposition declines, the decedent enters the advanced decay stage in which most of the flesh is gone and there is some bone exposure. When at least 50% of the soft tissues are gone from the remains, the skeletonization stage is reached (10).

To characterize the human bone decomposer microbial community during skeletonization, we placed six human donor subjects to decompose at the Southeast Texas Applied Forensic Science Facility (three in the spring and three in the summer) in Huntsville, TX. Our goals were to understand the source

of the microbial community, how it may differ across seasons, and determine whether microbial succession of decomposing bone could be used to estimate PMI. By placing decedents in two seasons, we sought to capture microbial succession within different environmental conditions, which could possibly affect the accuracy of PMI estimation models (11). Once naturally exposed (at least partially, see methods), an entire rib was collected from each decedent at eight time points for approximately every three weeks of decomposition, and 16S rRNA and 18S rRNA amplicon sequencing from DNA extracted from a sectioned, pulverized piece of the rib was used to characterize succession of the bacterial and microbial eukaryotic communities. Bayesian source tracking was used to predict the source of the bone bacterial decomposer community, and a random forest regression was used for predicting PMI.

Results and Discussion

Progression of Decomposition and Rib Sampling

In this study, we use Megyesi's system of total body scoring (10) based on the decomposition stages outlined by (12) to delineate between stages of decomposition. Photographs of the first 21 days of decomposition were used to calculate TBS and define fresh, active decay, and advanced decay stages. Each of the decedents reached the advanced decay stage within 8-11 days after placement. Since photographs were not available after the first 21 days, we use the first known occurrence of rib exposure as the beginning of skeletonization. Rib exposure, and sample initiation, began within approximately 4 weeks for the spring placement subjects and within a range of approximately 4-6 weeks for the summer placement subjects (see **Table S2.1**). Sample initiation occurred within a range of 592-1151 Accumulated Degree Day (ADD), which is a temperature-based temporal scale (see methods). Total sample collection ranged within the time frame of around 1-9 months of decomposition. Generally, we defined each stage of decomposition as; fresh (0-6 TBS, \sim <50 ADD), active decay (6-17 TBS, \sim 50-200 ADD), advanced decay (17-35 TBS, \sim 200-600 ADD), and skeletonization ($>$ 35 TBS, \sim >600 ADD). Decomposition stages often overlap, and are not always clearly defined, and this experiment was no exception. However, using the

TBS system and visual clues of skeletonization allowed us to place our sampling time frame of decomposition primarily within early skeletonization.

Quality of Amplicon Sequence Data

In the 16S rRNA dataset, a total of 1,270,545 reads were generated. After filtering out ASVs (amplicon sequence variants) with taxonomy assignments to mitochondria or chloroplast, there were 1,270,507 reads total with an average of 21,175 reads per sample, with sample sequence reads ranging from 712 to 39,169. We rarified 16S rRNA data at 17,098 reads as an optimal balance for retaining both reads and samples, as this number was the count of the lowest-count sample necessary to include all but three samples. For the 18S rRNA dataset, a total of 20,838,649 reads were generated. After filtering (see Materials and Methods), there were 18,178,587 reads total with an average of 288,549 reads per sample, with sample sequence reads ranging from 2,610 to 802,658. We rarified the 18S rRNA data at 214,940 sequences per sample, again, to optimize retaining both reads and samples in the data set, resulting in a loss of 10 samples. The taxonomic composition of negative controls can be seen in **Figure S2.1**.

What Microbes Invade the Bone, and Where are they Coming From?

We suspected that the diversity of microbes invading bone would increase as decomposition progressed, as more microbes from the environment (e.g., including the decedent, the surrounding soil) could likely access the internal bone as its structural integrity eroded. Our hypothesis was supported; the linear mixed effects model (which incorporates repeated measures) showed that there was a significant difference across time (ADD) for both bacteria and microbial eukaryotes ($p = 0.01$, $p = 0.002$) (**Figure 2.1A**; **Figure 2.1B**). Though, the positive trend in Faith's PD in the 18S rRNA data set appeared to be largely driven by a single individual (064), which is shown in red in **Figure 2.1B**. We discovered two potential alpha diversity data point outliers via volatility plots and Q-Q normality plots, which were removed prior to linear mixed effects modeling of the 16S rRNA data (065.R11 and 011.L08). Additionally, a single potential outlier was removed from the 18S rRNA data (064.R12). Kruskal-Wallis effect size calculations between seasons, hosts, and the 1st and last ADDs showed that ADD had the

highest effect on alpha diversity in all cases but one for both 16S rRNA and 18S rRNA datasets (**Table S2.3**).

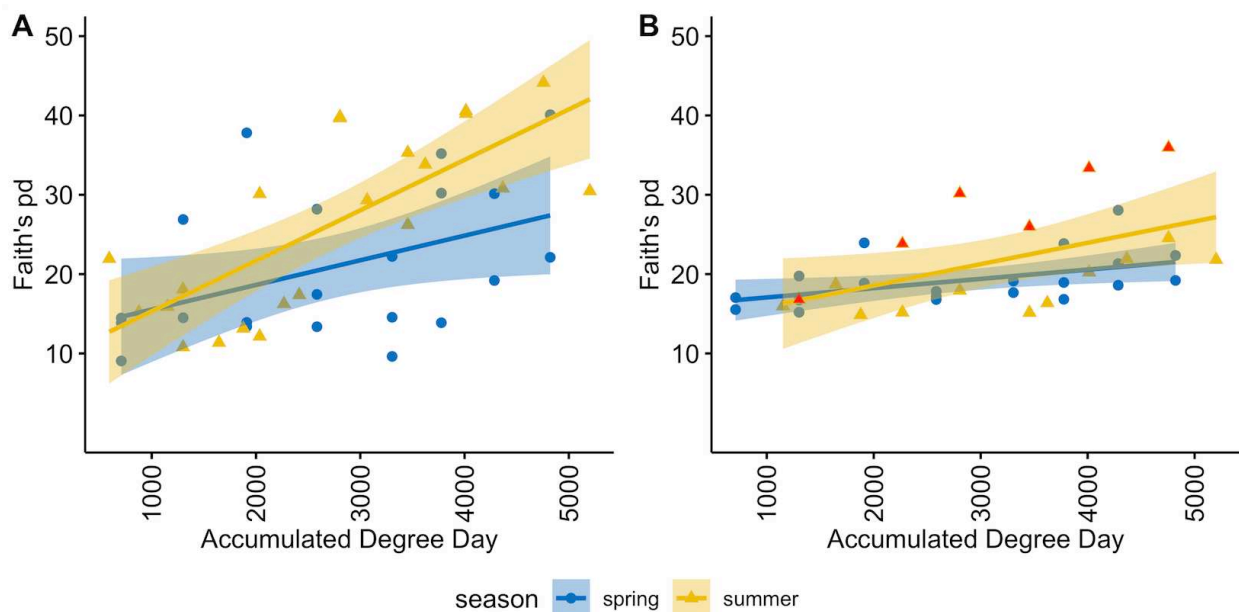


Figure 2.1. A measure of alpha diversity using Faith’s Phylogenetic Diversity Index with increasing ADD for 16S rRNA (A) and 18S rRNA (B) datasets. Red values are for visualization purposes and represent a single individual (064). Shaded areas around the line represent 95% confidence intervals. Linear mixed effects $p = 0.01$ and $p = 0.002$ over ADD for 16S rRNA and 18S rRNA datasets, respectively.

Exploring the taxonomic composition of the bone microbial decomposer communities revealed many similar taxa that were widely represented across rib bone samples, regardless of ADD or season (**Figure 2.2**). Core-features analysis showed that the core bacterial phyla included Proteobacteria, Firmicutes, Actinobacteria, and Bacteroidetes. In the core microbiome, each phylum was represented by several features, with most of those features (22 out of 42 total core bacteria) being within phylum Proteobacteria. The top five most prevalent core features (at the lowest identifiable level) included *Corynebacterium*, Pseudomonadaceae, *Trabulsiella farmeri*, *Sphingobacterium mizutaii*, and *Stenotrophomonas*. Outside of our defined core bacterial community, there were dozens to hundreds of different bacterial species, most of which had very low relative abundances. There were 86 total core microbial eukaryotic features. The top five most prevalent represented phyla (or subdivisions) included

Ascomycota, Nematoda, Basidiomycota, Apicomplexa, and Ochrophyta. The top five most prevalent core features at the lowest identifiable level included two orders of Rhabditida, Debaryomycetaceae, Apiotrichum, and *Candida bombi*.

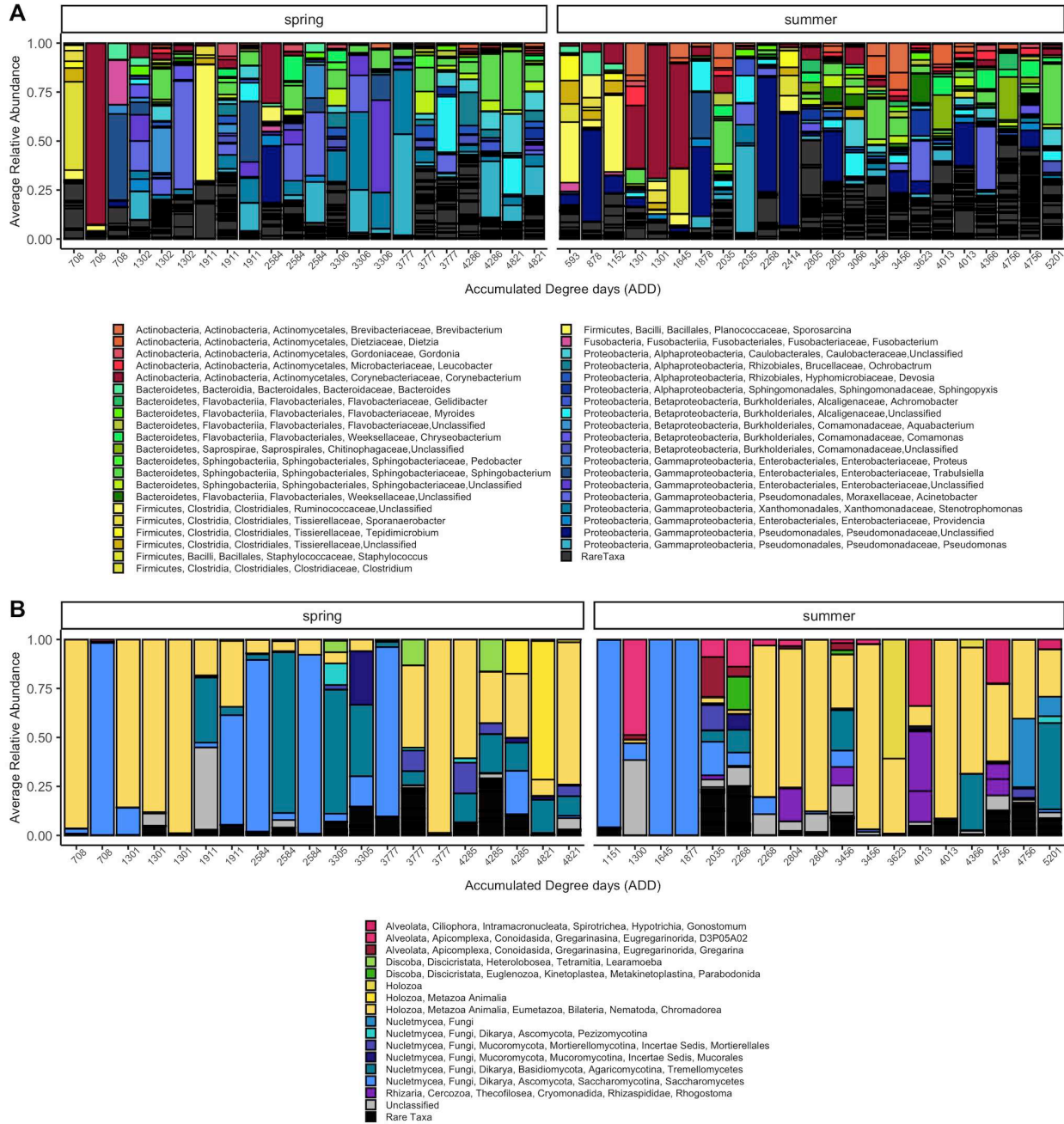


Figure 2.2. Relative abundance taxa plots of the bacterial communities (A) and microbial eukaryotic communities (B). Rare taxa include those with a mean relative abundance of 0.005 or lower within the

entire dataset. Unclassified features generally include those that were only able to be classified as Eukaryota, with approximately 14% of all unclassified features identified as Opisthokonts.

Many of these core bacterial and microbial eukaryotic taxa have been discovered in other decomposer bone (7, 13), skin (1, 4, 14), and vertebrate decomposition-associated soil (1, 4, 15–17) microbial communities, or have been found to decompose plant material and rotting wood (18, 19). There are likely many different processes occurring in this community, including the degradation and recycling of carcass derived nutrients (20) and symbiotic relationships between core organisms. For example, some members of the community could be degrading bone (21, 22), including *Pseudomonas* (23) and *Clostridium* organisms by releasing collagenases to break down bone collagen. Nematodes within the order Rhabditida are likely displaying their saprophagous characteristics, and feeding off bacterial biomass and the decaying organic matter provided by the decedent (24, 25). Ochrophyta is an algae that has shown evidence of a symbiotic relationship with wood- and leaf-litter decomposing fungi like Basidiomycota through acquiring carbon dioxide and protection from the sun, while providing the fungi a source of carbon and nitrogen (19). Additionally, some non-selected microbial processes known to occur in other environments such as the soil may also be occurring in the bone and contributing to the surrounding ecosystem. For example, decomposing bone taxa in the family Pseudomonadaceae likely contains phosphate solubilizing bacteria that are converting unavailable phosphorus into more accessible forms to be used by the surrounding soil and vegetation (26). Although this is not a comprehensive list of possible functional roles for these microbes within the bone decomposer community, it begins to represent the vast array of processes occurring that requires further investigation.

To better understand the source of rib decomposer microbes, we compared the rib microbial decomposer communities (~1-9 months after placement) to samples collected in earlier stages of decomposition for the same cadavers, including fresh (days 1 and 2 after placement) and advanced decay (days 19 - 21 after placement) skin and soil communities, as well as control soils that were not associated with a cadaver. The alpha diversity of decomposed rib bone bacterial communities was similar to those recovered from fresh skin and active decay skin and soil, which were all significantly lower than soils not

associated with decomposing cadavers (**Figure S2.2A and S2.2B**). The most prevalent taxa at the class level within the rib decomposer communities of both seasons were Gammaproteobacteria and Actinobacteria, with the most prevalent taxa comprising these classes being an unclassified Pseudomonadaceae, *Pseudomonas*, *Acinetobacter*, and two different *Corynebacterium* species. Of these common taxa, all were observed within the fresh and advanced decay cadaver skin and soil potential source communities (**Figure S2.3**), with *Corynebacterium* species being found primarily in the summer placement communities. However, the composition of bone communities appeared distinct from the skin and soil source communities, particularly if abundance was considered (**Figure 2.3A and Figure 2.3B**, **Figure S2.2C and S2.2D**).

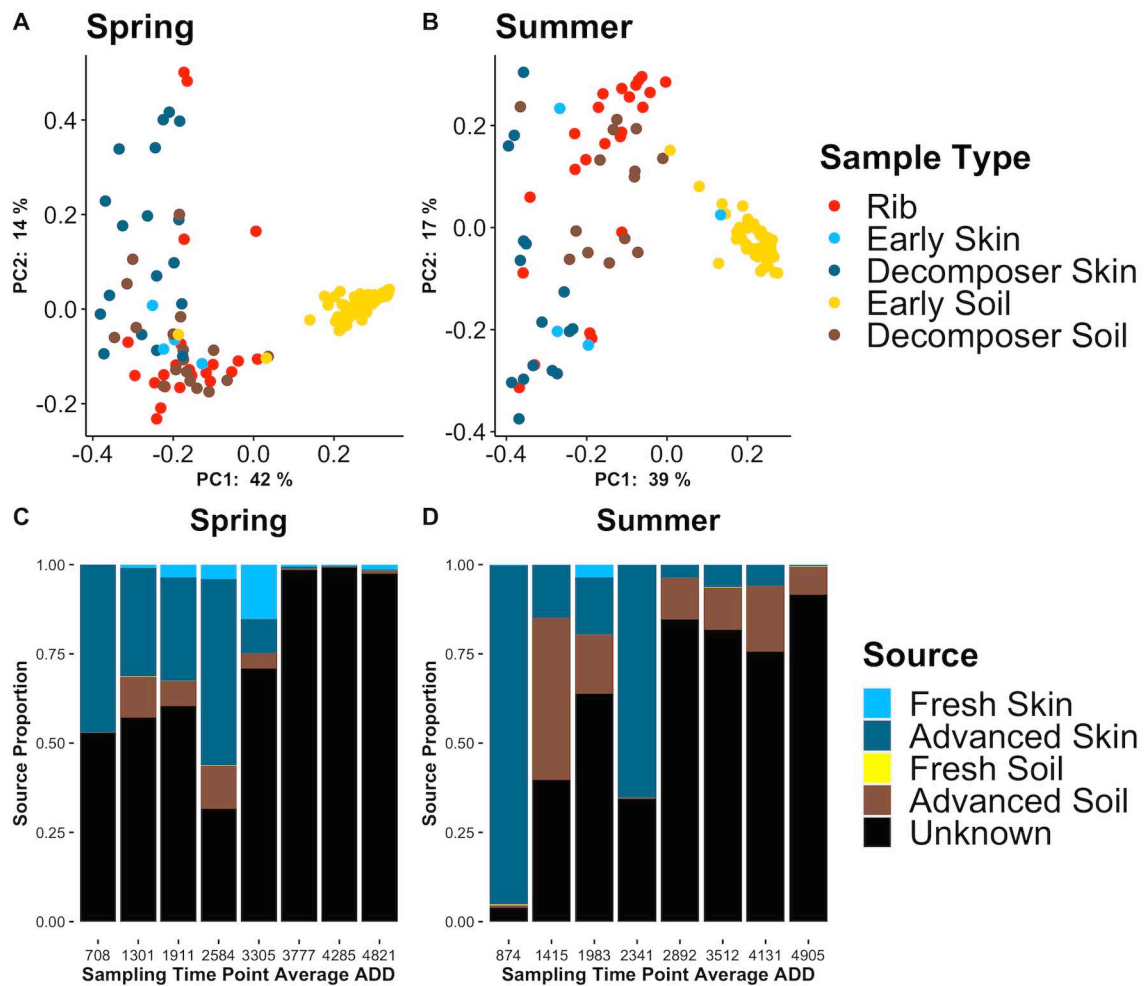


Figure 2.3. Principal Coordinates Analysis of 16S rRNA rib and source communities using the weighted UniFrac distance metric in the spring (A) and summer (B) placements. Spring pairwise PERMANOVA q

= 0.041 for Rib and Fresh Skin comparison, and $q = 0.001$ for all other spring comparisons. Summer pairwise PERMANOVA $q = 0.002$ for Rib and Fresh Skin comparison, and $q = 0.001$ for all other summer comparisons. There were 999 permutations for all comparisons. Succession of predicted portions of the fresh skin and soil (days 1 and 2) and advanced decay (days 19, 20, 21) communities of the 16S rRNA spring (C) and summer (D) placements. Samples are grouped into collection time points 1-8.

Despite the unique composition of rib bone decomposer communities, Bayesian source tracking did predict a proportion of sources from the skin and soil advanced decay decomposer communities, and a small proportion of the source from the fresh skin communities (**Figure 2.3C** and **Figure 2.3D**). These results suggest that rib bone decomposer communities are distinct from skin and soil communities (fresh or decomposition-associated), but likely originate, at least to some extent, from the surrounding environment of decomposing skin as well as soil bacteria. The rib bone environment likely selects a subset of microbes from cadaver skin and soil communities that are able to invade the bone and extract nutrients (27). More investigation is needed to determine whether additional microbial source(s) (e.g., nearby vegetation, rainfall, scavengers, insects) of the bone decomposer community exist.

Is there a Difference in the Microbial Community Assembly in Ribs from Cadavers Placed During Different Seasons?

Although we discovered similar microbial taxa across all decomposed rib bones, regardless of seasonal placement (**Figure 2.2**), there were significant differences in overall composition of bacterial and microbial eukaryotic communities in rib bones by season of placement (**Figure 2.4A**, **Figure S2.4**).

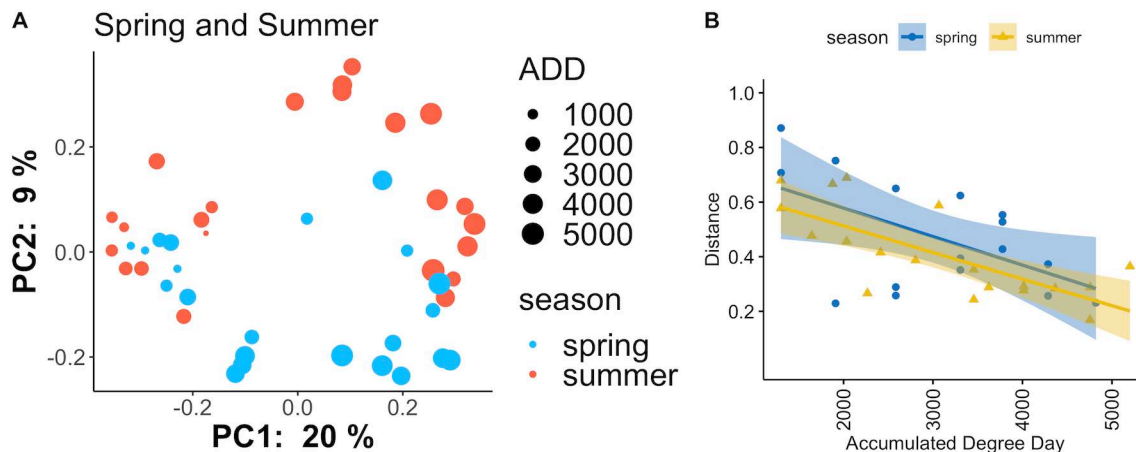


Figure 2.4. (A) A measure of beta diversity of 16S rRNA data using the unweighted UniFrac distance metric in both seasonal placements (PERMANOVA between seasons $p = 0.004$, pseudo-F (effect size) = 2.32, $df = 1$, with 999 permutations). (B) A measure of beta diversity of 16S rRNA data using the weighted UniFrac distance metric. Shaded areas around the line represent 95% confidence intervals. Linear mixed effects across ADD $p = 0.012$.

We discovered differential abundance/presence of an unclassified Pseudomonadaceae at the genus level, *Ochrobactrum intermedium* at the species level, and an unclassified *Stenotrophomonas* at the ASV level, which were also confirmed as drivers of beta diversity patterns using robust Aitchison PCA (28) via Emperor biplots (**Figure S2.5**). In the microbial eukaryotic communities, differences between rib bone microbial communities for bodies placed during different seasons included *Learamoeba* and an unclassified Eumetazoa at level seven, and an unclassified Colpodea at level eight. These differences in assembly between seasons may be explained by multiple factors. Given that the soil decomposer community is a source of microbes within decomposed bone (**Figure 2.3C** and **Figure 2.3D**), we hypothesize that differences in soil composition between seasons may be a factor contributing to variation in microbial assembly within decomposed bone. We see evidence of this in our data when observing the beta diversity and taxonomic composition of soil control (not associated with decomposition) microbial communities collected within the first 21 days of decomposition (**Figure S2.6**). This is unsurprising, as there is a wealth of evidence indicating that seasonality impacts microbial community composition (29–32). Variations in insect activity between seasons may also be affecting microbial assembly, as it is known that insects are less active in cooler seasons (9). Although ADDs were not very different between placements (Table S1), differences in temperature fluctuations over time between seasons may affect the relationship between insects and bacteria, fungi, protozoa, and nematodes (9), resulting in varied microbial community composition. Other differences in assembly between the spring and summer placements could be explained by variation in water content. While the amount of precipitation does not drastically differ between seasonal placements, the summer placement shows a higher accumulation of humidity (**Figure S2.7**). This may contribute to an increase in water content and subsequently the microbial composition (30) of the summer placement soil that is acting as a source of the bone microbes.

General differences in environmental stability may also be contributing to these differences. For example, there is greater diurnal temperature variation in spring and fall than in winter and summer, which would likely place constraints on bone microbial community assembly throughout our sampling time frame.

Can we use Microbial Invasion in Bone to Estimate PMI?

Bacterial community composition became increasingly different from the initial rib bone community as decomposition progressed (**Figure 2.4A**), with rate of change of community composition decreasing over ADD (**Figure 2.4B**), indicating a repeatable succession of invading microbes. Furthermore, effect size calculations showed that ADD had the highest effect on beta diversity in nearly every case (particularly for the 16S rRNA data, Table S3). Therefore, these data may be useful for predicting PMI of remains in an advanced stage of decomposition, in which the ribs have at least skeletonized. Microbial eukaryotic community composition also changed during decomposition, but with a less distinguishable pattern compared to 16S rRNA data (**Figure S2.4**). Because we detected microbial community differences for cadavers placed in different seasons (**Figure 2.4A**), we tested whether season-specific PMI models performed better (i.e., produced a lower mean absolute error).

Random forest models using only the 16S rRNA ASV-level data from summer placement cadavers provided the most accurate models (i.e., lowest range of mean absolute errors (MAEs)). The most accurate model had MAEs ranging from 724 - 853 ADD over a total of 5201 ADD for the summer data, which roughly equates to an error of +/- 39 days. Models including both the spring and summer placement data (i.e., the “combined” models) gave a higher range of MAEs, while models with just the spring placement data provided the highest range of MAEs within the 16S rRNA dataset (**Table 2.1**). In the 18S rRNA dataset, this pattern was the same. The lower Mean Absolute Error (MAE, i.e., increased accuracy) of the summer placement over the spring placement in both 16S rRNA and 18S rRNA datasets may be explained by the wider sample collection time frame (**Table S2.1**). Perhaps the increased information gained from an extra 2-3 months of sampling for bodies placed in the summer allowed for the model to account for more variability. Despite relatively similar ADDs within each season, it is possible

that once skeletonization occurs, a longer time-frame of collection is more important than combined temperature and time (i.e., ADD). Another factor explaining this difference could be the placement of all spring subjects on the same day, whereas the placement of summer subjects ranged over approximately two weeks (**Table S2.1**). This unintended occurrence was due to the limited availability of decedents in the summer placement. This may have allowed the summer models to capture more variability than the spring models, giving more accurate predictions.

Table 2.1. Random Forest regression modeling of amplicon data using features collapsed at different taxonomic levels. Model accuracy is assessed using mean absolute error (MAE). The range of MAEs resulting from modeling at all taxonomic levels is reported. The top five most important features within each model are arranged from the most to least important, as determined by the random forest regression. Note that some important features were not able to be classified all the way down to the same taxonomic level at which the model was performed (e.g., Metazoa). Underlined features include those commonly important between model types. Note that there are no commonly important features in the 18S rRNA models due differences in the most accurate levels, whereas in the 16S rRNA models all of the most accurate models were at the ASV level. MAEs for all levels are reported in Table S2.

Amplicon	Season(s)	Most accurate level	Range of MAEs	Top five important feature	Range of importances
16S rRNA	Spring and summer (“combined”)	ASV	793.33 – 851.41	<u>Phyllobacteriaceae</u> , <i>Defluviobacter</i> , <i>Corynebacterium</i> , <i>Shinella</i> , <u><i>Devosia</i></u>	0.040 to 0.023
16S rRNA	Spring	ASV	872.02 - 1074.76	<i>Gallicola</i> , <i>Cellulosimicrobium</i> , <i>Brachybacterium</i> , <i>Comamonas</i> , <i>Leucobacter</i>	0.075 to 0.042
16S rRNA	Summer	ASV	723.98 – 853.38	<u>Phyllobacteriaceae</u> , <i>Sphingopyxis</i> , <i>Alcaligenaceae</i> , <u><i>Devosia</i></u> , <i>Pseudaminobacter</i>	0.014 to 0.010
18S rRNA	Spring and summer (“combined”)	8	941.22 – 1128.13	Eurotiomycetes, Sordariomycetes, Metazoa, Saccharomycetes, Tremellomycetes	0.067 to 0.033
18S rRNA	Spring	5	1025.53 – 1443.86	Mucoromycota, Metazoa, Vannellida, Eumetazoa, Dikarya	0.102 to 0.047
18S rRNA	Summer	7	820.67 – 1083.95	Nematoda, Saccharomycotina, BOLA868, Alveolata, Eumetazoa	0.071 to 0.037

Modeling results indicate that the 16S rRNA data are more accurate in estimating PMI than the 18S rRNA data (**Table 2.1**). Nearly all ranges of MAEs obtained using 18S rRNA data were higher than those obtained using 16S rRNA data when comparing the same combination of seasons (e.g., the range of combined 18S rRNA MAEs was higher than the range of combined 16S rRNA MAEs). Modeling results for both datasets at each taxonomic level are provided in **Tables S2.2** and **S2.3**. At the ASV level, there

are over three times as many features in the 16S rRNA data than the 18S rRNA data (5,708 versus 1,696, respectively). The 16S rRNA model may have been able to effectively use an increased number of features to produce a lower MAE. This may also be explained by a less defined trend of dissimilarity with increasing ADD in the 18S rRNA data (**Figure S2.4**), indicating that the microbial eukaryotic community within decomposing bone is highly variable and less able to predict PMI. Further evidence of this is observed in the most accurate levels for 16S rRNA and 18S rRNA modeling (**Table 2.1**). Since the ASV level is the most accurate for all 16S rRNA models, this indicates that microbial succession within these data is defined well enough that the model is able to find patterns within these particular ASVs to predict PMI with some accuracy. This is also supported by effect size calculations in which host appears to have the highest effect on beta diversity in four cases (**Table S2.3**).

Across models using 16S rRNA ASV data, there were two commonalities in the top five important features, *Phyllobacteriaceae* and *Devosia* (shown underlined in **Table 2.1**). These taxa are both within the order Hyphomicrobiales (also known as Rhizobiales) and were shown to increase in prevalence at higher ADDs, which likely contributes to their high importance in these models. For example, for summer-placed cadavers between ADDs 592 - 2414, *Phyllobacteriaceae* is only present in 3/11 samples with a total of 45 reads while *Devosia* is prevalent in only 2/11 samples with a total of 100 reads. As decomposition progresses between ADDs 2804 - 5201, *Phyllobacteriaceae* and *Devosia* are present in all 12 samples with a total of 3303 and 2677 reads, respectively. This apparent trend across time suggests that these taxa may provide some useful information about the ecology of decomposed bone over time. For example, *Phyllobacteriaceae* consists of environmental (soil, water) and plant-associated bacteria that use oxygen as the terminal electron acceptor in respiratory metabolism (33). Perhaps increased porosity in the bone over decomposition contributes to higher levels of oxygen, allowing for this family to increase in prevalence. *Devosia*, a genus known for dominance in soil habitats, is known for encoding a large diversity of transporters that allow them to uptake short peptides for satisfying nutritional needs (34). This may facilitate their use of the variety of nutrients that are provided in the dynamic decomposition environment more efficiently than other bacteria, allowing for them to predictably thrive with increased

decomposition. The ability to fix nitrogen may also play a role in the importance of these organisms. *Devosia* is a nitrogen-fixing bacterium (35) and Phyllobacteriaceae is closely related to organisms known for nitrogen fixation (36). Perhaps they are using collagen of the bone as a source of nitrogen (37), and increasing in prevalence as more collagen becomes exposed with higher levels of porosity.

In the 18S rRNA models, several important features were representative at a range of taxonomic levels that consist of broadly defined taxa, including fungi, metazoans such as nematodes, and amoebae, which can flourish in a wide variety of habitats (**Table 2.1**). Just in the combined model, features include yeasts and fungi that have been isolated from environments including humans (38), soil and freshwater (39), plant material (18), or a combination including several of these listed environments (40). Although this wide range of important features in the 18S rRNA models provides less defined information about the ecology of decomposed bone over time, it nevertheless provides a picture of the suite of microbial eukaryotes that inhabit decomposed bone.

Conclusions and Limitations

This research demonstrates the potential use of postmortem bone microbial communities to predict time since death in human remains with PMIs of nine months or less. In the 16S rRNA spring and summer placement model, the lowest MAE of 793.33 roughly approximates to an error of +/- 34 days. Although much additional research is needed, this model has the potential to generate probative PMI estimates and it certainly represents progress toward improving medicolegal death investigations. To put this into the context of investigations involving skeletal remains that have been decomposing within a similar time frame of this study (~1-9 months), without other evidence, anthropologists are typically able to give PMI estimations with errors of several months or even years (41). Anthropologists typically provide PMI estimates in relative time based on qualitative information gathered from the death scene and the body itself. Otherwise, very few methods exist for estimating PMI within this time frame.

While these data represent an initial attempt to characterize the succession of postmortem bone microbial communities using a controlled research design at a decomposition research facility, there

remain limitations worth addressing. First, the sample size (48 rib bones from six human individuals) is small. Large numbers of willfully donated human decedents are difficult to obtain for the purposes of decomposition research despite the existence of decomposition research facilities, and not all decedents are available for destructive sampling, which is required for skeletal DNA analysis. This lack of biological replicates often pushes researchers toward the use of animal proxies, which do not often decompose in a similar manner to human remains (42). We opted to use human decedents to make this research more applicable to forensic contexts involving human remains. Although we did not see host having a larger effect than ADD or season in nearly every case (**Table S2.3**), we recognize that an increase in decedent sample size would mitigate any non-detectable host-host variations. The limited availability of human decedents also meant that some were frozen before placement. While there is some evidence that freeze-thawing affects the decay of soft tissues in rats (43), there is no known evidence that this affects the long-term microbial decomposition of human bone. Future studies should focus on a more consistent protocol (i.e., no individuals should ever be frozen). Second, there were some minor differences between the spring and summer seasons that contributed to our limitations. There was discordance in the placement protocol between spring and summer seasons such that in the spring, all decedents were placed on the same day, while in the summer, decedents were placed on different days. This may have resulted in a reduction in power for the spring season models by effectively making each placed decedent a pseudoreplicate. Furthermore, the spring placement cohort was uncaged whereas the summer cohort was caged to protect from scavengers. Lastly, the research design implemented here makes the assumption that all ribs have similar microbial communities at each time point. Two ribs collected from the same donor on the same time point indicate that this may not be true, and others have shown bone microbial community differences related to spatial positioning and bone type (13). Regardless of the validity of this assumption, random forest models were able to overcome differences in microbial community composition related to rib positioning.

To overcome these limitations, future research will attempt to increase sample sizes, stagger the placement of decedents, use only never-frozen individuals, and better characterize microbial differences

by bone location/type. Moreover, to better understand the ecological significance of predictive taxa and elucidate their potential role in skeletal degradation, future research will include other types of measured edaphic (e.g., soil moisture, phosphate, nitrate, and microbial biomass) and skeletal parameters (e.g., organic composition, histological indicators of microbial damage, and other indicators of skeletal degradation).

Despite these limitations and the observed variation in diversity, taxonomic composition, and important taxa between seasons and within PMI models, the model using data from both placements can still estimate PMI at an accuracy that is better than the currently used methods for skeletonized remains. As noted in (15), and supported by findings in this study, seasonality is likely important for developing a robust microbial clock to estimate PMI. This key point can now be extended to studies using decomposed bone. With future studies, the microbial ecology of decomposed bone and the surrounding environment can be further elucidated, providing insight into this unique ecosystem as well as new potential means for more accurately estimating PMI.

Materials and Methods

Decedent Placement and Sampling

Research was conducted in collaboration with the Southeast Texas Applied Forensic Science Facility (STAFS), previously known as the Applied Anatomical Research Center, an anthropological research center in Huntsville, TX. Willfully donated human decedents were placed outdoors, unclothed, and in the supine position to decompose under natural conditions. Three decedents were placed on 4/15/16, which are called our spring placement bodies. For our summer placement, decedents were placed outdoors as they became available to reduce time in cooled storage, during which time the decomposition process is slowed but not completely halted (44). As a result, two summer bodies were placed on 8/25/16, while the third was placed on 9/16/16. While some decedents were frozen, there is no known evidence that this affects the long-term microbial decomposition of human bone. Due to discordance between seasonal placements within the facility, the spring cohort was uncaged whereas the summer cohort was

caged and protected from scavengers. Sample collection was conducted in a similar manner as in Damann et al. (7). Collection of rib bones began once decomposition progressed sufficiently such that little dissection was needed. There was not a requirement for the rib to be fully exposed before collection. We were unable to calculate the percentage of rib exposure due to a lack of photos during sample collection, as per policy of the anthropological facility. It is important to note that sample collection of the spring placement decedents ranged from 5/16/16 - 10/11/16, and sample collection of the summer placement decedents ranged from 9/22/16 - 6/8/17. Therefore, while “spring” and “summer” both indicate certain times of the year, in this case it only refers to when the decedents were placed and not when samples were collected within other seasons of the year. Right and left lower ribs were selected by the field sampler based on ease of collection (i.e., ribs were collected based on the level of dissection required, with preference towards those requiring the least dissection). Samples were collected approximately every three weeks for a total of eight bones from each body (48 overall), with one exception, in which two ribs were mistakenly collected from the same decedent, resulting in one subject with nine time points and another subject with only seven time points. Each rib was individually bagged and immediately frozen at -10°C, then stored until shipping to Colorado State University for processing. Accumulated degree day (ADD) was estimated using weather data provided by the National Centers for Environmental Information (<https://www.ncdc.noaa.gov/>). Degree day on the day of placement was not included, and a base temperature of 0°C was used. ADD was calculated by adding together all average daily temperatures above 0°C for all prior days of decomposition, as in Megyesi et al. (10). A sampling summary is provided in **Table S2.1**.

Rib Bone Processing

The rib bones were shipped on dry ice to Colorado State University, then stored at -20°C until processing. Spring collections were processed in December 2016, and summer collections were processed in August 2017. A fume hood was cleaned with 20% bleach solution before processing and between each bone sample. Each rib was mechanically abraded with a handheld Dremel® Drill to remove any tissue

and superficial layers of cortical bone. An approximate 40 mm x 15 mm section of bone was removed from the rib angle. The remainder of the samples were stored at -20°C.

To remove microbial DNA from the exterior of ribs, each sample was weighed and ultraviolet irradiated at 254 nm for 30 minutes on each side. Each sample was wiped down with 3% bleach, then abraded again with the Dremel® Drill to ensure removal of the outer layer of bone. The sample was then divided into three equal segments, each of which were weighed and placed into a tube. Two segments were stored at -20C for potential future use, while the remaining sample was pulverized in a sterile Waring MC2 blender cup. The cup was washed and soaked in bleach for three minutes between each sample. Each of the bone powders were placed into a clean tube for extraction.

Extraction and Purification

DNA was extracted from 0.2-0.5 grams of pulverized bone. The samples were demineralized and lysed using 30 µl of 10% sodium dodecyl sulfate (SDS), 20 µl proteinase K, and 500 µl 0.5 M ethylenediaminetetraacetic acid (EDTA) (45). The samples were vortexed for two seconds and placed on a heating block at 55°C for one hour, with additional two-second vortexes every 15 minutes. The lysed samples were centrifuged at 10,000 x g for one minute at room temperature. The supernatant was removed, measured, and placed into a clean tube. The pellets were kept and frozen at -20°C. Fifteen extraction blanks were included to identify any potential contamination.

DNA was purified using the PowerSoil DNA Isolation Kit from MoBio (Carlsbad, CA) with a modified protocol. Solution C4 was added to the lysed supernatant at twice the volume of the supernatant. The addition of solution C5 and centrifugation was performed one extra time. Occasionally, additional centrifugation was used to pass the remaining supernatant through the filter when it became clogged with bone debris. All other steps were performed as per the manufacturer's instructions.

Amplification and Sequencing

The bacterial communities of the samples and extraction negative controls were characterized using the 16S ribosomal RNA (rRNA) V4 and 18S rRNA gene regions. Standard primer pairs and protocols according to the Earth Microbiome Project were followed (46). Sequencing was performed on the MiSeq Illumina platform for the 16S rRNA gene region (2 x 150 bp reads) and the HiSeq Illumina platform for the 18S rRNA gene region (2 x 150 bp reads) using standard protocols (Illumina, San Diego, CA, USA) at the University of California San Diego IGM Genomics Center.

Data Analysis

Sequencing information was uploaded onto QIITA (study 11553), an open-source microbial study management platform (47). Due to poor reverse read quality, only the raw forward read sequencing files were downloaded and imported into QIIME2 software 2018.4 for analysis (48).

16S rRNA Preprocessing

Reads were demultiplexed using uniquely assigned barcodes. Sequences were quality filtered using Deblur with a trim length of 150 base pairs. Taxonomy was assigned using the Naive Bayes classifier, which was trained on Greengenes 13_8 99% OTUs (49). After removal of mitochondria and chloroplasts, a tree was generated by inserting fragment sequences using SEPP into the Greengenes 13_8 reference phylogeny using the QIIME2 plugin. For core metrics phylogenetic analyses (50), the data were rarefied to 17,098 reads (see *Quality of amplicon sequence data* in Results), which removed all fifteen negative extraction controls and three samples with low numbers of reads (007.R11, 011.L09, and 064.L12). These samples were removed from all analyses.

18S rRNA Preprocessing

Similar to 16S rRNA processing, reads were demultiplexed using uniquely assigned barcodes. Sequences were quality filtered using Deblur with a trim length of 150 base pairs. Reference sequences

were obtained from the SILVA database at <https://www.arb-silva.de/download/archive/qiime> (SILVA_132_QIIME_release/rep_set/rep_set_18S_only/99/silva_132_99_18S.fna), which was then imported as a QIIME2 artifact. Taxonomy was assigned using a classifier trained on the full-length SILVA 132 99% 18S database (51) using the feature-classifier QIIME2 plugin (52). Sequence data representing non-microbial taxa were filtered out, including Archaeplastida, Arthropoda, Chordata, Mollusca, Bacteria, and Unassigned taxa. While there were many unclassified eukaryotes (50 in total), BLAST (53) results of these features generally consisted of yeasts, other fungi and nematodes (i.e., there were no obvious non-microbial taxa). A phylogenetic tree using fasttree (54) and mafft alignment was generated using the phylogeny plugin for core metrics analysis. For core metrics phylogenetic analyses (50), the data were rarefied to 214,940 reads, resulting in a loss of 10 samples (067.R12, 067.L11.march, 065.L11, 065.L09, 065.L10, 064.R09, 024.L10, 007.R10, 007.L09, 011.L09).

Diversity Estimates

A linear mixed effects model was used to consider alpha and beta diversity over time (fixed effect), and a random effect for subject was included to account for repeated measurements on the same subject across time. Alpha diversity was assessed using the rarefied data with Faith's Phylogenetic Diversity metric. The linear mixed effects, plot-feature-volatility, and volatility visualizers in the longitudinal plugin in QIIME2 were used to identify significant differences in community richness across ADD and between seasons. In addition to the linear mixed effects model, beta diversity was assessed using weighted and unweighted UniFrac distances (55), which were visualized using principal coordinates analysis (PCoA) and the data visualization tool Emperor (56, 57). Effect sizes between groups (season, hosts, and the first and last ADDs) were calculated using `kruskal_effsize()` in the `rstatix()` package (58) for alpha diversity and the pseudo-F output from the PERMANOVA (59) test in the beta-group-significance visualizer in the diversity plugin in QIIME2 was used for beta diversity.

Identifying Core Features and Features Different Between Seasons

Initial exploration of features within and between seasons was performed using taxa plots. Relative abundance taxa bar plots were generated using the taxonomically filtered and rarefied data (see below for software and packages used). To aid in interpretation of the taxa plots, taxa present at low relative abundances were lumped into rare taxa. These taxa were identified using mean relative abundances that ranged from 0.002 - 0.008 across the entire dataset (see each plot for the specific number). Core taxa within each season were identified using the core-features visualizer in the feature-table plugin in QIIME2 with the default setting of 0.5 as the minimum fraction of samples that a feature must be observed in to be considered a core feature. Taxa between seasons were compared using the ANCOM (60) visualizer in the composition plugin in QIIME2. Significance between beta diversity of seasons was determined using a non-pairwise PERMANOVA test with the beta-group-significance visualizer in QIIME2.

Source Tracking

To predict the environmental source of internal rib bacteria, initial analysis in QIIME2 (60) as well as the SourceTracker2 package (61) were used. Although no skin and soil samples were collected for this study, the same subjects from both spring and summer placements were included in another study in which skin and soil samples were collected daily for the first 21 days of decomposition. Amplification and sequencing of the 16S rRNA gene were performed following protocols in the Earth Microbiome Project (61). Fresh sources, those representing the unique, non-decomposer microbiome of the subject, include decedent skin (of the hip and face) and decedent soil (near the hip and face) samples collected on the day of placement and the day after placement (days one and two), as well as all soil control (non-decedent associated) samples. Note that previous studies have found that the human microbiome is stable up to two days after death (62). Samples of the advanced decay community similarly include skin and hip samples of the decedent skin and decedent soil collected on days 19, 20, and 21. Reference hit biom tables (trimmed at 150 bp) that included the samples to be used for source tracking were downloaded

from QIITA study 11271. These biom files were imported as QIIME2 artifacts using the BIOMV210Format and merged into a single feature table with the rib samples. Similarly, the reference-hit.seqs.fa files in QIITA study 11271 corresponding to source tracking samples were downloaded and imported as QIIME2 artifacts and merged into a single representative sequences file with the rib samples. Taxonomy was assigned similarly to the bone samples, using the Naive Bayes classifier, which was trained on Greengenes 13_8 99% OTUs (62). After filtering out mitochondria and chloroplasts, a fragment-insertion SEPP tree was generated for use in core metrics phylogenetic analyses. Diversity analyses of the rib and source communities were performed using the core metrics phylogenetic pipeline in the diversity plugin in QIIME2 at a sequencing depth of 17,321. This was to validate that the skin and soil sources were different from each other, and that the fresh and advanced decay communities were distinct. Alpha and beta diversity were assessed using the Shannon and unweighted UniFrac metrics, respectively. Significances between alpha diversity of sources and rib communities were calculated using the Wilcox test in the `stat_compare_means()` function in R (63), and significance between beta diversity of sources and the rib communities was determined using pairwise PERMANOVA in the beta-group-significance visualizer in QIIME2. To use in SourceTracker2 (61), the rarefied feature table was exported as a BIOM 2.1.0 table, and source predictions were generated using the Gibbs function. For analysis of the soil control data only (see **Figure S3**), relative abundance taxa plots were generated using a feature table rarefied at 10,177 reads per sample. The DEICODE plugin (63) in QIIME2 and the Aitchison Distance metric were used to generate a biplot with features that influence the principal component axes to help identify taxa that were driving differences between seasonal placements.

Note that SourceTracker2 analysis was not performed using the 18S rRNA data; this is due to exploration of diversity and modeling results indicating that the 16S rRNA communities were less noisy and more predictive of PMI, which directed the source tracking investigation to focus only on the 16S rRNA data.

Final result plots were generated using the packages phyloseq (64), qiime2R (65), tidyverse (66), RColorBrewer (67), randomcoloR (68), and ggpubr (69) in R software (v3.5.1) (63).

Model Testing

Feature abundance data were used to generate postmortem interval (PMI) prediction models using random forest regressors. The same rarefied feature tables that were produced during diversity analyses were converted to BIOM 2.1.0 tables and used for modeling. K-fold cross validation (non-nested) was performed so that the data were separated by individual, and data from the same individual was used in either the training (model-fitting) or the testing (postmortem interval-predicting) set, but not both. The number of estimators used in each model was 1000, and hyperparameter tuning was used to refine the model. All bootstrapping was set to false in the hyperparameter tuning grid. Mean absolute error, the average deviation between predicted and observed values, was used to measure the accuracy of the model. These methods were applied using data from both seasonal placements (spring and summer, termed “combined”), as well as only spring or only summer to determine if separate models could more accurately predict PMI. For each model type, models were produced at each taxonomic level to determine which was the most predictive. This was done by collapsing the rarefied feature table at all taxonomic levels in QIIME2, and then performing the same modeling methods as described above for each level. Since random forest innately assigns importance to features used in modeling, these data were extracted from the models and used to determine which features were most important in predicting PMI. Modeling and the extraction of important features was done with Python machine learning package scikit-learn (v19.0) (70).

REFERENCES

1. J. L. Metcalf, Z. Z. Xu, S. Weiss, S. Lax, W. Van Treuren, E. R. Hyde, S. J. Song, A. Amir, P. Larsen, N. Sangwan, D. Haarmann, G. C. Humphrey, G. Ackermann, L. R. Thompson, C. Lauber, A. Bibat, C. Nicholas, M. J. Gebert, J. F. Petrosino, S. C. Reed, J. A. Gilbert, A. M. Lynne, S. R. Bucheli, D. O. Carter, R. Knight, Microbial community assembly and metabolic function during mammalian corpse decomposition. *Science*. **351**, 158–162 (2016).
2. A. Belk, Z. Z. Xu, D. O. Carter, A. Lynne, S. Bucheli, R. Knight, J. L. Metcalf, Microbiome Data Accurately Predicts the Postmortem Interval Using Random Forest Regression Models. *Genes* . **9** (2018), doi:10.3390/genes9020104.
3. G. T. Javan, S. J. Finley, I. Can, J. E. Wilkinson, J. D. Hanson, A. M. Tarone, Human Thanatomicrobiome Succession and Time Since Death. *Sci. Rep.* **6**, 29598 (2016).
4. J. L. Metcalf, L. Wegener Parfrey, A. Gonzalez, C. L. Lauber, D. Knights, G. Ackermann, G. C. Humphrey, M. J. Gebert, W. Van Treuren, D. Berg-Lyons, K. Keepers, Y. Guo, J. Bullard, N. Fierer, D. O. Carter, R. Knight, A microbial clock provides an accurate estimate of the postmortem interval in a mouse model system. *Elife*. **2**, e01104 (2013).
5. J. L. Pechal, T. L. Crippen, M. E. Benbow, A. M. Tarone, S. Dowd, J. K. Tomberlin, The potential use of bacterial community succession in forensics as described by high throughput metagenomic sequencing. *Int. J. Legal Med.* **128**, 193–205 (2014).
6. J. M. DeBruyn, K. A. Hauther, Postmortem succession of gut microbial communities in deceased human subjects. *PeerJ*. **5**, e3437 (2017).
7. F. E. Damann, D. E. Williams, A. C. Layton, Potential Use of Bacterial Community Succession in Decaying Human Bone for Estimating Postmortem Interval. *J. Forensic Sci.* **60**, 844–850 (2015).
8. C. Cartozzo, T. Simmons, J. Swall, B. Singh, Postmortem submersion interval (PMSI) estimation

- from the microbiome of *Sus scrofa* bone in a freshwater river. *Forensic Sci. Int.*, 110480 (2020).
9. D. O. Carter, D. Yellowlees, M. Tibbett, Cadaver decomposition in terrestrial ecosystems. *Naturwissenschaften*. **94**, 12–24 (2007).
 10. M. S. Megyesi, S. P. Nawrocki, N. H. Haskell, Using accumulated degree-days to estimate the postmortem interval from decomposed human remains. *J. Forensic Sci.* **50**, 618–626 (2005).
 11. H. Gill-King, Chemical and ultrastructural aspects of decomposition. *Forensic taphonomy: the postmortem fate of human remains*, 93–108 (1997).
 12. A. Galloway, W. H. Birkby, A. M. Jones, T. E. Henry, B. O. Parks, Decay rates of human remains in an arid environment. *J. Forensic Sci.* **34**, 607–616 (1989).
 13. A. L. Emmons, A. Z. Mundorff, S. W. Keenan, J. Davoren, J. Andronowski, D. O. Carter, J. M. DeBruyn, Characterizing the postmortem human bone microbiome from surface-decomposed remains. *PLoS One*. **15**, e0218636 (2020).
 14. J. L. Pechal, T. L. Crippen, A. M. Tarone, A. J. Lewis, J. K. Tomberlin, M. E. Benbow, Microbial community functional change during vertebrate carrion decomposition. *PLoS One*. **8**, e79035 (2013).
 15. D. O. Carter, J. L. Metcalf, A. Bibat, R. Knight, Seasonal variation of postmortem microbial communities. *Forensic Sci. Med. Pathol.* **11**, 202–207 (2015).
 16. C. L. Lauber, J. L. Metcalf, K. Keepers, G. Ackermann, D. O. Carter, R. Knight, Vertebrate decomposition is accelerated by soil microbes. *Appl. Environ. Microbiol.* **80**, 4920–4929 (2014).
 17. S. J. Finley, M. E. Benbow, G. T. Javan, Microbial communities associated with human decomposition and their potential use as postmortem clocks. *Int. J. Legal Med.* **129**, 623–632 (2015).
 18. R. M. Cadete, M. R. Lopes, C. A. Rosa, in *Yeasts in Natural Ecosystems: Diversity*, P. Buzzini, M.-A. Lachance, A. Yurkov, Eds. (Springer International Publishing, Cham, 2017), pp. 265–292.
 19. V. A. Mukhin, E. N. Patova, M. D. Sivkov, I. V. Novakovskaya, N. V. Neustroeva, Diversity and

- Nitrogen-Fixing Activity of Phototrophic Mycetobionts of Xylotrophic Fungi. *Russian J. Ecol.* **49**, 406–412 (2018).
20. K. L. Cobough, S. M. Schaeffer, J. M. DeBruyn, Functional and Structural Succession of Soil Microbial Communities below Decomposing Human Cadavers. *PLoS One.* **10**, e0130201 (2015).
 21. A. M. Child, Microbial Taphonomy of Archaeological Bone. *Stud. Conserv.* **40**, 19–30 (1995).
 22. C. J. Hackett, Microscopical focal destruction (tunnels) in exhumed human bones. *Med. Sci. Law.* **21**, 243–265 (1981).
 23. H. Alipour, A. Raz, S. Zakeri, N. Dinparast Djadid, Therapeutic applications of collagenase (metalloproteases): A review. *Asian Pac. J. Trop. Biomed.* **6**, 975–981 (2016).
 24. P. Bohra, R. Sultana, ELEVEN SPECIES OF SAPROPHAGOUS NEMATODES AS NEW RECORD FROM RAJASTHAN. *Rec. zool. Surv. India.* **110**, 9–17 (2010).
 25. J. Abolafia, R. Peña-Santiago, Nematodes of the Order Rhabditida from Andalucía Oriental, Spain. The Genera *Protorhabditis* (Osche, 1952) Dougherty, 1953 and *Diploscapter* Cobb, 1913, with Description of *P. spiculocrestata* sp. n. and a Species *Protorhabditis* Key. *J. Nematol.* **39**, 263–274 (2007).
 26. E. T. Alori, B. R. Glick, O. O. Babalola, Microbial Phosphorus Solubilization and Its Potential for Use in Sustainable Agriculture. *Front. Microbiol.* **8**, 971 (2017).
 27. A. Balzer, G. Gleixner, G. Grupe, H.-L. Schmidt, S. Schramm, S. Turban-Just, IN VITRO DECOMPOSITION OF BONE COLLAGEN BY SOIL BACTERIA: THE IMPLICATIONS FOR STABLE ISOTOPE ANALYSIS IN ARCHAEOMETRY. *Archaeometry.* **39**, 415–429 (1997).
 28. C. Martino, J. T. Morton, C. A. Marotz, L. R. Thompson, A. Tripathi, R. Knight, K. Zengler, A Novel Sparse Compositional Technique Reveals Microbial Perturbations. *mSystems*, 4 (1): e00016--19 (2019).

29. G. V. Lacerda-Júnior, M. F. Noronha, L. Cabral, T. P. Delforno, S. T. P. de Sousa, P. I. Fernandes-Júnior, I. S. Melo, V. M. Oliveira, Land Use and Seasonal Effects on the Soil Microbiome of a Brazilian Dry Forest. *Front. Microbiol.* **10**, 648 (2019).
30. N. Shigyo, K. Umeki, T. Hirao, Seasonal Dynamics of Soil Fungal and Bacterial Communities in Cool-Temperate Montane Forests. *Front. Microbiol.* **10**, 1944 (2019).
31. M. Santalahti, H. Sun, A. Jumpponen, T. Pennanen, J. Heinonsalo, Vertical and seasonal dynamics of fungal communities in boreal Scots pine forest soil. *FEMS Microbiol. Ecol.* **92** (2016), doi:10.1093/femsec/fiw170.
32. K. Koorem, A. Gazol, M. Öpik, M. Moora, Ü. Saks, A. Uibopuu, V. Söber, M. Zobel, Soil nutrient content influences the abundance of soil microbes but not plant biomass at the small-scale. *PLoS One.* **9**, e91998 (2014).
33. A. Willems, in *The Prokaryotes: Alphaproteobacteria and Betaproteobacteria*, E. Rosenberg, E. F. DeLong, S. Lory, E. Stackebrandt, F. Thompson, Eds. (Springer Berlin Heidelberg, Berlin, Heidelberg, 2014), pp. 355–418.
34. C. Talwar, S. Nagar, R. Kumar, J. Scaria, R. Lal, R. K. Negi, Defining the Environmental Adaptations of Genus *Devosia*: Insights into its Expansive Short Peptide Transport System and Positively Selected Genes. *Sci. Rep.* **10**, 1151 (2020).
35. R. Rivas, E. Velázquez, A. Willems, N. Vizcaíno, N. S. Subba-Rao, P. F. Mateos, M. Gillis, F. B. Dazzo, E. Martínez-Molina, A new species of *Devosia* that forms a unique nitrogen-fixing root-nodule symbiosis with the aquatic legume *Neptunia natans* (L.f.) druce. *Appl. Environ. Microbiol.* **68**, 5217–5222 (2002).
36. K. Lindström, S. A. Mousavi, Effectiveness of nitrogen fixation in rhizobia. *Microb. Biotechnol.* **13**, 1314–1335 (2020).
37. Y.-Z. Zhang, L.-Y. Ran, C.-Y. Li, X.-L. Chen, Diversity, Structures, and Collagen-Degrading

- Mechanisms of Bacterial Collagenolytic Proteases. *Appl. Environ. Microbiol.* **81**, 6098–6107 (2015).
38. D. M. Geiser, C. Gueidan, J. Miadlikowska, F. Lutzoni, F. Kauff, V. Hofstetter, E. Fraker, C. L. Schoch, L. Tibell, W. A. Untereiner, A. Aptroot, Eurotiomycetes: Eurotiomycetidae and Chaetothyriomycetidae. *Mycologia.* **98**, 1053–1064 (2006).
 39. S. H. Lee, H. S. Park, T. T. T. Nguyen, H. B. Lee, Characterization of Three Species of Sordariomycetes Isolated from Freshwater and Soil Samples in Korea. *Mycobiology.* **47**, 20–30 (2019).
 40. X.-Z. Liu, Q.-M. Wang, M. Göker, M. Groenewald, A. V. Kachalkin, H. T. Lumbsch, A. M. Millanes, M. Wedin, A. M. Yurkov, T. Boekhout, F.-Y. Bai, Towards an integrated phylogenetic classification of the Tremellomycetes. *Stud. Mycol.* **81**, 85–147 (2015).
 41. K. J. Pinckard, N. I. Batalis, Academic Forensic Pathology: The Official Publication of the National Association of Medical Examiners (2016).
 42. A. Dautartas, M. W. Kenyhercz, G. M. Vidoli, L. Meadows Jantz, A. Mundorff, D. W. Steadman, Differential Decomposition Among Pig, Rabbit, and Human Remains. *J. Forensic Sci.* **63**, 1673–1683 (2018).
 43. M. S. Micozzi, Experimental study of postmortem change under field conditions: effects of freezing, thawing, and mechanical injury. *J. Forensic Sci.* **31**, 953–961 (1986).
 44. R. W. Mann, W. M. Bass, L. Meadows, Time since death and decomposition of the human body: variables and observations in case and experimental field studies. *J. Forensic Sci.* **35**, 103–111 (1990).
 45. O. M. Loreille, T. M. Diegoli, J. A. Irwin, M. D. Coble, T. J. Parsons, High efficiency DNA extraction from bone by total demineralization. *Forensic Sci. Int. Genet.* **1**, 191–195 (2007).
 46. L. R. Thompson, J. G. Sanders, D. McDonald, A. Amir, J. Ladau, K. J. Locey, R. J. Prill, A.

- Tripathi, S. M. Gibbons, G. Ackermann, J. A. Navas-Molina, S. Janssen, E. Kopylova, Y. Vázquez-Baeza, A. González, J. T. Morton, S. Mirarab, Z. Zech Xu, L. Jiang, M. F. Haroon, J. Kanbar, Q. Zhu, S. Jin Song, T. Kosciulek, N. A. Bokulich, J. Lefler, C. J. Brislawn, G. Humphrey, S. M. Owens, J. Hampton-Marcell, D. Berg-Lyons, V. McKenzie, N. Fierer, J. A. Fuhrman, A. Clauset, R. L. Stevens, A. Shade, K. S. Pollard, K. D. Goodwin, J. K. Jansson, J. A. Gilbert, R. Knight, Earth Microbiome Project Consortium, A communal catalogue reveals Earth's multiscale microbial diversity. *Nature*. **551**, 457–463 (2017).
47. A. Gonzalez, J. A. Navas-Molina, T. Kosciulek, D. McDonald, Y. Vázquez-Baeza, G. Ackermann, J. DeReus, S. Janssen, A. D. Swafford, S. B. Orchanian, J. G. Sanders, J. Shorenstein, H. Holste, S. Petrus, A. Robbins-Pianka, C. J. Brislawn, M. Wang, J. R. Rideout, E. Bolyen, M. Dillon, J. G. Caporaso, P. C. Dorrestein, R. Knight, Qiita: rapid, web-enabled microbiome meta-analysis. *Nat. Methods*. **15**, 796–798 (2018).
48. E. Bolyen, J. R. Rideout, M. R. Dillon, N. A. Bokulich, C. Abnet, G. A. Al-Ghalith, H. Alexander, E. J. Alm, M. Arumugam, F. Asnicar, Y. Bai, J. E. Bisanz, K. Bittinger, A. Brejnrod, C. J. Brislawn, C. Titus Brown, B. J. Callahan, A. M. Caraballo-Rodríguez, J. Chase, E. Cope, R. Da Silva, P. C. Dorrestein, G. M. Douglas, D. M. Durall, C. Duvall, C. F. Edwardson, M. Ernst, M. Estaki, J. Fouquier, J. M. Gauglitz, D. L. Gibson, A. Gonzalez, K. Gorlick, J. Guo, B. Hillmann, S. Holmes, H. Holste, C. Huttenhower, G. Huttley, S. Janssen, A. K. Jarmusch, L. Jiang, B. Kaehler, K. B. Kang, C. R. Keefe, P. Keim, S. T. Kelley, D. Knights, I. Koester, T. Kosciulek, J. Kreps, M. G. I. Langille, J. Lee, R. Ley, Y.-X. Liu, E. Loftfield, C. Lozupone, M. Maher, C. Marotz, B. Martin, D. McDonald, L. J. McIver, A. V. Melnik, J. L. Metcalf, S. C. Morgan, J. Morton, A. T. Naimey, J. A. Navas-Molina, L. F. Nothias, S. B. Orchanian, T. Pearson, S. L. Peoples, D. Petras, M. L. Preuss, E. Pruesse, L. B. Rasmussen, A. Rivers, I. I. Michael S Robeson, P. Rosenthal, N. Segata, M. Shaffer, A. Shiffer, R. Sinha, S. J. Song, J. R. Spear, A. D. Swafford, L. R. Thompson, P. J. Torres, P. Trinh, A. Tripathi, P. J. Turnbaugh, S. Ul-Hasan, J. J. J. van der Hooft, F. Vargas, Y. Vázquez-Baeza, E.

- Vogtmann, M. von Hippel, W. Walters, Y. Wan, M. Wang, J. Warren, K. C. Weber, C. H. D. Williamson, A. D. Willis, Z. Z. Xu, J. R. Zaneveld, Y. Zhang, R. Knight, J. Gregory Caporaso, “QIIME 2: Reproducible, interactive, scalable, and extensible microbiome data science” (e27295v1, PeerJ Preprints, 2018), , doi:10.7287/peerj.preprints.27295v1.
49. D. McDonald, M. N. Price, J. Goodrich, E. P. Nawrocki, T. Z. DeSantis, A. Probst, G. L. Andersen, R. Knight, P. Hugenholtz, An improved Greengenes taxonomy with explicit ranks for ecological and evolutionary analyses of bacteria and archaea. *ISME J.* **6**, 610–618 (2012).
50. S. Janssen, D. McDonald, A. Gonzalez, J. A. Navas-Molina, L. Jiang, Z. Z. Xu, K. Winker, D. M. Kado, E. Orwoll, M. Manary, S. Mirarab, R. Knight, Phylogenetic Placement of Exact Amplicon Sequences Improves Associations with Clinical Information. *mSystems.* **3** (2018), doi:10.1128/mSystems.00021-18.
51. C. Quast, E. Pruesse, P. Yilmaz, J. Gerken, T. Schweer, P. Yarza, J. Peplies, F. O. Glöckner, The SILVA ribosomal RNA gene database project: improved data processing and web-based tools. *Nucleic Acids Res.* **41**, D590-6 (2013).
52. N. A. Bokulich, B. D. Kaehler, J. R. Rideout, M. Dillon, E. Bolyen, R. Knight, G. A. Huttley, J. Gregory Caporaso, Optimizing taxonomic classification of marker-gene amplicon sequences with QIIME 2’s q2-feature-classifier plugin. *Microbiome.* **6**, 90 (2018).
53. S. F. Altschul, W. Gish, W. Miller, E. W. Myers, D. J. Lipman, Basic local alignment search tool. *J. Mol. Biol.* **215**, 403–410 (1990).
54. M. N. Price, P. S. Dehal, A. P. Arkin, FastTree 2--approximately maximum-likelihood trees for large alignments. *PLoS One.* **5**, e9490 (2010).
55. C. Lozupone, R. Knight, UniFrac: a new phylogenetic method for comparing microbial communities. *Appl. Environ. Microbiol.* **71**, 8228–8235 (2005).
56. Y. Vázquez-Baeza, A. Gonzalez, L. Smarr, D. McDonald, J. T. Morton, J. A. Navas-Molina, R.

- Knight, Bringing the Dynamic Microbiome to Life with Animations. *Cell Host Microbe*. **21**, 7–10 (2017).
57. Y. Vázquez-Baeza, M. Pirrung, A. Gonzalez, R. Knight, EMPeror: a tool for visualizing high-throughput microbial community data. *Gigascience*. **2**, 16 (2013).
 58. M. Tomczak, E. Tomczak, The need to report effect size estimates revisited. An overview of some recommended measures of effect size. *Trends in Sport Sciences* (2014) (available at <https://www.semanticscholar.org/paper/8c08127f9e736e8db15bec81d69f547d672f9f58>).
 59. M. J. Anderson, Permutational Multivariate Analysis of Variance (PERMANOVA). *Wiley StatsRef: Statistics Reference Online*, 1–15 (2017).
 60. S. Mandal, W. Van Treuren, R. A. White, M. Eggesbø, R. Knight, S. D. Peddada, Analysis of composition of microbiomes: a novel method for studying microbial composition. *Microb. Ecol. Health Dis.* **26**, 27663 (2015).
 61. D. Knights, J. Kuczynski, E. S. Charlson, J. Zaneveld, M. C. Mozer, R. G. Collman, F. D. Bushman, R. Knight, S. T. Kelley, Bayesian community-wide culture-independent microbial source tracking. *Nat. Methods*. **8**, 761–763 (2011).
 62. J. L. Pechal, C. J. Schmidt, H. R. Jordan, M. E. Benbow, A large-scale survey of the postmortem human microbiome, and its potential to provide insight into the living health condition. *Sci. Rep.* **8**, 5724 (2018).
 63. R Core Team, R: A Language and Environment for Statistical Computing (2017) (available at <https://www.R-project.org/>).
 64. P. J. McMurdie, S. Holmes, phyloseq: an R package for reproducible interactive analysis and graphics of microbiome census data. *PLoS One*. **8**, e61217 (2013).
 65. J. E. Bisanz, qiime2R: Importing QIIME2 artifacts and associated data into R sessions (2018),

(available at <https://github.com/jbisanz/qiime2R>).

66. H. Wickham, M. Averick, J. Bryan, W. Chang, L. D. McGowan, R. François, G. Grolemund, A. Hayes, L. Henry, J. Hester, Others, Welcome to the Tidyverse. *Journal of Open Source Software*. **4**, 1686 (2019).
67. E. Neuwirth, ColorBrewer Palettes (2014) (available at <https://cran.r-project.org/web/packages/RColorBrewer/RColorBrewer.pdf>).
68. R. Ammar, Generate Attractive Random Colors (2019) (available at <https://cran.r-project.org/web/packages/randomcoloR/randomcoloR.pdf>).
69. A. Kassambara, “ggplot2” Based Publication Ready Plots (2020) (available at <https://cran.r-project.org/web/packages/ggpubr/ggpubr.pdf>).
70. F. Pedregosa, G. Varoquaux, A. Gramfort, V. Michel, B. Thirion, O. Grisel, M. Blondel, P. Prettenhofer, R. Weiss, V. Dubourg, J. Vanderplas, A. Passos, D. Cournapeau, M. Brucher, M. Perrot, É. Duchesnay, Scikit-learn: Machine Learning in Python. *J. Mach. Learn. Res.* **12**, 2825–2830 (2011).

CHAPTER 3: THE MICROBIOME OF BLOW FLY ORGANS AND FLY-HUMAN MICROBIAL TRANSFER DURING DECOMPOSITION³

Summary

In the early stages of decomposition, blow flies lay eggs and acquire nutrients, and bring their microbes with them. While blow flies have a unique core microbiome, it is not known whether this is altered in a decomposition environment. Differences in the blow fly microbiome may influence the types of microbes transmitted from the flies to the cadaver, therefore potentially affecting assembly of the human decomposer microbiome. This is because fly interactions with cadavers vary by season, and because it is likely that external fly parts (i.e., the labellum and tarsi) make more direct contact and are likely involved in increased mechanical transmission with the cadaver than internal parts such as the oocyte. The second purpose of this study was to determine if the blow fly microbes contribute to the human decomposer microbiome. To accomplish these aims, ten human cadavers were placed outdoors across three seasons and allowed to decompose. The first waves of colonizing flies were collected and dissected by organ (labellum, tarsi, and oocyte). In addition to fly collections, samples from the cadavers were collected using a sterile swab at sites including the face, inner cheek, bicep, torso, and anus. Overall, blow flies associated with human cadavers have a similar microbiome to blow flies not associated with human cadavers. Furthermore, there were differences in the microbiome between seasons and blow fly organs. We also show evidence that blow flies act as a microbial source to the human decomposer microbiome, which is important for understanding the ecological mechanisms of human cadaver microbial community assembly.

³ This work has been submitted for publication: Deel, H., Montoya, S., King, K., Emmons, A. L., Huhn, C., Lynne, A., Metcalf, J. L., Bucheli, S. (2021). The microbiome of blow fly organs and fly-human microbial transfer during decomposition. Submitted to *Forensic Science International*.

Introduction

The decomposition of vertebrate remains is a dynamic process that is partially driven by the actions of microbes (1–5). As decomposition progresses through successive stages as defined by Galloway et al. (6), the microbial roles change as cadaver derived nutrients change (7). Immediately after death and in the fresh stage, enteric microbes are no longer influenced by the host immune system (7). Those that can survive with little oxygen flourish (7, 8), initiating a shift from the individual host microbiome (9) to a decomposer microbiome that is more consistent across cadavers (10). During this time frame, flies (primarily female) are also interacting with the cadaver, as they are attracted to the nutrients and volatile compounds produced by microbes (11). Flies will lay eggs in the eyes, nose, and ears, as well as in the hair and in body-body and body-ground interfaces (7). Typically, blow flies (Calliphoridae) are the first to colonize a cadaver and so they are of particular interest and importance for forensics (12).

Studies, a few of which have focused on blow flies (13, 14), have shown that flies have their own microbiome (13–15). This core blow fly microbiome is composed of the phyla Proteobacteria, Firmicutes, and Bacteroidetes (13, 14), with a small number of species identified within phylum Actinobacteria (16). Some of the more common bacterial genera associated with blow flies included *Enterococcus*, *Proteus*, *Serratia*, *Wolbachia*, *Pseudomonas*, *Corynebacterium*, *Providencia*, *Lactobacillus*, *Lactococcus*, *Morganella*, and *Myroides*, although this is not a comprehensive list of every genus found on blow flies. Additionally, body part specific analyses have been conducted, in which it was found that *Providencia* spp. were more abundant on the blow fly abdomen (13) and *Lactobacillus*, *Proteus*, *Diaphorobacter*, and *Morganella* were dominant in the salivary gland (14). Another experiment studying the bacterial profiles by organ showed that *Pseudomonas* was a key contributor to all bacterial profiles studied, with notable differences between the digestive tract, salivary gland, and reproductive organs (17). While these studies were useful for characterizing the blow fly bacterial microbiome and discovering bacterial differences between body parts, very few studies have been performed in a decomposition environment. Wohlfahrt et al. used decomposed beef liver as an attractant for blow fly species *Lucilia sericata* and *Phormia regina*

in order to characterize the bacterial communities associated with different life stages (18). In both blow fly species, Bacilli and Gammaproteobacteria (classes that are both common to other blow fly microbiome studies) comprised >95% of all bacterial classes across all life stages. In the same year, Maleki-Ravasan et al. published a study showing that blow flies collected using chicken liver baited traps contained bacteria within genera *Enterococcus*, *Myroides*, *Proteus*, *Providencia*, and *Serratia*, all of which are also common blow fly genera (16). However, more experiments studying the blow fly microbiome in the context of human decomposition are needed.

The interaction of blow flies with carrions and the potential transfer of microbes between hosts in the process makes characterization of the blow fly microbiome in a human decomposition setting of entomological and forensic importance. There are several studies showing evidence of a mechanical transfer of microbes between flies and carrions, including viruses (19) and bacteria (18, 20–22). This can occur through several ways, including physical contact between the fly and the cadaver (18, 20), fly defecation or regurgitation (22), and oviposition (16). These processes often begin to occur immediately after death, during which the human decomposer microbiome begins to assemble (10). Therefore, characterizing the microbiome of blow flies associated with human cadavers and understanding the mechanical transfer of microbes onto human cadavers is relevant to elucidating the ecological dynamics of the human decomposer microbiome assembly.

The first purpose of this study was to characterize the blow fly microbiome in a human decomposition environment because to the authors' knowledge, this has never been performed before. To do this, human cadavers were placed to decompose outdoors, unclothed, aboveground, and in the supine position at the Southeast Texas Applied Forensic Facility in Huntsville, TX. A total of 10 cadavers were placed across three seasons (two winter placements, two spring placements, and one summer placement represented by February, April, and July, respectively). Seasonal placements were conducted because fly colonization and the amount that flies interact with the cadavers can vary by season (23), which may in turn affect the decomposition fly microbiome. The first wave of colonizing flies was collected (ranging from immediately after placement to hours after placement), and the microbiomes of the labellum (mouth

parts), tarsi (leg parts), and oocytes were characterized using 16S ribosomal RNA gene sequencing following the Human Microbiome Project standard protocols (24). The labellum and tarsi were sampled because they make direct contact with the cadaver, while the oocytes were chosen to preliminarily screen for transovarial transmission (i.e., the transmission of microbes from parent to offspring via infection of the developing egg (25)). Since blow flies interact with human cadavers during the transitional stage from the individual host microbiome to the decomposer microbiome (26), the second purpose of this study was to determine if the blow fly microbes contribute as a source to the human decomposer microbiome, as well as to investigate if this source contribution differs between seasons. We predicted that organ-specific analyses would show that the labellum and tarsi, external fly organs which come into direct contact with the cadavers, would have more similar microbial compositions to each other compared to the oocyte. Furthermore, we also predicted that the labellum and tarsi, which are involved in a higher rate of mechanical transmission of microbes (26), would be shown to contribute to the human decomposer microbial community assembly using source tracking analysis.

Results and Discussion

Fly Occurrence

The fly species that were collected across the five different placements (February, April, and July 2014, and February and April 2015) are summarized in **Figure 3.1** by month and year. These data are consistent with the collection times from other years for these species of fly for our geographic region (unpublished data available from Sam Houston State University entomological collection).

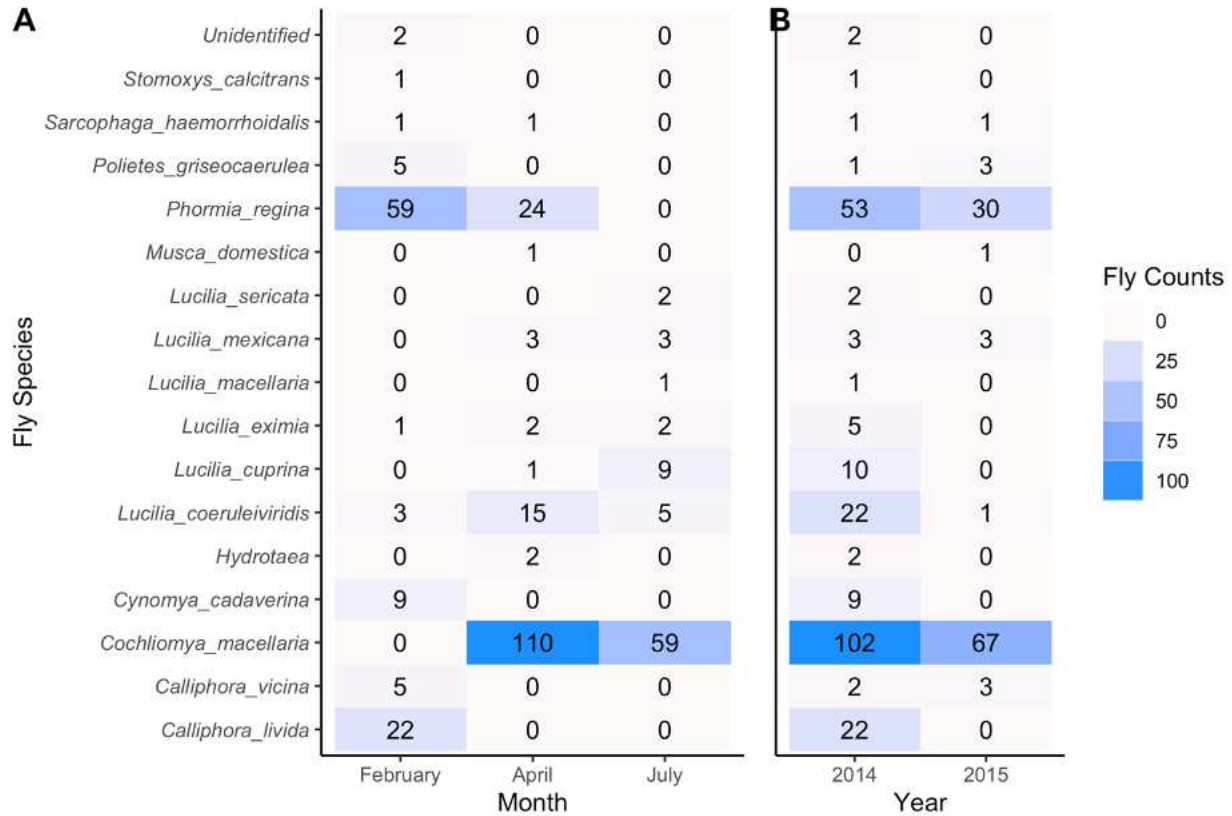


Figure 3.1. Summary of fly collections by month (A) and year (B). The “unidentified” fly species is a member of the family Muscidae, and the species of *Hydrotaea* could not be identified but is likely *Hydrotaea aenescens*.

Quality of Amplicon Sequence Data

A total of 16,970,884 reads were generated. Filtering of reads assigned to chloroplast and mitochondria resulted in a total of 16,235,066 reads with a mean frequency per sample of 13,461 and a range of 2 - 55,152 reads. To normalize, the data were rarefied at 5,937 reads per sample as an optimal balance for retaining enough samples and observed features. This retained approximately 74% of all samples (890/1,206), with the percent of retained samples for each sample type as follows: 69% fly, 81% bicep, 82% face, 84% fecal, 81% inner cheek, and 84% torso.

The Core Fly Microbiome

The main phyla found in every organ type of every species included in the analyses are Proteobacteria, Firmicutes, Bacteroidetes, and Actinobacteria (**Figure 3.2**). This result agrees with several other studies that observed the fly microbiome (11, 13–15, 27). One notable exception is the relatively smaller abundance of Actinobacteria in February (**Figure 3.2**). In this dataset, the top three most relatively abundant taxa that comprise phylum Actinobacteria are within genus *Corynebacterium* (including an unclassified *Corynebacterium*, *Corynebacterium urealyticum*, and *Corynebacterium propinquum*, in decreasing order). Since this genus grows best within a temperature range of 30-37°C (86-98.6°F) (28), perhaps *Corynebacterium* can't survive within the colder February temperatures. A temperature profile for each season can be seen in **Figure S3.1**.

A total of seven core features were identified using the QIIME2 core-features plugin, and these were (in decreasing order of frequency) genera *Tumebacillus*, *Vagococcus*, *Wolbachia*, *Providencia*, *Pseudomonas*, *Staphylococcus*, and family *Comamonadaceae*. Although *Wohlfahrtiimonas*, a common fly-associated bacterium (29), was found in the fly microbiome (**Figure 3.2**), it was not identified as a core feature in this dataset. *Tumebacillus*, the most relatively abundant core feature, is not commonly associated with flies (11, 13–15, 27), but it is a gram-positive aerobic organism that has previously been found in non-rhizosphere soils (30) and was likely transferred onto the flies from the surrounding outdoor environment. *Vagococcus*, *Providencia*, *Pseudomonas*, and *Staphylococcus* are all known to be present on blow flies from previous studies (13–16, 18, 22, 26, 29). *Wolbachia* is known for its endosymbiotic relationships with arthropods, including reproductive manipulations as well as protection against pathogens (31). In blow flies in particular, *Wolbachia* is the most abundant and ubiquitous organism for all body parts (13). In our dataset, *Wolbachia* varied in its presence. For example, *Wolbachia* was present in all fly organs and represented the majority of features in nearly all samples for blow flies *Lucilia coeruleiviridis*, *Lucilia eximia*, and *Lucilia mexicana*, but for *Phormia regina*, *Wolbachia* presence ranged from dominating all samples from all organs (typically in the April placements) to being low in frequency or undetectable (typically in the February placements). There were also several other blow fly species

including *Calliphora vicina*, *Cynomya cadaverina*, *Calliphora livida*, *Lucilia cuprina*, and *Lucilia sericata* in which *Wolbachia* had little presence. However, it is important to note that many of these *Wolbachia*-lacking species were collected only in one seasonal placement, so it is difficult to determine whether this is a species or seasonal effect. The last core feature, family *Comamonadaceae*, is a diverse bacterial family that comprises over 100 species in at least 29 genera (32). To the authors' knowledge, this family has not been well highlighted in fly microbiomes.

Five different amplicon sequence variants (ASVs) assigned to genus *Dysgonomonas* were identified (**Figure 3.2**). This taxon has been isolated from environments like the human gallbladder (33), abdominal drains (34), and wounds (35). While it has also been isolated from the gut of a termite (36), it seems more likely that the flies acquired *Dysgonomonas* through their continued interaction with decomposing humans rather than termites, which are not common and have not been recorded in association with decomposing human remains at STAFS. However, it is also possible that *Dysgonomonas* is naturally occurring in the fly microbiome. It is interesting to note that *Dysgonomonas* had a noticeably higher relative abundance in April compared to other seasonal placements, the reason for which requires further investigation. Although this was not a deep investigation, it indicates that blow flies likely can pick up human-derived bacteria from cadavers after only a few hours of decomposition.

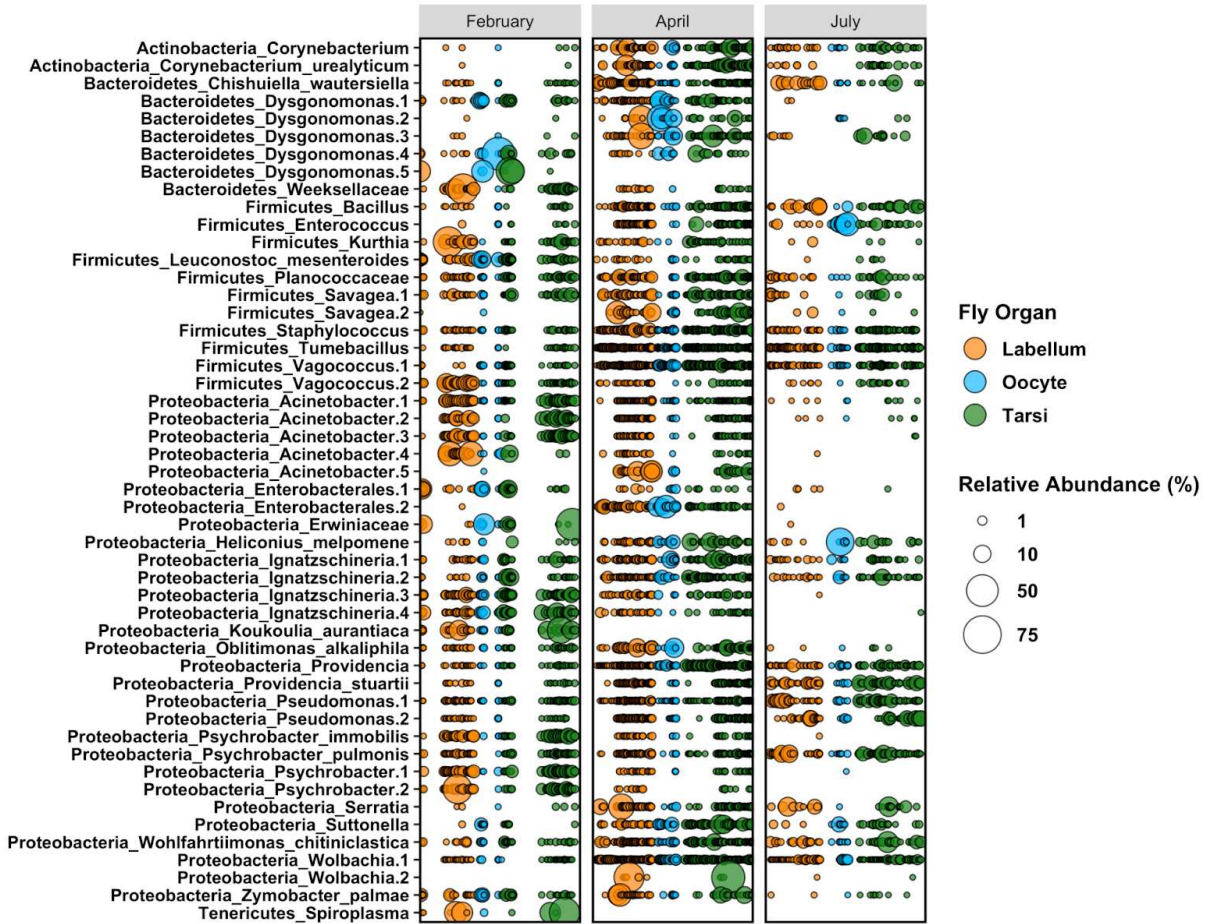


Figure 3.2. A bubble chart of the relative abundance of the top 50 fly taxa colored by organ and separated by placement season. Taxa are sorted by phylum, and each taxon name contains the phylum and the taxonomically lowest identifiable name. Each column represents the community of a single fly organ within the indicated season. Taxa with number assignments represent different amplicon sequence variants that were assigned to the same taxon.

How Does the Fly Microbiome Compare Between Organs (Tarsi, Oocyte, Labellum)?

Pairwise comparisons between the beta diversity of fly organs (**Figure 3.3A**) were all significant for all beta group unweighted UniFrac and beta group weighted UniFrac tests (PERMANOVA $q = 0.001$ for all comparisons, 999 permutations). Comparisons including the oocyte had higher pseudo-F values for both unweighted UniFrac (pseudo-F = 11.89 and pseudo-F = 15.07 compared to the labellum and tarsi, respectively) and weighted UniFrac (pseudo-F = 11.05 and pseudo-F = 11.33 compared to the labellum and tarsi, respectively) metrics compared to labellum versus tarsi comparisons (pseudo-F = 3.05 and

pseudo-F = 4.24 for unweighted UniFrac and weighted UniFrac, respectively). These statistics indicate that the bacterial composition of the oocyte is significantly different from the tarsi and labellum. Pairwise comparisons using the ANCOM plugin in QIIME2 identified 14 differentially abundant features between fly organs (**Table 3.1**). Notable features included *Chishuiella wautersiella*, which was more frequent in labellum compared to the tarsi and oocyte, *Ignatzschineria*, which was more abundant in the tarsi compared to the labellum, *Suttonella*, which was more abundant in the tarsi and oocyte compared to the labellum, and several other features that were more abundant in the labellum and tarsi compared to the oocyte such as *Tumebacillus*, *Psychrobacter pulmonis*, and *Pseudomonas* (**Table 3.1**). Genus *Chishuiella* is a gram-negative, strictly aerobic bacterium that has been isolated from freshwater (37). STAFS is located at the Center for Biological Field Studies, a 250-acre land designation. There are two main watersheds in the area, Wynne and Harmon, with smaller tributaries which cross throughout the area, including within the STAFS facility (38). *Ignatzschineria* is a bacterium that is commonly associated with myiasis, or infection by fly larvae of human tissue though its exact role in maggot biology is not understood (14, 39–47). While we expected to find this common fly bacterium on both the tarsi and the labellum, it is more common on the tarsi. This may be simply because the surface of the tarsi are in contact with cadaver tissues for longer than the labellum and allows for increased transfer of bacteria. Interestingly, *Suttonella* has been found to be associated with human respiratory disease (48). This may be further evidence of two things. First, blow flies can pick up human-derived bacteria from cadavers during decomposition. While it has been known for several decades that flies can pick up bacteria from other sources, this knowledge can potentially be extended to include blow flies picking up bacteria in a human decomposition environment. Second, not only do flies pick up bacteria, but these bacteria then may become integrated into the fly microbiome. Even when a new bacterium is introduced into an environment, it is possible that the ecological dynamics of the microbiome in the environment do not support the integration of the new bacterium into the microbial community structure (citation for this). Therefore, it is interesting that the blow fly microbial community dynamics support integration of bacteria from human cadavers into their microbiome. Our prediction that several features would be differentially

abundant in the labellum and tarsi was confirmed. This is likely due to the increased interaction of these surface organs with the surrounding environment compared to the internal oocytes, which has a larger physical barrier that probably prevents it from participating in microbial transfer and the fact that bacteria present in the oocytes are there most likely due to transovarial transmission (49). While contamination of oocytes during dissection is possible, steps were taken to minimize the possibility (flies were washed and sterile dissection techniques were employed).

Table 3.1. The top five differentially abundant taxa that were identified using the ANCOM plugin in QIIME2. The W-value represents the number of ANCOM sub-hypotheses that have passed for each individual taxon. Note that the labellum vs. tarsi comparison only contained four total differentially abundant taxon. A full table is available in the supplementary files.

Comparison	Taxon	Group taxon is higher in	W-value
labellum vs. tarsi	<i>Chishuiella wautersiella</i>	labellum	1274
	<i>Vagococcus</i>	tarsi	1266
	<i>Ignatzschineria</i>	tarsi	1264
	<i>Suttonella</i>	tarsi	1202
labellum vs. oocyte	<i>Suttonella</i>	oocyte	746
	<i>Tumebacillus</i>	labellum	744
	<i>Psychrobacter pulmonis</i>	labellum	744
	<i>Chishuiella wautersiella</i>	labellum	725
	<i>Pseudomonas</i>	labellum	713
tarsi vs. oocyte	Enterobacterales	oocyte	935
	<i>Psychrobacter pulmonis</i>	tarsi	932
	<i>Tumebacillus</i>	tarsi	924
	<i>Pseudomonas</i>	tarsi	916
	<i>Corynebacterium urealyticum</i>	tarsi	899
April vs. February	<i>Providencia</i>	April	1093
	<i>Ignatzschineria</i>	February	1092
	<i>Vagococcus</i>	April	1091

	<i>Wolbachia</i>	April	1091
	<i>Tumebacillus</i>	April	1091
April vs. July	<i>Pseudomonas</i>	July	1163
	<i>Wolbachia</i>	April	1161
	<i>Psychrobacter pulmonis</i>	July	1160
	<i>Actinomycespora</i>	July	1155
	<i>Corynebacterium</i>	July	1154
February vs. July	<i>Actinetobacter</i>	February	624
	<i>Ignatzschineria</i>	February	624
	<i>Tumebacillus</i>	July	624
	<i>Providencia stuartii</i>	July	620
	Comamonadaceae	July	619

How Does the Fly Microbiome Compare Between Seasons?

Beta diversity analyses show clustering by the season of fly collection, in which February is distinct from both April and July, the latter of which overlap (**Figure 3.3B**). All seasons were significantly different from each other ($q = 0.001$ for all pairwise PERMANOVA comparisons for unweighted and weighted UniFrac metrics). The pseudo-F value (effect size) was higher for season than organ for both unweighted (9.15 and 17.59 for organ and season, respectively) and weighted (8.36 and 27.09 for organ and season, respectively) UniFrac metrics, indicating that season has a larger effect on the fly microbiome than the type of organ. This seasonal effect may be due to less fly activity during cooler months (50), as the average April and July placement temperatures (20.21°C and 27.71°C, respectively) are closer together than they are to the average February placement temperature of 10.23°C. Furthermore, it is possible that variation in species occurrence between seasons (**Figure 3.1A**) may play a role in seasonal differences. However, to the authors' knowledge, the microbiomes of individual blow fly species have not been studied and thus the influence of blow fly species occurrence on seasonal microbiome variation would require more investigation. Pairwise analysis using the ANCOM plugin in QIIME2

identified a total of 135 differentially abundant features between flies collected in different seasons. Notable differentially abundant features include *Ignatzschineria*, which was more frequent in February, *Wolbachia*, which was more abundant in April, along with *Tumebacillus* and two features belonging to genus *Providencia*, which were more abundant in the warmer months April and July. While literature on the seasonal fly microbiome is lacking, one study by Wei et al. (40) did observe that the *Lucilia sericata* microbiome differs between seasons, in which *Staphylococcus* increased in the spring, *Ignatzschineria* increased in the summer, and *Vagococcus*, *Dysgonomonas*, and an unclassified Acetobacteraceae increased in the fall. These results do not agree with those of our dataset (e.g., our results instead showed a differential increase of *Ignatzschineria* in the winter as opposed to the summer). There may be several reasons for this, including differences in geographic location, local animals and vegetation, solar irradiation, or that Wei et al. (40) did not conduct their study in a decomposition environment.

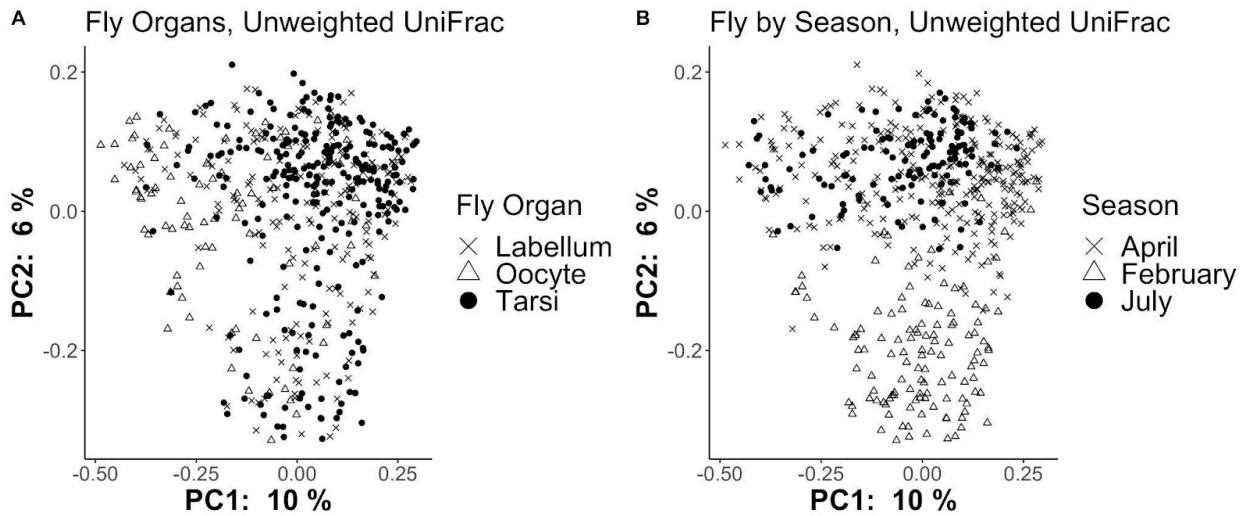


Figure 3.3. Unweighted UniFrac beta diversity of fly microbiomes by organ and season. For all unweighted PERMANOVA pairwise comparisons (i.e., all organs compared to all organs and all seasons compared to all seasons, see methods), $q = 0.001$ (999 permutations). The weighted UniFrac version of this can be seen in **Figure S3.2**.

Do Fly-Associated Bacteria Appear in the Human Decomposition Microbiome, and How Does this Differ Between Placement Seasons?

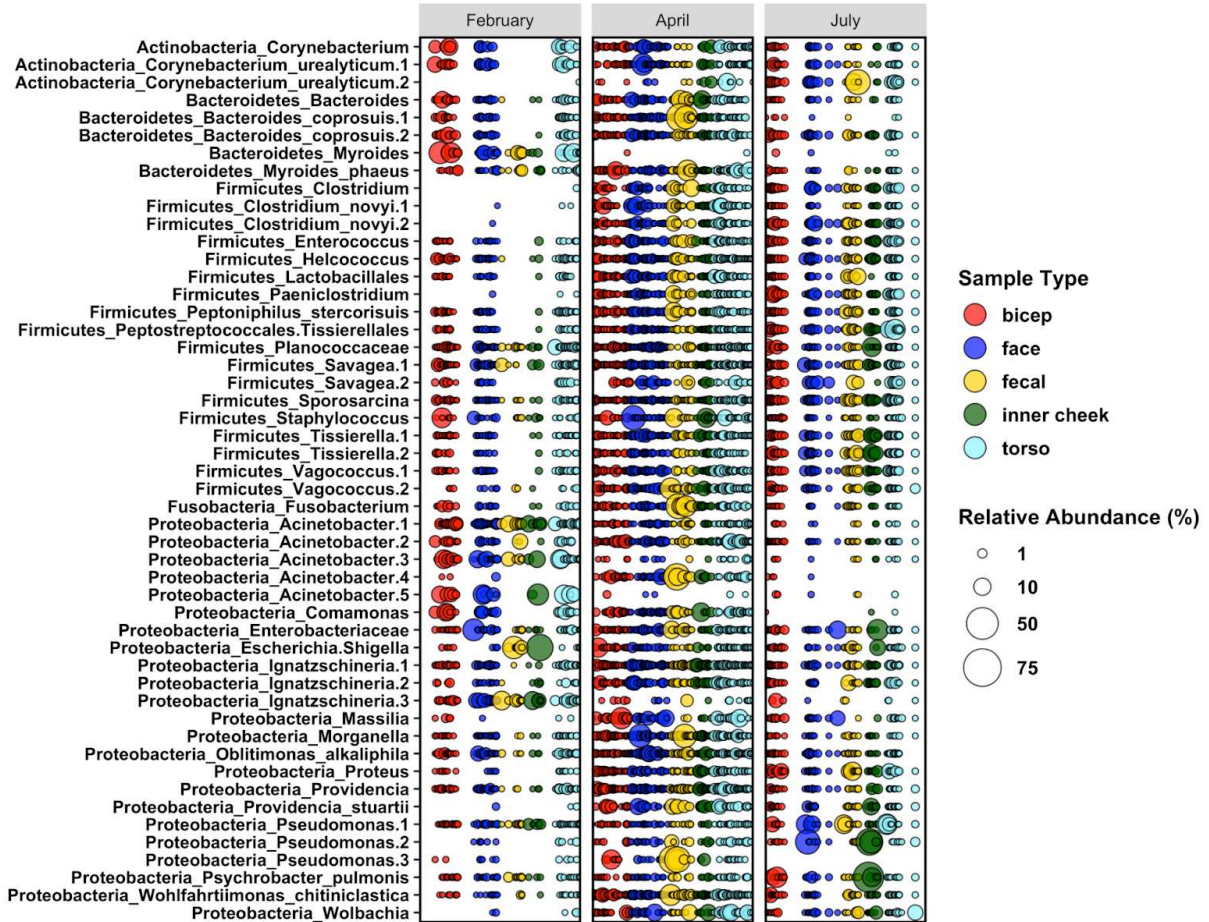


Figure 3.4. A bubble chart of the relative abundance of the top 50 human-associated microbial taxa colored by sample type and separated by placement season. Taxa are sorted by phylum, and each taxon name contains the phylum and the taxonomically lowest identifiable name. Each column represents the microbial community of a single human sample within the indicated season. Taxa with number assignments represent different amplicon sequence variants that were assigned to the same taxon.

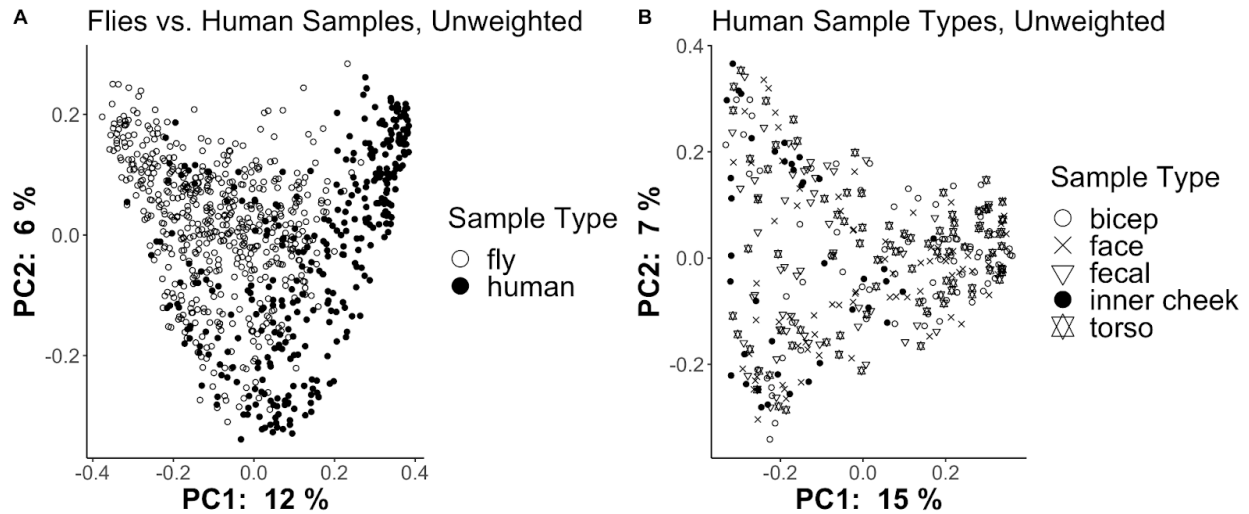


Figure 3.5. Unweighted UniFrac beta diversity of human vs. fly samples (A) and the different sample types within the human data (B). PERMANOVA comparisons showed that the fly samples were significantly different from human samples ($p = 0.001$, 999 permutations, pseudo- $F = 58.10$), and pairwise PERMANOVA comparisons showed that some human sample types were significantly different from each other (fecal and inner cheek samples were different from each other as well as all other sample types $q = 0.001$ for all unweighted comparisons, 999 permutations). Other human sample types (bicep, face, torso), were not significantly different from each other ($0.11 < q < 0.75$ for all comparisons, 999 permutations). The weighted UniFrac version of this can be seen in **Figure S3.3**.

Many of the same phyla found in the fly data were also found in the human sample types, including Actinobacteria, Bacteroidetes, Firmicutes, and Proteobacteria (**Figure 3.4**). An exception is the presence of one ASV classified as taxon *Fusobacterium* within phylum Fusobacteria. This is unsurprising, as *Fusobacterium* is typically a human pathogen (51). At a lower taxonomic level, many of the fly genera were similarly found in the human samples, including common fly associated bacteria like *Wolbachia*, *Ignatzschineria*, and *Wohlfahrtiimonas* (**Figure 3.4**). Beta diversity analyses using the unweighted UniFrac metric showed that fly sample types clustered away from human sample types (**Figure 3.5A**, PERMANOVA $p = 0.001$ for both unweighted and weighted UniFrac). Fecal and inner cheek sample types were significantly different from each other and from all other sample types for both unweighted UniFrac and weighted UniFrac for all pairwise PERMANOVA comparisons ($q = 0.001$, 999 permutations) except for one case, in which the fecal and inner cheek samples were not significantly different when compared using the weighted UniFrac metric ($q = 0.126$). In all comparisons for both

metrics, the bicep, face, and torso samples were not significantly different from each other ($0.11 < q < 0.75$ for all comparisons, 999 permutations). This indicates that the area of skin in which blow flies interact with may not affect the microbes they acquire, but that their interaction with other more distinct sample types such as feces and the inner mouth may have greater influence. Furthermore, flies are more likely to oviposit in moist, protected areas like the mouth and anus (52). To track the transfer of fly microbes more accurately onto humans during decomposition, SourceTracker2 was used. Source tracking analyses showed that in February, the tarsi microbiome is a higher contributor to the human decomposition microbiome, with the labellum microbiome acting as a smaller source and the oocyte microbiome a relatively nonexistent source (Figure 3.6A). As the months become warmer, the labellum source proportion increases, the tarsi source proportion decreases, and the oocyte microbiome begins to contribute to the human decomposition microbiome, albeit minimally (Figure 3.6B and 3.6C). Therefore, blow flies are likely a source of microbes during human decomposition, and the fly source organ varies between seasons. In general, these seasonal trends held regardless of the human sample type, with one notable exception being that tarsi appeared to contribute a higher source proportion of the inner cheek community in July (Figure 3.6C).

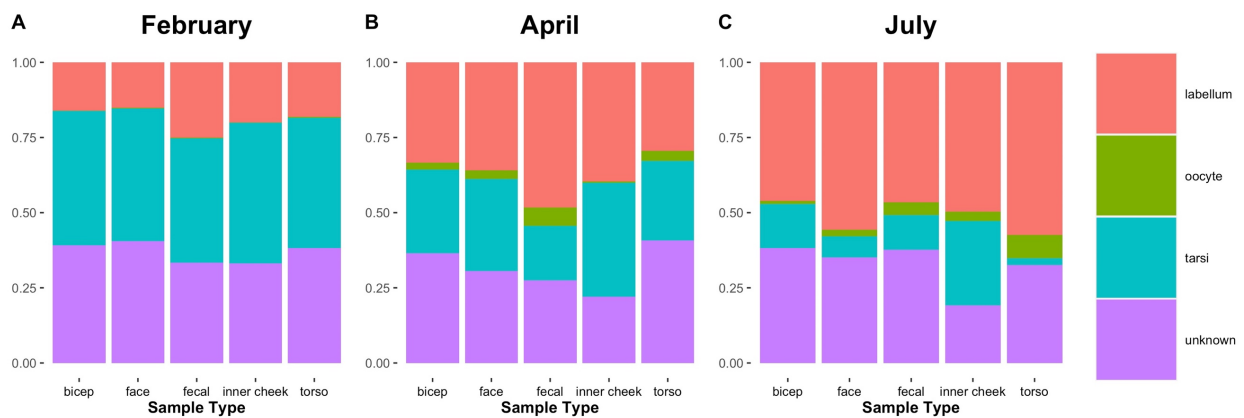


Figure 3.6. The predicted source proportions of fly organ microbes on human sample types, separated by placement season.

Conclusions

The core fly microbiome observed in our dataset had several commonalities with other fly microbiome studies, indicating a “universal” fly microbiome that persists even in a decomposition environment. Despite this, there were still notable differences between fly organs and seasons. While there was a statistically significant signal in beta diversity between the labellum, tarsi, and oocyte, seasonal placement had a stronger effect on the fly bacterial communities. Fly species occurrence may play a role in seasonal differences, which would require further investigation. Furthermore, blow flies can pick up human-derived bacteria from the cadaver within only a few hours after placement, and they likely act as substantial bacterial sources of the human decomposer bacterial community, with the source contribution per fly organ varying based on the time of year. This study has characterized the blow fly microbiome by organ during different seasons, and it has provided evidence that the fly microbiome contributes to the human decomposer microbial community assembly.

Materials and Methods

Study Site

The Southeast Texas Applied Forensic Science Facility (STAFS, formerly the Applied Anatomical Research Center, AARC) is a willed-body donation facility housed at the Center for Biological Field Studies (CBFS), Sam Houston State University, Huntsville, Texas. It is a research facility with a focus on the study of applications of forensic science of the human body. The facility lies in the Pineywoods ecoregion of Southeast Texas and has a subtropical, humid environment with a moderate covering of pine trees and herbaceous underbrush. The soil is acidic, well-draining, and sandy (53).

Cadaver Placement and Monthly Temperature Calculations

As part of a larger 3-year study looking at the ecology of decomposition, ten human cadavers were placed outdoors over five seasons and allowed to decompose under natural conditions with no

clothing (5, 39). Cadavers were not autopsied and were either cooled, frozen, or underwent both before placement. A summary of cadaver information including age, sex, storage conditions, height, weight, ancestry, and medical history is provided in **Table S3.1**. The average monthly temperatures for seasonal placements were calculated by collecting monthly summary data from Weather Underground, and averaging both February placement months (2014 and 2015) together to get the overall February average, and averaging both April placement months (2014 and 2015) together to get the overall April average. There was only one July placement (2014), and the monthly average for this one month was used. A breakdown of the average monthly weather data is provided in **Figure S3.1**, including average monthly temperatures, average monthly precipitation, and average dew points.

Fly Collections

Once the bodies were placed, the goal was to collect the first wave of colonizing flies that were in contact with the cadaver as this would target those flies associated with the earliest stage of decomposition and would represent possible sources of bacteria. The time for collection ranged from immediately after placement to hours after placement. The wide range in time was mainly dependent on time necessary for the body to thaw (affecting fly attraction to the remains), and the outside temperature (affecting fly availability and fly activity). To collect the flies, three different methods were used: collection by hand, collection by aerial sweep nets, and collection directly into conical tubes. Upon collection, flies were kept in separate sterilized conical tubes, placed in a bag labeled with the body accession number, and frozen until dissection.

Human Sampling

Samples from cadavers were collected at the same time as fly collection using sterile dual-tipped BD SWUBE Applicator (REF 281130) swabs by rubbing the sample site lightly for approximately 30 seconds over an area of approximately 2 cm square. Cadaver sample sites were: bicep, face, fecal through anus, inner cheek, and torso.

Identification of Flies

Flies were identified to family, genus, and species using the Whitworth key to the genera and species of blow flies (Diptera: Calliphoridae) of America North of Mexico (54) and Field Guide to the Insects of America: North of Mexico (55). Specimens were cross-checked against a reference collection housed at the Sam Houston State University Museum.

Dissections

Flies were dissected to obtain all tarsi from one side of their body (the right), the labellum, and the oocytes (if female). All dissections were conducted under sterile conditions using a laminar flow hood. After the tarsi and labellum were isolated but before the oocytes were dissected, the flies were washed in soapy water and rinsed in EtOH. All fly organs were placed separately in sterile cryotubes and labeled with fly accession number, fly organ, dissection date, and dissector identification. Samples were stored at -80° C until they were sent to the Alkek Center for Metagenomics and Microbiome Research at Baylor College of Medicine for sequencing.

Sample Processing and Sequencing

The bacterial communities for all fly parts and human swab samples were assessed by genetic identification employing next-generation techniques. Amplification of 16S ribosomal RNA (rRNA) gene amplification, and Illumina sequencing were conducted at the Alkek Center for Metagenomics and Microbiome Research at Baylor College of Medicine following protocols benchmarked as part of the Human Microbiome Project (24). DNA was extracted from the fly organs or human swabs using the MoBio PowerSoil DNA isolation kit following manufacturer's instructions. Negative controls that were included in the extraction process did not show evidence of amplification following gel electrophoresis, and were thus not included in sequencing. 16S rRNA gene sequencing was performed using Illumina MiSeq with barcoded primers targeting the V4 region: GGACTACHVGGGTWTCTAAT and GTGCCAGCMGCCGCGGTAA.

Data Cleaning and Analysis

Data cleaning and most analyses were performed using the microbiome analysis package, QIIME2 (56). All raw data files were imported into QIIME2 version 2021.4 using EMPPairedEndSequences file types, except for one sequencing pool in which only the already merged reads were available and thus the EMPSingleEndSequences file type was used. Each pool was demultiplexed using the demux plugin, and all forward and reverse reads were merged using VSEARCH (57). Quality filtering using the q-score was performed using the quality-filter plugin (58) and the default parameters. Denoising to create amplicon sequence variants (ASVs) was performed using the denoise-16S method in the deblur (59) plugin with a left trim length of 0 and a right trim length of 250 (i.e., the entire sequences were kept for all pools due to high quality). All feature tables and representative sequence files were merged using the feature-table merge and merge-seqs methods, and all subsequent analyses were performed on merged data.

Taxonomy was assigned using a Naive Bayes classifier trained on SILVA 138 99% OTUs from the 515F/806R region of sequences (60–62). Taxa assigned to chloroplasts and mitochondria were filtered from the dataset. To visualize the observed taxa, the barplot visualizer in the taxa plugin was used. These data were exported to a .csv file and imported into R software 4.0.3 (63) for bubble chart visualization (see below for packages used). To create the bubble chart, taxa relative abundances were first calculated within the entire dataset, and the top 50 taxa from this table were visualized. A phylogenetic tree was created using the fragment-insertion plugin (64–67) and the SEPP (68) method using the SILVA 128 SEPP reference database. For simplicity, duplicate seasonal placements (i.e., both winter and both spring placements) were combined for group analyses. Core metric phylogenetic analyses were performed using the insertion tree and with a rarefying depth of 5,937 reads per sample as an optimal balance for retaining observed features and samples. From this pipeline, the unweighted UniFrac (69) and weighted UniFrac metrics were used for assessing beta diversity. To compare groups, the permutational multivariate analysis of variance (PERMANOVA) (70) test output from the beta-group-significance visualizer in the diversity plugin was used, with the pseudo-F value used to estimate effect size and the p-value used to

assess significance (or q-value for pairwise comparisons). Core taxa within fly and human samples were identified using the core-features visualizer in the feature-table plugin with the default setting of 0.5 as the minimum fraction of samples that a feature must be observed in to be considered a core feature.

Differentially abundant taxa between groups were identified using analysis of composition of microbiomes (ANCOM) (71) in the composition plugin. To do pairwise ANCOM analyses, feature tables containing only two categories within a group (e.g., tarsi and labellum, tarsi and oocyte, labellum and oocyte) were created. ANCOM was applied to each table, and the results between tables were compared. This method was also used for pairwise ANCOM analyses between seasonal placements.

For source tracking, separate feature tables were created for each seasonal placement and each table was exported from QIIME2 as a BIOM 2.1.0 table. These tables were used to generate per season source predictions with the Gibbs function in SourceTracker2 (72) in which fly organs were used as sources and human sample types were used as sinks. Since rarefied BIOM tables were used, source rarefaction depth and sink rarefaction depth were 0 in all cases.

All visualizations were made in R software 4.0.3 (63) using the following packages: ggplot2 (73), reshape and reshape2 (74), ggpubr, qiime2R (75), tidyverse (76), ggpattern, plyr (77), and sf (78).

Data Availability

All data are available in QIITA study 13301 and all analysis and visualization code files are provided at https://github.com/Metcalf-Lab/fly_human_2021_Deel.

REFERENCES

1. A. A. Vass, Others, Beyond the grave-understanding human decomposition. *Microbiol. Today*. 28, 190–193 (2001).
2. E. B. Mondor, M. N. Tremblay, J. K. Tomberlin, E. M. Benbow, A. M. Tarone, T. L. Crippen, The ecology of carrion decomposition. *Nat Educ Knowledge*. 3, 21 (2012).
3. D. W. Hopkins, in *Soil analysis in forensic taphonomy* (CRC Press, 2008), pp. 65–78.
4. J. L. Metcalf, L. Wegener Parfrey, A. Gonzalez, C. L. Lauber, D. Knights, G. Ackermann, G. C. Humphrey, M. J. Gebert, W. Van Treuren, D. Berg-Lyons, K. Keepers, Y. Guo, J. Bullard, N. Fierer, D. O. Carter, R. Knight, A microbial clock provides an accurate estimate of the postmortem interval in a mouse model system. *Elife*. 2, e01104 (2013).
5. J. L. Metcalf, Z. Z. Xu, S. Weiss, S. Lax, W. Van Treuren, E. R. Hyde, S. J. Song, A. Amir, P. Larsen, N. Sangwan, D. Haarmann, G. C. Humphrey, G. Ackermann, L. R. Thompson, C. Lauber, A. Bibat, C. Nicholas, M. J. Gebert, J. F. Petrosino, S. C. Reed, J. A. Gilbert, A. M. Lynne, S. R. Bucheli, D. O. Carter, R. Knight, Microbial community assembly and metabolic function during mammalian corpse decomposition. *Science*. 351, 158–162 (2016).
6. A. Galloway, W. H. Birkby, A. M. Jones, T. E. Henry, B. O. Parks, Decay rates of human remains in an arid environment. *J. Forensic Sci.* 34, 607–616 (1989).
7. H. Deel, S. Bucheli, A. Belk, S. Ogden, A. Lynne, D. O. Carter, R. Knight, J. L. Metcalf, in *Microbial Forensics (Third Edition)*, B. Budowle, S. Schutzer, S. Morse, Eds. (Academic Press, 2020), pp. 171–191.
8. V. Mesli, C. Neut, V. Hedouin, Postmortem bacterial translocation. *Forensic microbiology*, 192–211 (2017).

9. Human Microbiome Project Consortium, Structure, function and diversity of the healthy human microbiome. *Nature*. **486**, 207–214 (2012).
10. J. L. Pechal, C. J. Schmidt, H. R. Jordan, M. E. Benbow, A large-scale survey of the postmortem human microbiome, and its potential to provide insight into the living health condition. *Sci. Rep.* **8**, 5724 (2018).
11. J. K. Tomberlin, T. L. Crippen, A. M. Tarone, M. F. B. Chaudhury, B. Singh, J. A. Cammack, R. P. Meisel, A Review of Bacterial Interactions With Blow Flies (Diptera: Calliphoridae) of Medical, Veterinary, and Forensic Importance. *Ann. Entomol. Soc. Am.* **110**, 19–36 (2016).
12. C. P. Campobasso, G. Di Vella, F. Introna, Factors affecting decomposition and Diptera colonization. *Forensic Sci. Int.* **120**, 18–27 (2001).
13. A. C. M. Junqueira, A. Ratan, E. Acerbi, D. I. Drautz-Moses, B. N. V. Premkrishnan, P. I. Costea, B. Linz, R. W. Purbojati, D. F. Paulo, N. E. Gaultier, P. Subramanian, N. A. Hasan, R. R. Colwell, P. Bork, A. M. L. Azeredo-Espin, D. A. Bryant, S. C. Schuster, The microbiomes of blowflies and houseflies as bacterial transmission reservoirs. *Sci. Rep.* **7**, 16324 (2017).
14. B. Singh, T. L. Crippen, L. Zheng, A. T. Fields, Z. Yu, Q. Ma, T. K. Wood, S. E. Dowd, M. Flores, J. K. Tomberlin, A. M. Tarone, A metagenomic assessment of the bacteria associated with *Lucilia sericata* and *Lucilia cuprina* (Diptera: Calliphoridae). *Appl. Microbiol. Biotechnol.* **99**, 869–883 (2015).
15. S. Bahrndorff, N. de Jonge, H. Skovgård, J. L. Nielsen, Bacterial Communities Associated with Houseflies (*Musca domestica* L.) Sampled within and between Farms. *PLoS One*. **12**, e0169753 (2017).
16. N. Maleki-Ravasan, N. Ahmadi, Z. Soroushzadeh, A. A. Raz, S. Zakeri, N. Dinparast Djadid, New Insights Into Culturable and Unculturable Bacteria Across the Life History of Medicinal Maggots *Lucilia sericata* (Meigen) (Diptera: Calliphoridae). *Front. Microbiol.* **11**, 505 (2020).

17. N. E. Gasz, M. J. Geary, S. L. Doggett, M. L. Harvey, Bacterial association observations in *Lucilia sericata* and *Lucilia cuprina* organs through 16S rRNA gene sequencing. *Appl. Microbiol. Biotechnol.* **105**, 1091–1106 (2021).
18. D. Wohlfahrt, M. S. Woolf, B. Singh, A survey of bacteria associated with various life stages of primary colonizers: *Lucilia sericata* and *Phormia regina*. *Sci. Justice.* **60**, 173–179 (2020).
19. S. Wanaratana, S. Panyim, S. Pakpinyo, The potential of house flies to act as a vector of avian influenza subtype H5N1 under experimental conditions. *Med. Vet. Entomol.* **25**, 58–63 (2011).
20. T. Chaiwong, T. Srivoramas, P. Sueabsamran, K. Sukontason, M. R. Sanford, K. L. Sukontason, The blow fly, *Chrysomya megacephala*, and the house fly, *Musca domestica*, as mechanical vectors of pathogenic bacteria in Northeast Thailand. *Trop. Biomed.* **31**, 336–346 (2014).
21. G. Daeschlein, K. Reese, M. Napp, R. Spitzmueller, P. Hinz, M. Juenger, A. Kramer, Maggots as potential vector for pathogen transmission and consequences for infection control in waste management. *GMS Hyg Infect Control.* **10**, Doc07 (2015).
22. Y. Uriel, R. Gries, L. Tu, C. Carroll, H. Zhai, M. Moore, G. Gries, The fly factor phenomenon is mediated by interkingdom signaling between bacterial symbionts and their blow fly hosts. *Insect Sci.* **27**, 256–265 (2020).
23. M. E. Benbow, A. J. Lewis, J. K. Tomberlin, J. L. Pechal, Seasonal necrophagous insect community assembly during vertebrate carrion decomposition. *J. Med. Entomol.* **50**, 440–450 (2013).
24. P. J. Turnbaugh, R. E. Ley, M. Hamady, C. M. Fraser-Liggett, R. Knight, J. I. Gordon, The human microbiome project. *Nature.* **449**, 804–810 (2007).
25. N. A. Bergren, R. C. Kading, The Ecological Significance and Implications of Transovarial Transmission among the Vector-Borne Bunyaviruses: A Review. *Insects.* **9** (2018), doi:10.3390/insects9040173.

26. J. G. Stoffolano, Fly foregut and transmission of microbes. *Adv. In Insect Phys.* **57**, 27–95 (2019).
27. A. E. Douglas, Multiorganismal insects: diversity and function of resident microorganisms. *Annu. Rev. Entomol.* **60**, 17–34 (2015).
28. K. A. Bernard, G. Funke, Corynebacterium. *Bergey's Manual of Systematics of Archaea and Bacteria* (2015), pp. 1–70.
29. N. Wiktorczyk-Kapischke, K. Skowron, J. Kwiecińska-Piróg, A. Białucha, E. Wałęcka-Zacharska, K. Grudlewska-Buda, Z. Kraszewska, E. Gospodarek-Komkowska, Flies as a potential vector of selected alert pathogens in a hospital environment. *Int. J. Environ. Health Res.*, 1–20 (2021).
30. J.-H. Kim, W. Kim, *Tumebacillus soli* sp. nov., isolated from non-rhizosphere soil. *Int. J. Syst. Evol. Microbiol.* **66**, 2192–2197 (2016).
31. R. R. S. Manoj, M. S. Latrofa, S. Epis, D. Otranto, Wolbachia: endosymbiont of onchocercid nematodes and their vectors. *Parasit. Vectors.* **14**, 245 (2021).
32. A. Willems, in *The Prokaryotes: Alphaproteobacteria and Betaproteobacteria*, E. Rosenberg, E. F. DeLong, S. Lory, E. Stackebrandt, F. Thompson, Eds. (Springer Berlin Heidelberg, Berlin, Heidelberg, 2014), pp. 777–851.
33. T. Hofstad, I. Olsen, E. R. Eribe, E. Falsen, M. D. Collins, P. A. Lawson, *Dysgonomonas* gen. nov. to accommodate *Dysgonomonas gadei* sp. nov., an organism isolated from a human gall bladder, and *Dysgonomonas capnocytophagoides* (formerly CDC group DF-3). *Int. J. Syst. Evol. Microbiol.* **50 Pt 6**, 2189–2195 (2000).
34. P. A. Lawson, E. Falsen, E. Inganäs, R. S. Weyant, M. D. Collins, *Dysgonomonas mossii* sp. nov., from human sources. *Syst. Appl. Microbiol.* **25**, 194–197 (2002).

35. P. A. Lawson, P. Carlson, S. Wernersson, E. R. B. Moore, E. Falsen, *Dysgonomonas hofstadii* sp. nov., isolated from a human clinical source. *Anaerobe*. **16**, 161–164 (2010).
36. X. Sun, Y. Yang, N. Zhang, Y. Shen, J. Ni, Draft Genome Sequence of *Dysgonomonas macrotermitis* Strain JCM 19375T, Isolated from the Gut of a Termite. *Genome Announc.* **3** (2015), doi:10.1128/genomeA.00963-15.
37. R.-G. Zhang, X. Tan, Y. Liang, T.-Y. Meng, H.-Z. Liang, J. Lv, Description of *Chishuiella changwenlii* gen. nov., sp. nov., isolated from freshwater, and transfer of *Wautersiella falsenii* to the genus *Empedobacter* as *Empedobacter falsenii* comb. nov. *Int. J. Syst. Evol. Microbiol.* **64**, 2723–2728 (2014).
38. J. R. Wozniak, M. L. Thies, J. A. Bytheway, W. I. Lutterschmidt, A hydrologic retention system and water quality monitoring program for a human decomposition research facility: concept and design. *J. Forensic Sci.* **60**, 54–60 (2015).
39. E. R. Hyde, D. P. Haarmann, J. F. Petrosino, A. M. Lynne, S. R. Bucheli, Initial insights into bacterial succession during human decomposition. *Int. J. Legal Med.* **129**, 661–671 (2015).
40. T. Wei, R. Ishida, K. Miyanaga, Y. Tanji, Seasonal variations in bacterial communities and antibiotic-resistant strains associated with green bottle flies (Diptera: Calliphoridae). *Appl. Microbiol. Biotechnol.* **98**, 4197–4208 (2014).
41. K. Reed, S. B. Reynolds, C. Smith, The First Case of *Ignatzschineria ureiclastica*/larvae in the United States Presenting as a Myiatic Wound Infection. *Cureus*. **13**, e14518 (2021).
42. Barker Heather S., Snyder James W., Hicks Adam B., Yanoviak Stephen P., Southern Paul, Dhakal Bijaya K., Ghimire Giri R., Couturier Marc R., Forbes B. A., First Case Reports of *Ignatzschineria* (*Schineria*) *indica* Associated with Myiasis. *J. Clin. Microbiol.* **52**, 4432–4434 (2014).

43. L. T. DiFranza, M. K. Annavajhala, A.-C. Uhlemann, D. A. Green, The brief case: A maggot mystery-Ignatzschineria larvae sepsis secondary to an infested wound. *J. Clin. Microbiol.* **59** (2021), doi:10.1128/JCM.02279-20.
44. T. B. Lysaght, M. E. Wooster, P. C. Jenkins, L. G. Koniaris, Myiasis-induced sepsis: a rare case report of Wohlfahrtiimonas chitiniclastica and Ignatzschineria indica bacteremia in the continental United States. *Medicine* . **97**, e13627 (2018).
45. C. Le Brun, M. Gombert, S. Robert, E. Mercier, P. Lanotte, Association of Necrotizing Wounds Colonized by Maggots with Ignatzschineria-Associated Septicemia. *Emerg. Infect. Dis.* **21**, 1881–1883 (2015).
46. D. Rodríguez-Zúñiga, N. González-Galiano, Á. Leal-Negrado, E. Hidalgo-Pérez, First case of sepsis by Ignatzschineria in Spain associated with myiasis. Description of a case and review of the literature. *Enferm. Infecc. Microbiol. Clin.* **37**, 64–65 (2019).
47. H. Muse, R. L. Jenkins, M. B. Oliver, S. Kim, R. L. Grantier, B. K. Malhotra, J. J. Parham, K. R. Stover, A Case of Ignatzschineria indica Bacteremia following Maggot Colonization. *Case Rep. Infect. Dis.* **2017** (2017), doi:10.1155/2017/3698124.
48. E. H. Yang, K. Poon, P. Pillutla, M. J. Budoff, J. Chung, Pulmonary embolus caused by Suttonella indologenes prosthetic endocarditis in a pulmonary homograft. *J. Am. Soc. Echocardiogr.* **24**, 592.e1–3 (2011).
49. M. Riegler, S. L. O’Neill, in *The Prokaryotes: Volume 5: Proteobacteria: Alpha and Beta Subclasses*, M. Dworkin, S. Falkow, E. Rosenberg, K.-H. Schleifer, E. Stackebrandt, Eds. (Springer New York, New York, NY, 2006), pp. 547–561.
50. D. O. Carter, D. Yellowlees, M. Tibbett, Cadaver decomposition in terrestrial ecosystems. *Naturwissenschaften.* **94**, 12–24 (2007).

51. K. Afra, K. Laupland, J. Leal, T. Lloyd, D. Gregson, Incidence, risk factors, and outcomes of *Fusobacterium* species bacteremia. *BMC Infect. Dis.* **13**, 264 (2013).
52. S. Fatchurochim, C. J. Geden, R. C. Axtell, Filth fly (Diptera) oviposition and larval development in poultry manure of various moisture levels. *J. Entomol. Sci.* **24** (1989), doi:10.18474/0749-8004-24.2.224.
53. N. K. Lindgren, M. S. Sisson, A. D. Archambeault, B. C. Rahlwes, J. R. Willett, S. R. Bucheli, Four Forensic Entomology Case Studies: Records and Behavioral Observations on Seldom Reported Cadaver Fauna With Notes on Relevant Previous Occurrences and Ecology. *J. Med. Entomol.* **52**, 143–150 (2015).
54. T. Whitworth, Keys To the Genera and Species of Blow Flies (Diptera: Calliphoridae) of America North of Mexico. *Proc. Entomol. Soc. Wash.* **108**, 689–725 (2006).
55. . . Klots Alexander B. (Alexander Barrett), A Field Guide to the Insects of America, North of Mexico by Donald J. Borror, Richard E. White. *J. N. Y. Entomol. Soc.* **78**, 192–192 (1970).
56. E. Bolyen, J. R. Rideout, M. R. Dillon, N. A. Bokulich, C. C. Abnet, G. A. Al-Ghalith, H. Alexander, E. J. Alm, M. Arumugam, F. Asnicar, Y. Bai, J. E. Bisanz, K. Bittinger, A. Brejnrod, C. J. Brislawn, C. T. Brown, B. J. Callahan, A. M. Caraballo-Rodríguez, J. Chase, E. K. Cope, R. Da Silva, C. Diener, P. C. Dorrestein, G. M. Douglas, D. M. Durall, C. Duvall, C. F. Edwardson, M. Ernst, M. Estaki, J. Fouquier, J. M. Gauglitz, S. M. Gibbons, D. L. Gibson, A. Gonzalez, K. Gorlick, J. Guo, B. Hillmann, S. Holmes, H. Holste, C. Huttenhower, G. A. Huttley, S. Janssen, A. K. Jarmusch, L. Jiang, B. D. Kaehler, K. B. Kang, C. R. Keefe, P. Keim, S. T. Kelley, D. Knights, I. Koester, T. Kosciulek, J. Kreps, M. G. I. Langille, J. Lee, R. Ley, Y.-X. Liu, E. Loftfield, C. Lozupone, M. Maher, C. Marotz, B. D. Martin, D. McDonald, L. J. McIver, A. V. Melnik, J. L. Metcalf, S. C. Morgan, J. T. Morton, A. T. Naimey, J. A. Navas-Molina, L. F. Nothias, S. B. Orchanian, T. Pearson, S. L. Peoples, D. Petras, M. L. Preuss, E. Priesse, L. B. Rasmussen, A. Rivers, M. S. Robeson, P. Rosenthal, N. Segata, M. Shaffer, A. Shiffer, R. Sinha, S. J. Song, J. R. Spear, A. D. Swafford, L. R. Thompson, P. J. Torres, P. Trinh, A. Tripathi, P. J.

- Turnbaugh, S. Ul-Hasan, J. J. J. van der Hooft, F. Vargas, Y. Vázquez-Baeza, E. Vogtmann, M. von Hippel, W. Walters, Y. Wan, M. Wang, J. Warren, K. C. Weber, C. H. D. Williamson, A. D. Willis, Z. Z. Xu, J. R. Zaneveld, Y. Zhang, Q. Zhu, R. Knight, J. G. Caporaso, Reproducible, interactive, scalable and extensible microbiome data science using QIIME 2. *Nat. Biotechnol.* (2019), doi:10.1038/s41587-019-0209-9.
57. T. Rognes, T. Flouri, B. Nichols, C. Quince, F. Mahé, VSEARCH: a versatile open source tool for metagenomics. *PeerJ.* **4**, e2584 (2016).
58. N. A. Bokulich, S. Subramanian, J. J. Faith, D. Gevers, J. I. Gordon, R. Knight, D. A. Mills, J. G. Caporaso, Quality-filtering vastly improves diversity estimates from Illumina amplicon sequencing. *Nat. Methods.* **10**, 57–59 (2013).
59. A. Amir, D. McDonald, J. A. Navas-Molina, E. Kopylova, J. T. Morton, Z. Zech Xu, E. P. Kightley, L. R. Thompson, E. R. Hyde, A. Gonzalez, R. Knight, Deblur Rapidly Resolves Single-Nucleotide Community Sequence Patterns. *mSystems.* **2** (2017), doi:10.1128/mSystems.00191-16.
60. N. Bokulich, M. Robeson, M. Dillon, M. Ziemski, B. Kaehler, D. O'Rourke, *bokulich-lab/RESCRIPT: 2021.8.0.dev0* (2021; <https://zenodo.org/record/4811136>).
61. N. A. Bokulich, B. D. Kaehler, J. R. Rideout, M. Dillon, E. Bolyen, R. Knight, G. A. Huttley, J. Gregory Caporaso, Optimizing taxonomic classification of marker-gene amplicon sequences with QIIME 2's q2-feature-classifier plugin. *Microbiome.* **6**, 90 (2018).
62. C. Quast, E. Pruesse, P. Yilmaz, J. Gerken, T. Schweer, P. Yarza, J. Peplies, F. O. Glöckner, The SILVA ribosomal RNA gene database project: improved data processing and web-based tools. *Nucleic Acids Res.* **41**, D590–6 (2013).
63. R Core Team, R: A Language and Environment for Statistical Computing (2017) (available at <https://www.R-project.org/>).

64. S. R. Eddy, Accelerated Profile HMM Searches. *PLoS Comput. Biol.* **7**, e1002195 (2011).
65. S. Janssen, D. McDonald, A. Gonzalez, J. A. Navas-Molina, L. Jiang, Z. Z. Xu, K. Winker, D. M. Kado, E. Orwoll, M. Manary, S. Mirarab, R. Knight, Phylogenetic Placement of Exact Amplicon Sequences Improves Associations with Clinical Information. *mSystems*. **3** (2018), doi:10.1128/mSystems.00021-18.
66. F. A. Matsen, R. B. Kodner, E. V. Armbrust, pplacer: linear time maximum-likelihood and Bayesian phylogenetic placement of sequences onto a fixed reference tree. *BMC Bioinformatics*. **11**, 538 (2010).
67. F. A. Matsen, N. G. Hoffman, A. Gallagher, A. Stamatakis, A format for phylogenetic placements. *PLoS One*. **7**, e31009 (2012).
68. S. Mirarab, N. Nguyen, T. Warnow, SEPP: SATé-enabled phylogenetic placement. *Pac. Symp. Biocomput.*, 247–258 (2012).
69. C. Lozupone, R. Knight, UniFrac: a new phylogenetic method for comparing microbial communities. *Appl. Environ. Microbiol.* **71**, 8228–8235 (2005).
70. M. J. Anderson, Permutational Multivariate Analysis of Variance (PERMANOVA). *Wiley StatsRef: Statistics Reference Online*, 1–15 (2017).
71. S. Mandal, W. Van Treuren, R. A. White, M. Eggesbø, R. Knight, S. D. Peddada, Analysis of composition of microbiomes: a novel method for studying microbial composition. *Microb. Ecol. Health Dis.* **26**, 27663 (2015).
72. D. Knights, J. Kuczynski, E. S. Charlson, J. Zaneveld, M. C. Mozer, R. G. Collman, F. D. Bushman, R. Knight, S. T. Kelley, Bayesian community-wide culture-independent microbial source tracking. *Nat. Methods*. **8**, 761–763 (2011).
73. A. Kassambara, “ggplot2” Based Publication Ready Plots (2020) (available at <https://cran.r-project.org/web/packages/ggpubr/ggpubr.pdf>).

74. H. Wickham, Reshaping Data with the reshape Package. *Journal of Statistical Software, Articles*. **21**, 1–20 (2007).
75. J. E. Bisanz, qiime2R: Importing QIIME2 artifacts and associated data into R sessions (2018), (available at <https://github.com/jbisanz/qiime2R>).
76. H. Wickham, M. Averick, J. Bryan, W. Chang, L. D. McGowan, R. François, G. Grolemund, A. Hayes, L. Henry, J. Hester, Others, Welcome to the Tidyverse. *Journal of Open Source Software*. **4**, 1686 (2019).
77. H. Wickham, The Split-Apply-Combine Strategy for Data Analysis. *Journal of Statistical Software, Articles*. **40**, 1–29 (2011).
78. E. Pebesma, Simple features for R: Standardized support for spatial vector data. *R J.* **10**, 439 (2018).

CHAPTER 4: CONCLUSIONS AND FUTURE DIRECTIONS

Human decomposition is a complex process that is subject to many environmental influences. The progression of decomposition through the fresh, early decomposition, advanced decomposition, and skeletonization stages is partially driven by the actions of microbes. Chapter 1 provides background information about this succession of microbes as well as how high throughput sequencing may be used to develop microbial-based models for estimating postmortem interval. Importantly, it describes how these techniques are used with bone microbiome data for developing PMI models in the advanced decomposition and skeletonization stages of decomposition.

In Chapter 2, some of the methods described in Chapter 1 are implemented. Using microbial succession data in bone, postmortem interval was estimated within +/- 34 days over a 1-9-month time frame of decomposition. Typically, anthropologists can estimate postmortem interval of skeletal remains with errors ranging from months to years. Therefore, the approximate error of one month as described in this dissertation seems like a promising start to contributing new PMI estimation methods to the forensic sciences. There are several ways that this model may be refined to increase accuracy in the future. First, it is important to test the optimal sampling frequency for obtaining the lowest mean absolute error (i.e., would sampling more frequently than every three weeks more accurately estimate PMI?). Second, developing a model using samples collected within all seasons of the year is critical for understanding if PMI models need to be seasonally specific. Finally, future work should include testing which time frame of decomposition that bone is most useful for when developing PMI models (e.g., is bone most predictive of PMI between 1-9 months or 12-24 months of decomposition?). These are all ongoing questions that will be critical to investigate before incorporating this method into the criminal justice system.

Chapter 3 builds upon some of the concepts described in Chapter 1 by investigating the influence of the fly microbiome on the human cadaver decomposer microbiome assembly. During the first 48 hours of decomposition, the individual human microbiome transitions to a decomposer microbiome that is consistent between human remains. When flies interact with the remains during this time frame, it is

likely that there is a mechanical transfer of microbes onto the cadaver. Results of this study showed that the fly labellum and tarsi act as substantial microbial sources of the human decomposer microbiome, with source contributions varying between seasons. This conclusion provides insight into the ecological dynamics of human cadaver microbial community assembly. In the future, it may be interesting to investigate whether flies have a similar influence on the human decomposer microbiome within different geographies. Additionally, it would be useful to conduct another source tracking experiment that investigates the source of the fly microbiome. This may provide insight into whether microbes found on the flies are due to natural infections or if the flies acquire them from the surrounding environment (i.e., bodies of water, vegetation, soil, etc.).

Overall, this dissertation contributes to the field of forensic sciences by furthering methods for estimating postmortem interval and providing insight into the influence of flies on human cadaver microbial community assembly.

APPENDIX A: CHAPTER 2 SUPPLEMENTARY MATERIAL

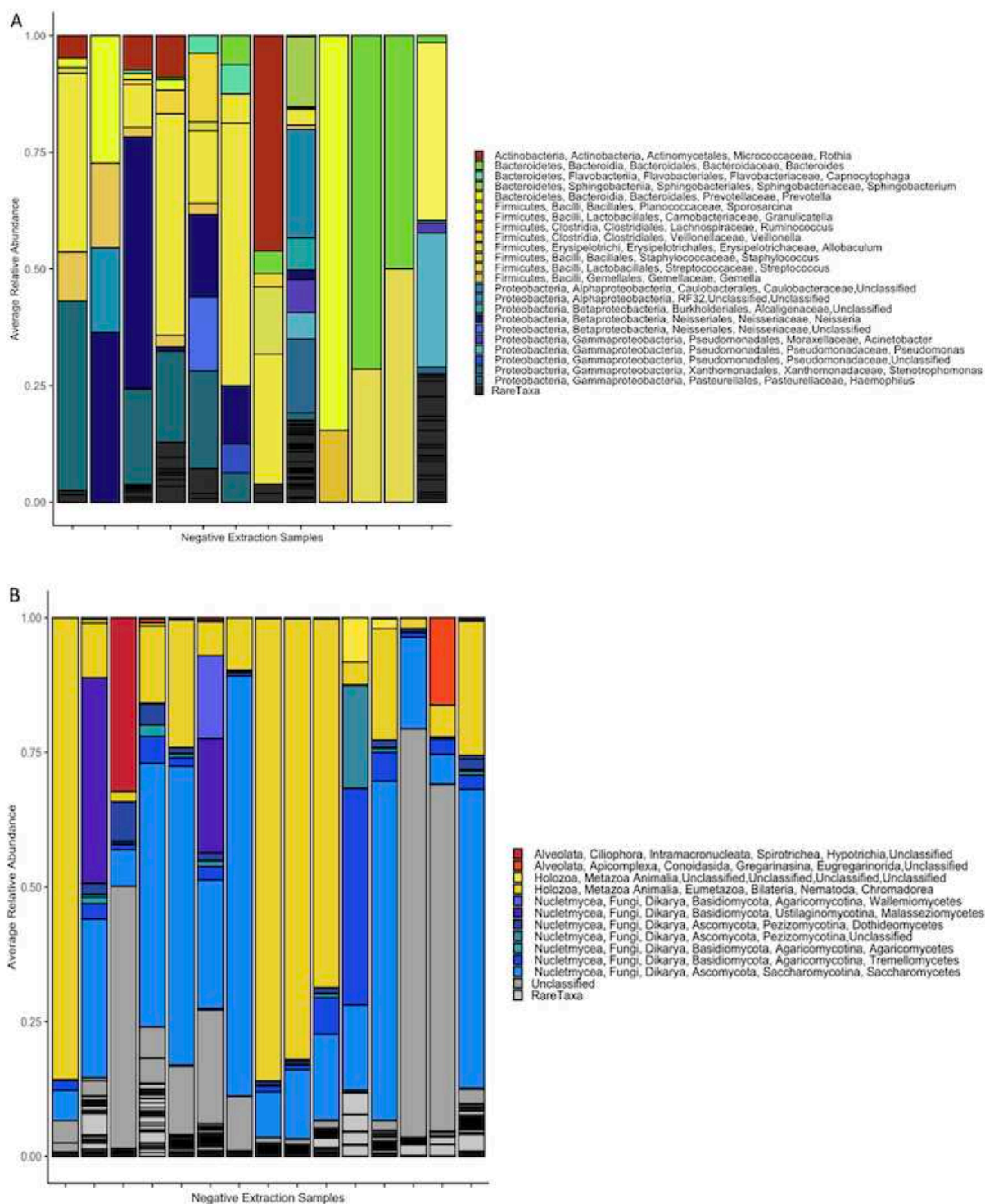


Figure S2.1. Taxonomic composition of negative controls of 16S rRNA (A) and 18S rRNA (B) datasets. Rare taxa include those with a mean relative abundance of 0.005 or lower in both plots. We included 15 negative extraction controls, of which 12 had enough detectable signal to be included in the sequencing pool of the 16S rRNA data. These 12 samples (A) averaged 387 reads, ranging from 4 - 2,232 reads. In

the 16S rRNA data (B), there was an average of 12,187 reads per sample, ranging from 1,189 - 39,663 reads.

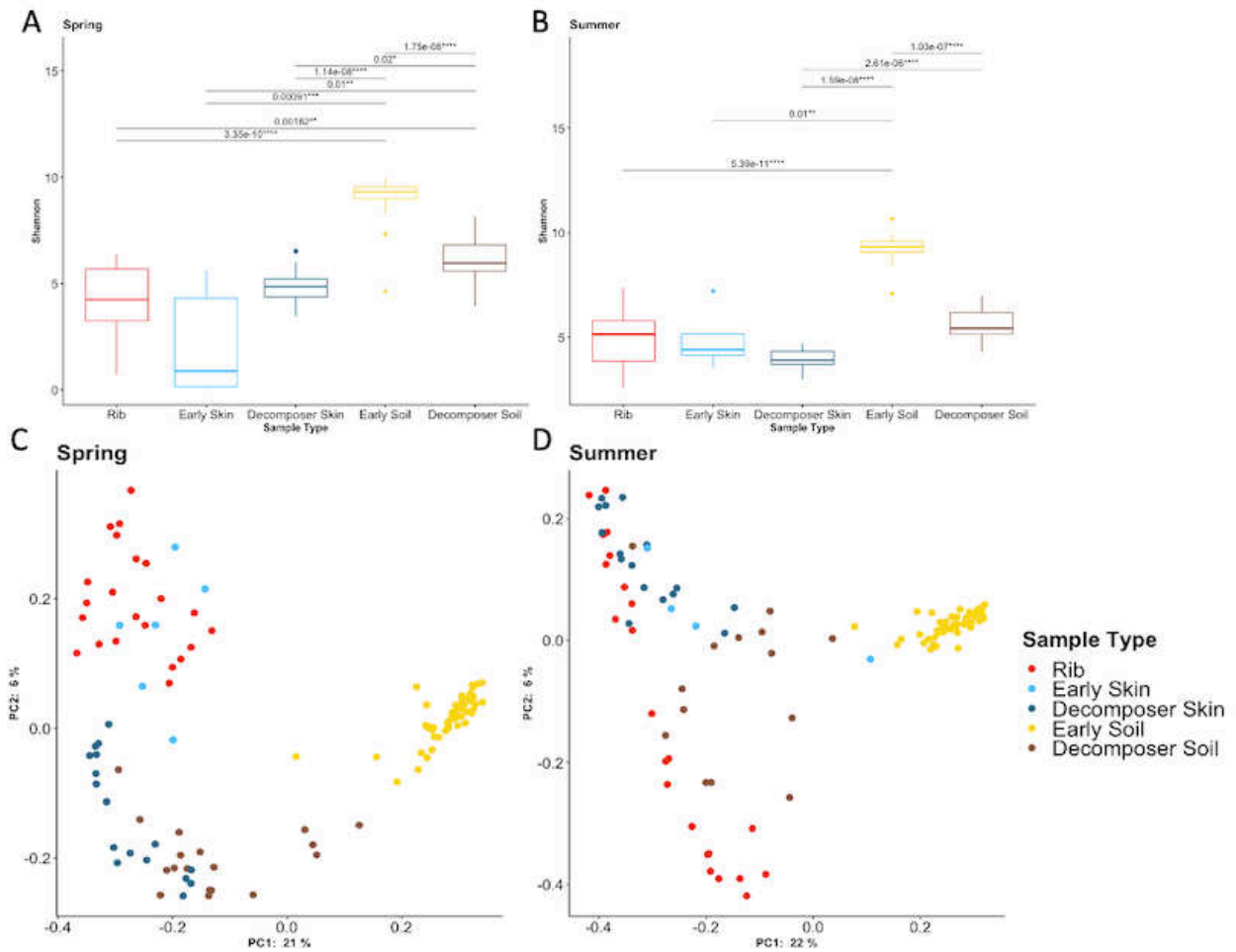


Figure S2.2. 16S rRNA alpha diversity of the rib and source communities in the spring (A) and summer (B) placements, measured by Shannon index. Principal Coordinates Analysis of rib and potential source community 16S rRNA data using the unweighted UniFrac distance metric in the spring (C) and summer (D) placements.

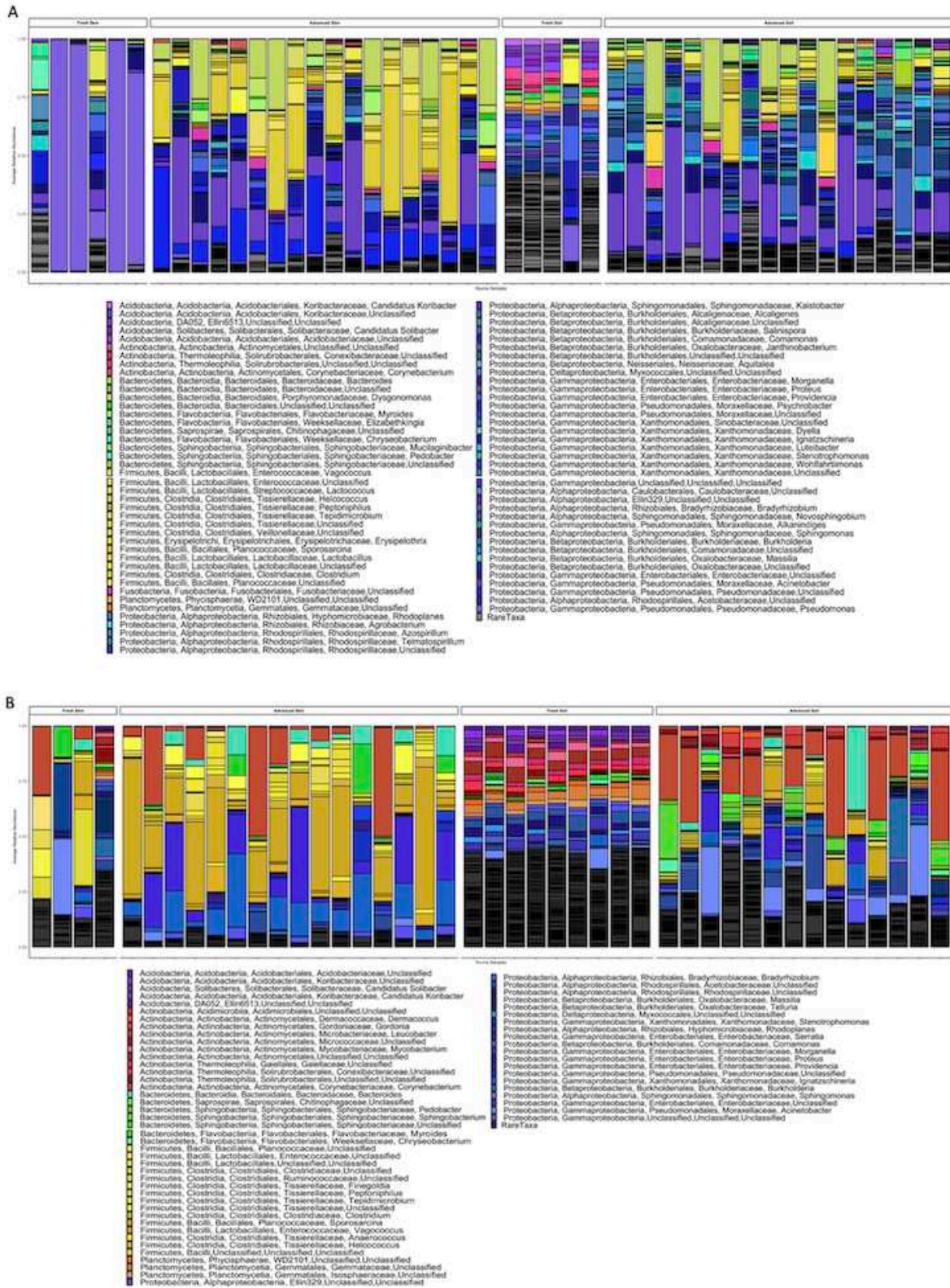


Figure S2.3. Taxa plots of the 16S rRNA spring (A) and summer (B) placement source data collected from days 1, 2, 19, 20, and 21 of decomposition (not including soil controls, see Figure S5 for these data).

Rare taxa include those with a mean relative abundance of 0.002 or lower in the spring and 0.003 or lower in the summer.

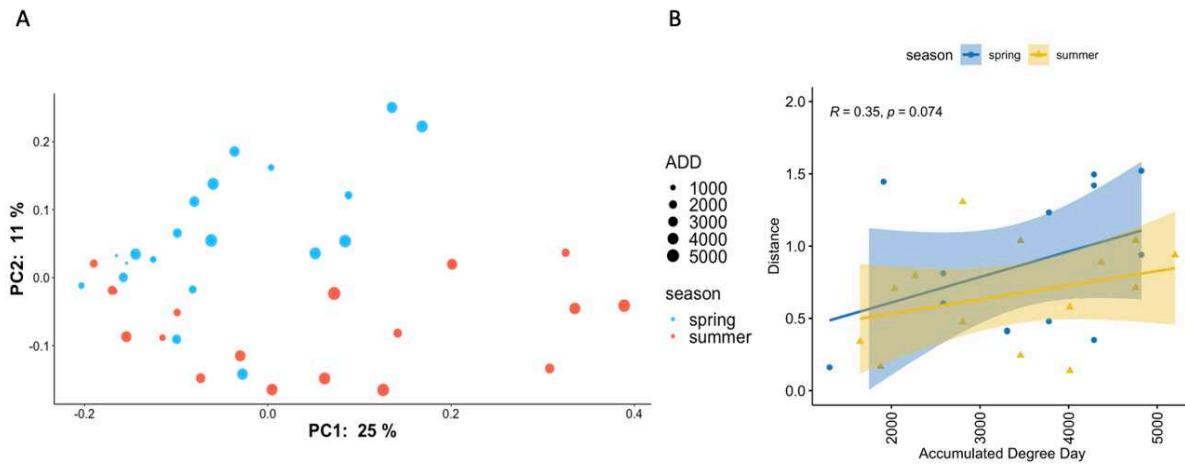


Figure S2.4. (A) A measure of beta diversity of 18S rRNA data using the unweighted UniFrac distance metric (PERMANOVA between seasons $p = 0.004$, pseudo-F (effect size) = 3.07, $df = 1$ with 999 permutations). (B) A measure of beta diversity of 18S rRNA data using the weighted UniFrac distance metric. Shaded areas around the line represent 95% confidence intervals. Linear mixed effects across ADD $p = 0.109$.

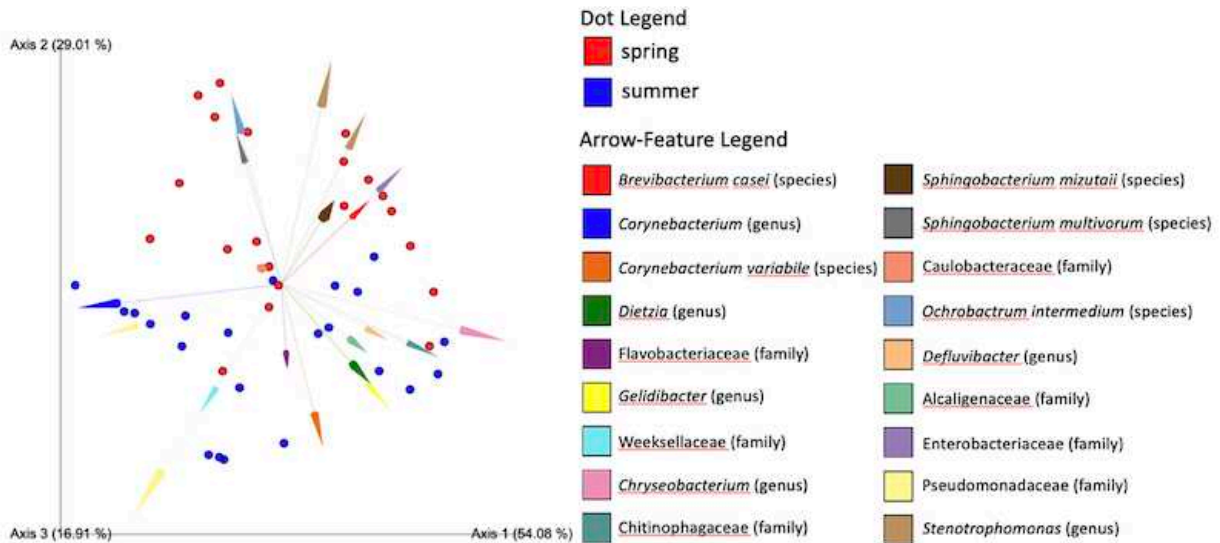


Figure S2.5. Principal Coordinates Analysis of the rib sample 16S rRNA data using the Aitchison distance metric from bodies placed in spring and summer.

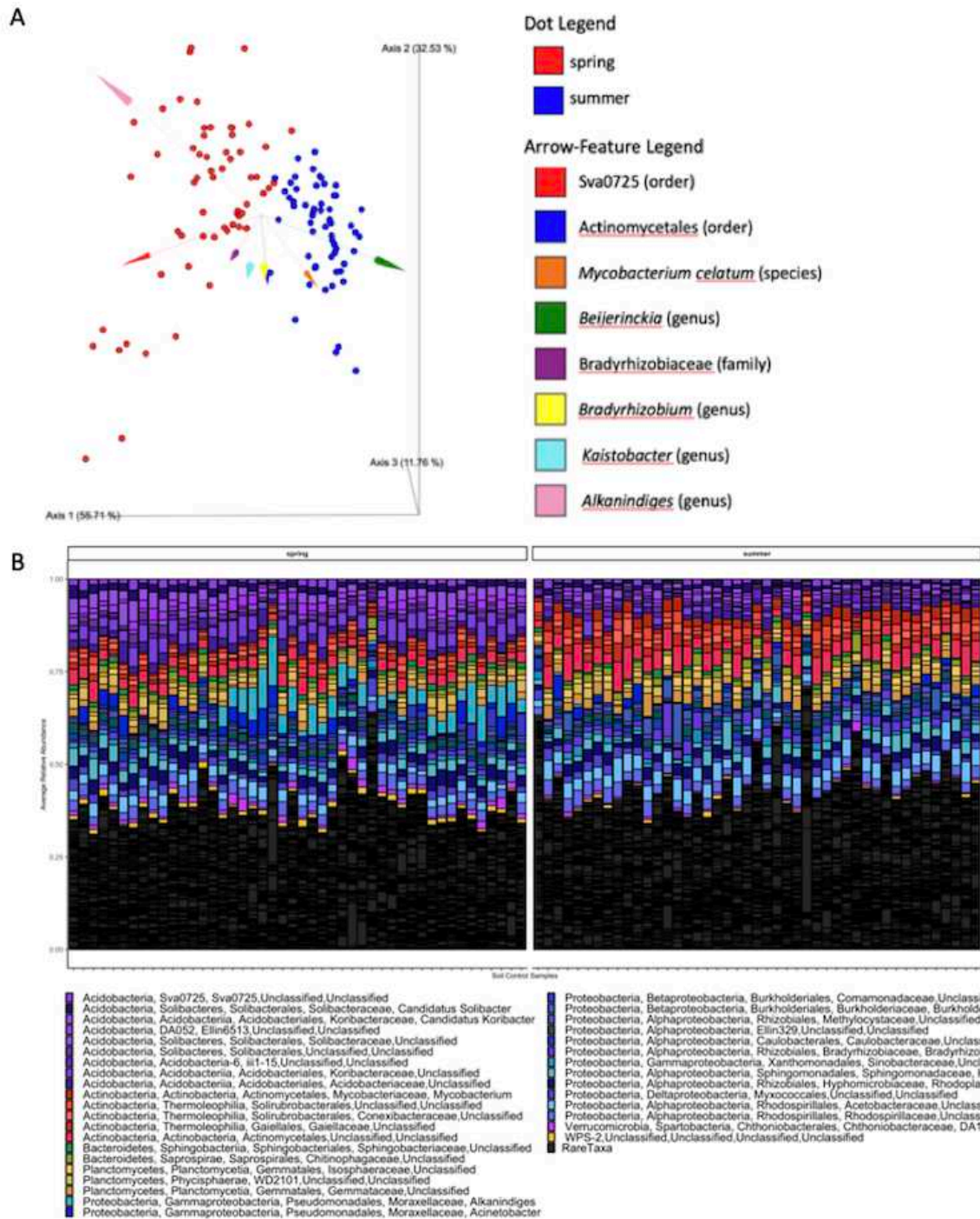


Figure S2.6. (A) Principal Coordinates Analysis of the 16S rRNA spring and summer placement soil control communities using the Aitchison distance metric. Features driving clustering differences between seasons are labeled, PERMANOVA between seasons $p = 0.001$, pseudo-F (effect size) = 68.72, $df = 1$ with 999 permutations. (B) Taxa plots of the 16S rRNA data of soil controls collected within the first 21 days of decomposition in the spring and summer placements. Rare taxa include those with a mean relative abundance of 0.008 or lower.

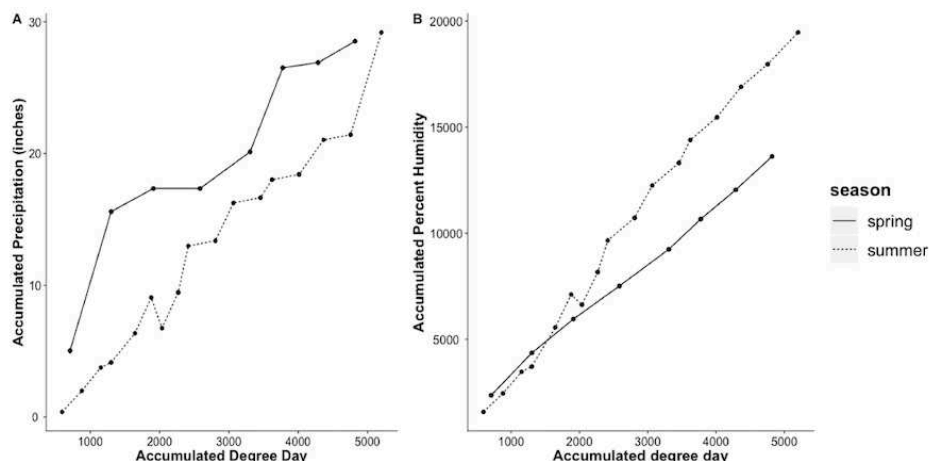


Figure S2.7. Accumulated precipitation (A) and humidity (B) data between day of placement and last day of collection for the spring and summer placements. Accumulated precipitation was calculated by adding average inches of precipitation per day, while accumulated humidity was calculated by adding average percent humidity per day. Weather data were collected from the Easterwood Airport Station using Weather Underground (<https://www.wunderground.com/>).

Table S2.1. Summary of rib bones collected from human cadavers placed at STAFS. The beginning date of the range of collection indicates the first known occurrence of rib exposure.

Season	Body ID	Day of placement	Advanced decay reached	Date range of collection	Ribs collected	ADD range
Spring	007	4/15/16	4/25/16	5/16/16 – 10/11/16	L9-12, R9-12	708-4821
	011	4/15/16	4/25/16	5/16/16 – 10/11/16	L8-12, R8-10, R12	708-4821
	024	4/15/16	4/25/16	5/16/16 – 10/11/16	L9-12, R9, R11-12	708-4821
Summer	064	8/25/16	9/02/16	9/22/16 – 5/05/17	L9-12, R9-12	592-4756
	065	8/25/16	9/02/16	10/4/16 – 5/05/17	L9-12, R8-11	877-4756
	067	9/16/16	9/23/16	11/01/16 – 6/08/17	L9-12, R9-12	1151-5201

Table S2.2. Random forests regression modeling of 16S rRNA and 18S rRNA data using features collapsed at different taxonomic levels. Model accuracy is assessed using mean absolute error (MAE). The model with the lowest error within each season (spring and summer together, spring only, summer only) is in bold.

Data type	Season	Level	MAE
16S rRNA	Spring and summer	ASV	793.33
		L7	822.28
		L6	822.37
		L5	851.41
		L4	839.88
		L3	842.20
		L2	807.77
	Spring	ASV	872.02
		L7	904.18
		L6	884.32
		L5	941.63
		L4	1025.01
		L3	987.59
	Summer	L2	1074.76
		ASV	723.98
		L7	729.09
		L6	746.90
		L5	788.10
		L4	834.82
		L3	853.38
	18S rRNA	Spring and summer	L2
ASV			1013.78
L12			952.92
L11			963.61
L10			964.84
L9			966.57
L8			956.64
L7			941.22
L6			1095.19
L5			1040.01
L4			1125.68
L3			1128.13
L2			1042.47
		ASV	1128.14
	L12	1044.26	
	L11	1074.59	
	L10	1084.54	
	L9	1110.03	

18S rRNA	Spring	L8	1113.28
		L7	1187.64
		L6	1202.75
		L5	1025.53
		L4	1168.03
		L3	1181.39
		L2	1443.86
	Summer	ASV	990.91
		L12	877.59
		L11	864.45
		L10	858.58
		L9	870.40
		L8	886.16
		L7	820.67
		L6	867.09
		L5	942.52
		L4	904.18
		L3	958.75
		L2	1083.95

Table S2.3. Effect size calculations for alpha (Faith’s PD and Shannon Index) and beta (weighted and unweighted UniFrac) diversity of the 16S rRNA and 18S rRNA data. The effect sizes (eta squared) of alpha diversity metrics were calculated using the H-value output of the Kruskal-Wallis test and the equation given by `kruskal_effsize()` in R. Effect sizes of beta diversity metrics are reported as pseudo-F values, which were provided in the beta-group-significance PERMANOVA outputs in QIIME2. Effect sizes were calculated for between seasons, hosts, and the first and last ADDs. Results are reported for calculations including both seasons as well as within season. Note that since effect size calculations were different between alpha and beta diversity metrics, results should only be compared within alpha or within beta diversity, but not between.

Data Type	Season(s)	Diversity Metric	Grouped by	Effect Size
16S rRNA	Spring and Summer	Faith’s PD	Season	0.02
			Host	0.12
			1 st and last ADD	0.31
		Shannon	Season	0.05
			Host	0.08
			1 st and last ADD	0.44
		Unweighted UniFrac	Season	2.32
			Host	1.73
			1 st and last ADD	4.22
		Weighted UniFrac	Season	2.42
			Host	1.78
			1 st and last ADD	5.20
	Spring	Faith’s PD	Host	0.24
			1 st and last ADD	0.13
Shannon		Host	0.07	
		1 st and last ADD	0.37	

		Unweighted UniFrac	Host	1.46	
			1 st and last ADD	2.12	
		Weighted UniFrac	Host	1.77	
			1 st and last ADD	1.41	
		Summer	Faith's PD	Host	0.10
				1 st and last ADD	0.79
	Shannon		Host	0.15	
			1 st and last ADD	0.50	
	Unweighted UniFrac		Host	1.66	
			1 st and last ADD	3.45	
	Weighted UniFrac	Host	1.40		
		1 st and last ADD	6.24		
	18S rRNA	Spring and Summer	Faith's PD	Season	0.04
				Host	0.22
1 st and last ADD				0.73	
Shannon			Season	0.04	
			Host	0.09	
			1 st and last ADD	0.73	
Unweighted UniFrac			Season	2.90	
			Host	2.44	
			1 st and last ADD	2.53	
Weighted UniFrac			Season	0.85	
			Host	2.32	
			1 st and last ADD	0.60	
Spring		Faith's PD	Host	0.07	
			1 st and last ADD	0.80	
		Shannon	Host	0	
			1 st and last ADD	0.80	
		Unweighted UniFrac	Host	1.56	
			1 st and last ADD	1.67	
Weighted UniFrac		Host	0.80		
		1 st and last ADD	0.20		
Summer		Faith's PD	Host	0.41	
			1 st and last ADD	0.60	
		Shannon	Host	0.33	
			1 st and last ADD	0.60	
	Unweighted UniFrac	Host	2.38		
		1 st and last ADD	1.28		
	Weighted UniFrac	Host	6.10		
		1 st and last ADD	4.24		

APPENDIX B: CHAPTER 3 SUPPLEMENTARY MATERIAL

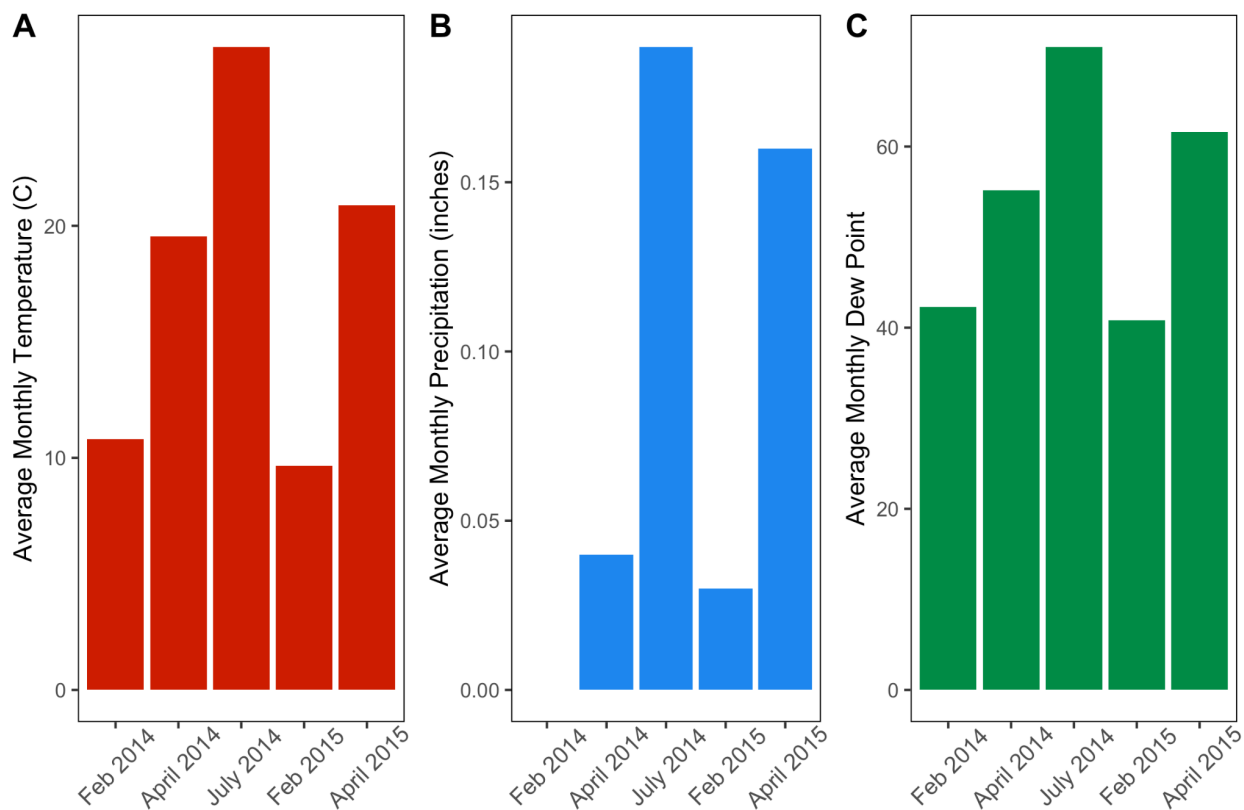


Figure S3.1. Weather data for each seasonal placement, including average monthly temperatures (A), average monthly precipitation (B), and average monthly dew point (C). No precipitation was recorded in February 2014.

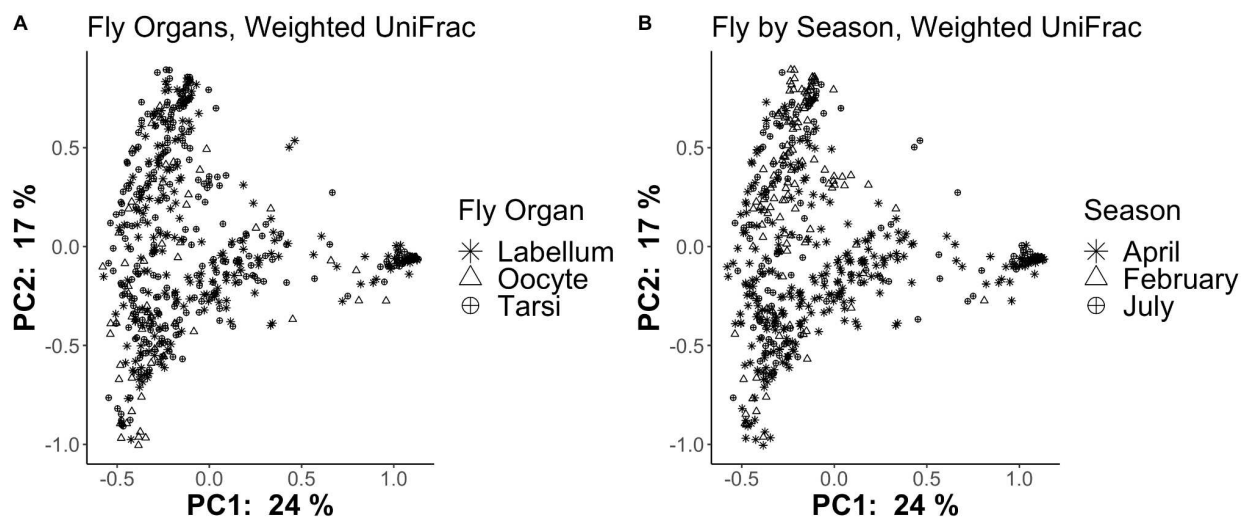


Figure S3.2. Weighted UniFrac beta diversity of fly microbiomes by organ and season. For all weighted PERMANOVA pairwise comparisons (i.e., all organs compared to all organs and all seasons compared to all seasons), $q = 0.001$ (999 permutations).

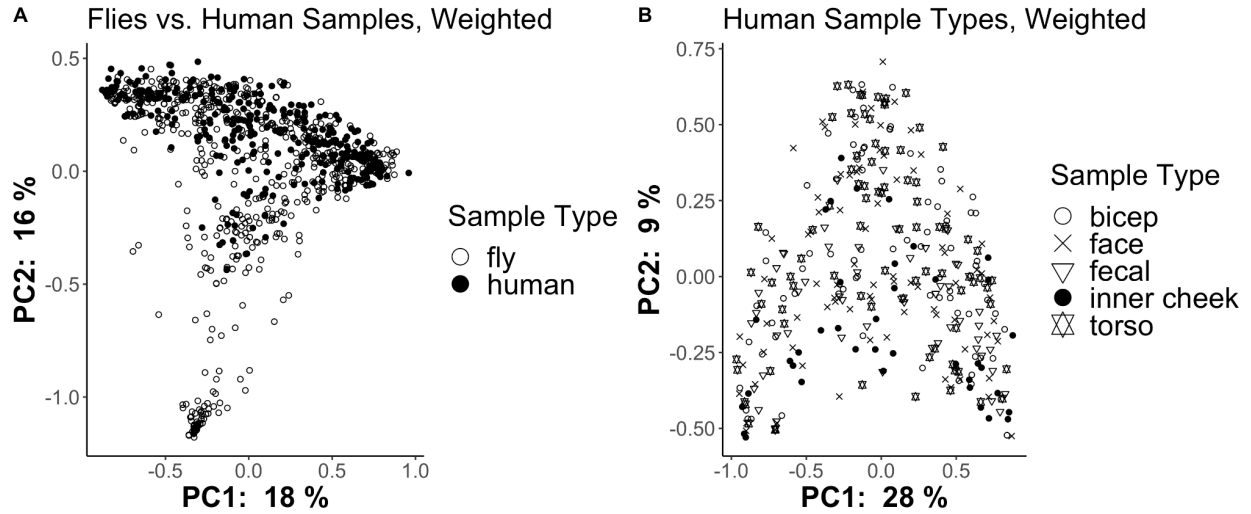


Figure S3.3. Weighted UniFrac beta diversity of human vs. fly samples (A) and the different sample types within the human data (B). PERMANOVA comparisons showed that the fly samples were significantly different from human samples ($p = 0.001$, 999 permutations, pseudo- $F = 41.95$), and pairwise PERMANOVA comparisons showed that some human sample types were significantly different from each other while others were not. Fecal samples were different from all other sample types ($0.005 < q < 0.006$, 999 permutations) except the inner cheek ($q = 0.13$, 999 permutations). The inner cheek was significantly different from the bicep, face, and torso ($q = 0.006$ for all comparisons, 999 permutations). Other human sample types (bicep, face, torso) were not significantly different from each other ($0.19 < q < 0.52$ for all comparisons, 999 permutations). The bicep, face, and torso were not significantly different from each other ($0.19 < q < 0.52$ for all comparisons, 999 permutations).

Table S3.1. Summary of cadavers included in this study. For storage condition, c = days in the cooler and f = days in the freezer.

Accession	Age	Sex	Storage	Height (m)	Ancestry	Medical
STAFS2014.006	47	M	c=26/f=21	1.78/81.64	European	Unknown
STAFS2014.009	71	M	c=29/f=11	unknown	European	Unknown
STAFS2014.004	62	M	c=2/f=98	1.9/99.79	European	Unknown
STAFS2014.028	58	M	c=6/f=14	?/158.75	European	Unknown
STAFS2014.052	62	M	c=35	1.73/72.57	European descent	Hypertension; cardiovascular
STAFS2014.053	68	M	c=19	1.88/40.82	European descent	failure to thrive; severe malnutrition;
STAFS2015.015	66	M	c=25	1.83/108.86	European	Unknown
STAFS2015.017	55	M	c=26	1.78/?	European	Unknown
STAFS2014.042	80	F	f=327	1.73/83.65	Unknown	congestive heart failure;
STAFS2014.066	87	F	c=2/f=244	1.52/36.28	European	Unknown